

**Dynamics In Primary Somatosensory Cortex: A Role For SI In The Processing Of
Tactile Information.**

Stephen B. Simons

A dissertation submitted to the faculty of the University of North Carolina at Chapel Hill
in partial fulfillment of the requirements for the degree of Doctor of Philosophy in the
Department of Biomedical Engineering.

Chapel Hill
2007

Approved by:

Mark Tommerdahl

Oleg Favorov

Bob Dennis

Jeff MacDonald

Sean Gomez

ABSTRACT

Stephen B. Simons: Dynamics In Primary Somatosensory Cortex: A Role For SI In The Processing Of Tactile Information.

(Under the direction of Mark Tommerdahl)

Traditional views of primary somatosensory cortex (SI) and its role in the processing of tactile information have limited its function as a dynamic component in the somatosensory pathway. Here I present evidence that the response in SI to stimuli at a given skin site is systematically modified with changes in the stimulus parameters and displays considerable dynamics. Optical intrinsic signal (OIS) imaging was used to study the responses (*in vivo*) evoked by 25 Hz (flutter) vertical skin displacement stimuli to the forelimb of squirrel monkey and cat. Responses to electrical stimulation were also measured in rat sensorimotor cortical slices using OIS imaging and local field potential (LFP) recordings. Results indicate that, contrary to traditional views, the intensive but not spatial attributes of the SI response are modified by increases in stimulus amplitude. Increasing the duration of flutter stimulation evokes increases in response magnitude in cortical regions near to the maximally responding center and simultaneous decreases in surrounding cortical regions; the net effect of this is the spatial sharpening of the SI response during prolonged stimulation. The distribution of decreased absorbance in surrounding cortex was non-uniform, indicating the possibility of stronger intracortical

inhibition along the proximodistal axis of the body representation. Cortical slices in the sagittal and coronal planes of the rat somatosensory cortex demonstrated a similar anisotropy in the distribution and impact of GABAergic inhibition on the horizontal spread of activity, and lend support to the idea that the non-uniformity observed *in vivo* may contain functional relevance. Bilateral stimulation of both forelimbs demonstrated that, although input to SI has been traditionally regarded as exclusively contralateral, not only can the response to an ipsilateral stimulus be measured in SI, but when stimulation is applied bilaterally the spatiotemporal characteristics of the evoked response cannot be accounted for by the responses of either stimulus alone or by the linear summation of the pair. All of these results taken together present a strong case for the necessity of strong dynamics in SI and the role of SI as an important site of cortical information processing in the somatosensory pathway.

*For my parents Ross and Sheila, whose love and support have carried me,
further than I ever thought possible.*

ACKNOWLEDGEMENTS

I would like to acknowledge all those people who have assisted in the completion of this work. Special thanks go to my colleagues, the members of my committee and, most especially to my advisor Mark Tommerdahl whose guidance and drive has been an inspiration to me.

TABLE OF CONTENTS

TABLE OF FIGURES	ix
CHAPTER 1: Introduction	1
CHAPTER TWO: Experimental Methods	5
In Vivo Methods	5
<i>Cat preparation</i>	6
<i>Imaging Protocol in vivo</i>	7
<i>Histological procedures/identification of cytoarchitectural boundaries</i>	8
In vitro preparation	9
<i>In vitro OIS and stimulation protocol</i>	10
<i>Evoked field potential recordings</i>	10
CHAPTER THREE: SI Response to Changes in Stimulus Amplitude	12
Background	12
Analytical Methods	14
<i>Imaging and Stimulus Protocol</i>	14
<i>Spatial Histogram</i>	14
<i>Correlation Maps</i>	14
Results	15
Discussion	30
Conclusions	34
CHAPTER FOUR: The Effects of Bilateral Stimulation	35

Background	35
Methods	36
<i>Stimulus Protocols</i>	36
<i>Cluster Analysis</i>	36
Results	37
<i>Squirrel Monkey SI</i>	37
<i>Cat SI</i>	39
<i>Cat SII</i>	46
Discussion	50
CHAPTER FIVE: SI Response to Changes in Stimulus Duration	55
Background	55
Methods	57
<i>Stimulus Protocol</i>	57
<i>Response Recovery</i>	58
<i>Determination of ROI</i>	58
<i>Correlational Methodology</i>	59
<i>Radial Histograms</i>	60
<i>Surround Anisotropy Plots (SAPs)</i>	60
Results	60
<i>Characterization of the temporal response within the maximally activated region</i> ..	61
<i>Changes in degree of correlated activity with increasing stimulus duration</i>	65
<i>Effects of stimulus duration on spatial extent</i>	67
<i>Anisotropy in magnitude of surround suppression</i>	68

<i>Characterization of the temporal response in the surround</i>	71
<i>Stimulus site specific suppression</i>	72
Discussion	76
<i>Prolonged stimulation reduces the spatial extent of the responding population</i>	77
<i>Stimulus site-specific SI suppression</i>	78
<i>Functional implications</i>	79
CHAPTER SIX: In Vitro Examination of Pericolumnar Excitability	81
Background	81
Analytical Methods	83
Results	83
Discussion	98
References	103

TABLE OF FIGURES

Figure 3.1. OIS response to low vs. high amplitude stimulation.....	16
Figure 3.2. Spatial histograms of activity at different amplitudes.....	18
Figure 3.3. Absorbance time course and anatomical registration in SI.....	20
Figure 3.4. Time course of absorbance change averaged across all subjects (n=5).....	22
Figure 3.5. Radial time space plots.....	24
Figure 3.6. Time course of absorbance change surrounding the ROI across all subjects (n=5).....	25
Figure 3.7. Correlation maps for amplitudes of 50 (left) and 400 (right) microns.....	27
Figure 3.8. Spatial plots of activity evoked by low (50mm) and high (400mm) amplitudes of stimulation.....	29
Figure 4.1. OIS response evoked by flutter stimulation of the thenar pad in two subject.....	38
Figure 4.2. Optical responses recorded in cat SI and SII to 25 Hz vibrotactile stimulation of the forepaws.....	41
Figure 4.3. Surface plots of absorbance evoked in SI by contralateral, ipsilateral, and bilateral stimulation.....	43
Figure 4.4. Time course of the absorbance change within the region of interest (ROI) in SI.....	44
Figure 4.5. Comparison of averaged normalized absorbance values (n=5) evoked under 3 different stimulus conditions.....	45
Figure 4.6. Optical responses in cat SI and SII to 25 Hz vibrotactile stimulation of the central pad in 2 subjects.....	47
Figure 4.7. Time course of the absorbance change in the anterior and posterior SII cortical regions evoked by flutter stimulation of the central pad in 2 subjects.....	48
Figure 4.8. Cluster plots of ipsilateral vs. contralateral response of 2 subjects.....	49
Figure 5.1. Difference images evoked by stimulation of the contralateral thenar pad in two exemplary subjects.....	62

Figure 5.2. Absorbance time course in one subject.....	63
Figure 5.3. Across-subjects absorbance time courses.....	64
Figure 5.4. Maps of correlated activity in two exemplary subjects.....	66
Figure 5.5. Radial absorbance trends across subjects (n=5).....	68
Figure 5.6. Surround Anisotropy Plots (SAPs) for one exemplary subject.....	70
Figure 5.7. Time course in medial/posterior region of surround.....	72
Figure 5.8. Surround Anisotropy Plots (SAPs) for two different stimulus sites in the same subject.....	74
Figure 5.9. Corresponding skin sites to locations of strongest suppression.....	76
Figure 6.1. OIS images in sensorimotor cortical slices during perfusion with normal ACSF and after application of 2mmol bicuculline methiodide (BMI).....	85
Figure 6.2. OIS images in cortical slices before and after perfusion with the NMDA antagonist D-AP5.....	88
Figure 6.3. Differential effects of GABA _A block with BMI and NMDA block with D-AP5 on the distribution of activity in layer 2/3.....	90
Figure 6.4. Recordings of local field potential across layer 2/3.....	93
Figure 6.5. Distribution of local field potential across layer 2/3 in coronal and sagittal slices.....	96
Figure 6.6. OIS responses evoked by multisite stimulation.....	98

CHAPTER 1: Introduction

Traditionally, primary somatosensory cortex (SI) has been depicted as a stage of the central nervous system that relays with only minor transformation, somatosensory information to higher centers that carry out the higher-order processing required for perception and discrimination. In this scenario, the SI cortical network displays little to no dynamics in response to transient stimuli, but instead produces a predictable response which is not significantly affected by nearby sensory inputs or the network's short term sensory history (Hubel and Wiesel 1962; Ferster 1992). Opposition to this viewpoint considers activity in SI as more significantly impacted by the intrinsic intracortical circuitry. In this case, thalamic input serves as a general framework for which cortical territories are activated but the more diverse activity patterns which arise can be mostly attributed to feedback excitation and inhibition from the complex intracortical network (Ahmed et al. 1994; Douglas et al. 1995; Somers et al. 1995). Recent studies in support of this view have shown that corticocortical synapses in fact greatly outnumber thalamocortical synapses (Ahmed et al. 1994; Douglas et al. 1995). To this end, the extensive lateral arborization of the cortex suggests that responses both in single neurons and populations of neurons are capable of modification by inputs to cortical sites which may be spatially remote.

Recent studies have shown that single SI neurons do in fact exhibit significant temporal dynamics when exposed to more prolonged periods of stimulation (Lee and Whitsel 1992; Whitsel et al. 2000; Whitsel et al. 2003). Comparison of 2DG experiments

and receptive field mapping experiments gave the first evidence of a time-dependent process involved in the formation of somatosensory cortical activity patterns (Whitsel and Juliano 1984; Whitsel 1987; Tommerdahl 1989). Discrepancies in the results of these experiments conducted with contrasting methodologies led to the investigation into the response of SI cortex to repetitive stimulation and the possible role that cortical dynamics played in SI pattern formation. These studies (Diamond et al. 1986; Whitsel 1987; Whitsel and Kelly 1988; Whitsel et al. 1989; Whitsel and Franzen 1989) revealed that the initial cortical response to a tactile stimulus is not the selective activation of a relatively few, highly tuned neurons, but rather a complex spatio-intensive pattern of activity involving very large numbers of neurons. With repetitive stimulation, this extensive and less differentiated initial activity pattern becomes rapidly sculpted by a dynamic cortical inhibitory mechanism into a more stimulus-specific spatiotemporal pattern. The spatial sharpening of the cortical response by lateral inhibition is one example of a dynamic process in SI.

Multiple animal studies have demonstrated that repetitive stimulation is reliably coupled with systematic reductions in neuronal responsivity at both peripheral and central levels of the somatosensory nervous system. For example, such stimulation is accompanied by a sustained decrease of the responsivity of skin mechanoreceptors located in the vicinity of the stimulated skin region (Leung 1995), a long-lasting depression of the responsivity of neurons in the cuneate nucleus of the brainstem ipsilateral to the stimulus site (OMara et al. 1988), a decrease in the thalamic and cortical firing rate (Chung et al. 2002) and a persistent reduction in the spatial extent of the SI region that responds to mechanical stimulation of a discrete skin site (Juliano et al. 1981;

Juliano et al. 1983; Kleinfeld and Delaney 1996; Tommerdahl and Whitsel 1996a; Tommerdahl et al. 1999a). Reduction in the spatial extent of the responding population in SI is presumably caused by mechanisms of surrounding cortical inhibition in regions remote from maximally stimulated neurons. This has been directly shown in the rat barrel cortex at the population level using voltage sensitive dyes (Kleinfeld and Delaney 1996; Derdikman et al. 2003) and with single cell recordings (Brumberg et al. 1996). The presence of SI surround inhibition associated with repetitive stimulation has also been suggested by imaging studies which have used the optical intrinsic signal (OIS). Although the intrinsic signal is an indirect measure of neuronal activity, many studies have demonstrated a decrease in signal strength to levels below tonic activity in surrounding regions of cortex, which has been suggested to reflect underlying inhibition (Tommerdahl et al. 1999a; Simons et al. 2005; Simons et al. 2007). The importance of surround inhibition in normal cortical function is poorly understood. One view has been that intracortical inhibition is nonspecific and serves to maintain the ability of neurons to selectively respond to stimuli which maximally drive them (Somers et al. 1995). Another possibility is that surrounding inhibition exists to suppress the response of neurons which are more weakly activated by intracortical lateral excitatory connections (rather than directly by thalamocortical connections). In this case, the function of such lateral inhibition in SI could be the precise localization of responses to more specific cortical sites for the purpose of behaviors involved in spatial discrimination. This type of mechanism could be particularly important in regions of SI which represent the hand, because of its large role in tactile sensibility and its superior spatial discriminative capacity.

The majority of studies which have examined primate SI have used the glabrous hand as the principal site for sensory input, primarily because of the expansive cortical territory that is devoted to its representation, and also because in most primates this region occupies a highly accessible territory (i.e. not buried in a sulcus in cerebral cortex). In primates, the glabrous hand is the primary means for not only tactile exploration of the environment but also for voluntary manipulations (such as gripping objects) of this environment. Completion of tasks involving grip requires not only the coordination of movement but also the continuous incorporation of sensory feedback. Similar to the rest of the body the glabrous hand is mapped in a highly orderly manner in SI. However, unlike processing of tactile information from almost all other regions of the body (i.e. trunk, forearm, legs), proper interpretation of tactile input from the hand likely requires the integration of information from any number of skin sites that function cooperatively during tactile exploration. For this reason, the selective dynamic interaction of multiple cortical regions in SI representing functionally interconnected sites on the hand seems not only plausible, but almost likely. Understanding cortical dynamics in normal functioning cortex is necessary to the subsequent comprehension and treatment of illnesses which originate from cortical dysfunction such as autism and schizophrenia. Additionally, if the activity in SI is significantly impacted by intracortical dynamics it could in turn affect the way in which dynamics are viewed across multiple sensory cortices.

CHAPTER TWO: Experimental Methods

In Vivo Methods

Squirrel monkey preparation

All methods and procedures involving the use of squirrel monkeys are consistent with USPHS policies and guidelines on animal care and welfare in biomedical research. They were reviewed and approved by an institutional committee prior to initiation of the experiments. Squirrel monkeys were used as subjects in studies aimed at the specific characterization of responses in primary somatosensory cortex (SI). Due to the large region of SI which is accessible for imaging (on the surface) as well as the fact that the primate representation of the glabrous hand in SI is extensive, squirrel monkeys make excellent subjects for investigating the response in SI. Following induction of anesthesia with 4% halothane in a 50/50 mix of nitrous oxide (N₂O) and oxygen, the trachea was intubated. A veterinary anesthesia machine (Forreger Compac-75) provided an anesthetic gas mix whose composition could be adjusted (typically 1.5 –3.0% halothane in 50/50 N₂O/oxygen) to maintain a stable level of surgical anesthesia. Methylprednisolone sodium succinate (20 mg/kg) and gentamicin sulfate (2.5 mg/kg) were injected intramuscularly to lessen the probability of halothane-induced cerebral edema and prevent bacterial septicemia, respectively. Placement of a valved polyethylene catheter into a superficial hindlimb vein enabled administration of 5%glucose, 0.9%NaCl, and drugs.

A 1.5 cm opening was trephined in the skull overlying SI cortex. A recording chamber (25 mm i.d.) was placed over the opening and cemented to the skull with dental acrylic. Wound margins were infiltrated with local anesthetic, closed with sutures and bandaged, and the dura overlying SI was resected. After the completion of all surgical procedures subjects were immobilized with norcuron (loading dose 0.25 - 0.5 mg/kg, i.v.; maintenance dose 0.025 – 0.05 mg/kg/hr). From this point on, the animal was ventilated with a 50/50 mix of N₂O and oxygen and the concentration of halothane was adjusted (typically between 0.5 and 1.0%) to maintain heart rate, blood pressure, and the EEG at values consistent with general anesthesia. Rate and depth of ventilation were adjusted to maintain end-tidal CO₂ between 3.0 and 4.5%. Under these experimental/anesthetic conditions both SI neuron spontaneous and stimulus-evoked spike discharge activity patterns are highly reproducible over even prolonged (>1 hr) time periods.

Cat preparation

Cats were used as subjects in experiments involving acquisition of optical data from secondary somatosensory cortex (SII), as well as bilateral studies of SI activity. The decision to use cats as subjects was made due to the large region of SII which lies exposed on the pial surface of the cortex, making it easy to image. All surgical procedures were carried out under deep general anesthesia (1 - 4% halothane in a 50/50 mixture of oxygen and nitrous oxide). After induction of general anesthesia the trachea was intubated with a soft tube and a polyethylene cannula was inserted in the femoral vein to allow administration of drugs and fluids (5% dextrose and 0.9% NaCl). For each subject, a 1.5 cm diameter opening was made in the skull overlying somatosensory cortex, a chamber was mounted to the skull over the opening with dental acrylic, and the

dura overlying anterior parietal cortex was incised and removed. Following the completion of the surgical procedures all wound margins were infiltrated with long-lasting local anesthetic, the skin and muscle incisions were closed with sutures, and each surgical site outside the recording chamber was covered with a bandage held in place by adhesive tape.

Subjects were immobilized with Norcuron and ventilated with a gas mixture (a 50/50 mix of oxygen and nitrous oxide; supplemented with 0.1 - 1.0% halothane when necessary) delivered via a positive pressure respirator 1-3 hours prior to the data acquisition phase of the OIS imaging experiments. Respirator rate and volume were adjusted to maintain end-tidal CO₂ between 3.0 - 4.0%; EEG and autonomic signs (slow wave content; heart rate, etc.) were monitored and titrated (by adjustments in the anesthetic gas mixture) to maintain levels consistent with light general anesthesia. Rectal temperature was maintained (using a heating pad) at 37.5 °C.

Euthanasia was achieved by intravenous injection of pentobarbital (45 mg/kg) and by intracardial perfusion with saline followed by fixative (10% formalin). Following perfusion fiducial marks were placed to guide removal, blocking, and subsequent histological sectioning of the cortical region studied. All procedures were reviewed and approved in advance by an institutional committee and are in full compliance with current NIH policy on animal welfare.

Imaging Protocol in vivo

After obtaining an image of the exposed cortical surface, the recording chamber was filled with artificial cerebrospinal fluid and hydraulically sealed using a clear glass plate. The imaging system consisted of a computer-interfaced CCD camera (Quantix 510

or Cascade 512b from Roper Scientific), light source, guide and filters required for near-infrared (833 ± 15 nm) illumination of the cortical surface, a focusing device, and a recording chamber capped by an optical window. Images of the exposed anterior parietal and surrounding cortical surface were acquired 250 ms before stimulus onset (“reference images”) and continuously thereafter for 9.75 sec after stimulus onset (“poststimulus images”) at a rate of one image every 250 msec. Difference images were generated by subtracting the reference image from each post-stimulus image. Averaged difference images typically show regions of both increased light absorption (decreased reflectance) and decreased light absorption (increased reflectance), which are believed widely (Grinvald 1985; Grinvald et al. 1991; Grinvald et al. 1991) to be accompanied by increases and decreases in neuronal activation, respectively.

All images were examined prior to their inclusion for analysis. Images containing random high amplitude noise were excluded, and the remaining trials (typically 10-15) were averaged to improve the signal to noise ratio. Images were analyzed using custom routines written in Matlab. Computational methods for analysis of the optical data varied depending on the experimental goal and will thus be described in later sections in which they were used.

Histological procedures/identification of cytoarchitectural boundaries

At the conclusion of each experiment (*in vivo*), the imaged cortical region was removed immediately following intracardial perfusion with saline and fixative. The region then was blocked, postfixed, cryoprotected, frozen, sectioned serially at 30 μm , and stained with cresyl fast violet. The boundaries between adjacent cytoarchitectonic areas were identified by scanning individual sagittal sections separated by no more than

300 μm and were plotted at high resolution using a microscope with a drawing tube attachment. The resulting plots then were used to reconstruct a two-dimensional surface map of the cytoarchitectonic boundaries within the region studied with optical and neurophysiological recording methods. The locations of microelectrode tracks and electrolytic lesions evident in the histological sections were projected radially to the pial surface and transferred to the map of cytoarchitectonic boundaries reconstructed from the same sections. As the final step, the cytoarchitectonic boundaries (along with the locations of microelectrode tracks and lesions whenever present) identified in each brain were mapped onto the images of the stimulus-evoked intrinsic signal obtained from the same subject, using fiducial points (made by postmortem applications of india ink or needle stabs) as well as morphological landmarks (e.g., blood vessels and sulci evident both in the optical images and in histological sections). Locations of cytoarchitectonic boundaries were identified using established criteria (Powell and Mountcastle 1959a; Jones and Porter 1980; Sur et al. 1982).

In vitro preparation

Young adult (21 – 35 day old) wistar rats were used as subjects. Subjects were immobilized using a conical soft plastic enclosure and decapitated. The whole brain was excised and immediately transferred to ice cold artificial cerebrospinal fluid (ACSF; NaCl replaced by sucrose). Composition of ACSF was (in mM) 124 NaCl, 3.0 KCl, 2.5 CaCl_2 , 25 NaHCO_3 , 1 MgSO_4 , 1.25 NaH_2PO_4 , and 10 glucose. The hindbrain was cut away using a straight razor blade and the left and right hemispheres were separated. Special care was taken to ensure that sections were taken from the region of the brain corresponding to SI. Coronal and sagittal brain slices (400 μm thickness) were cut serially

using an oscillating tissue slicer (OTS-4000, Electron Microscopy Sciences) and placed in a reservoir containing warmed (30°C) and oxygenated (using a 95% O₂ – 5% CO₂ gas mix) ACSF. Slices remained in the reservoir a minimum of 1 hour prior to being transferred (via pipette) into the recording chamber. While in the recording chamber slices were held in place using a fine nylon mesh and continuously perfused at a rate of 2-3 ml/min with oxygenated ACSF at room temperature. In experiments in which GABA_A block was performed bicuculline methiodide was added to the ACSF at a final concentration of 2μM and perfused normally. Stimulation was stopped for 10 minutes to allow for complete perfusion.

In vitro OIS and stimulation protocol

Slices were transilluminated using unfiltered light from a halogen light source (Oriol) and images were obtained at 2x magnification using an inverted microscope (Diaphot 200, Nikon) and a cooled CCD camera (Quantix 5714, Photometrics). Images were acquired continuously for 4s before stimulus onset and 11s following stimulus onset (15s total acquisition time) at a rate of 2 fps. Difference images were generated by subtracting the first image acquired from each subsequent image. Acquisition of a full 4s of pre-stimulus data allows for easy demonstration of baseline levels before stimulus delivery. Stimulation was delivered using a 50μm tip bipolar electrode at the layer VI/white matter (WM) border. The standard stimulus for evoking an OIS was delivered with a current amplitude of 150-200μA at a frequency of 20Hz for 1 second using a programmable pulse generator (Master A; AMPI).

Evoked field potential recordings

Measures of neural population electrical activity were made using a glass micropipette pulled with a vertical puller (Narishige PP-83) and filled with 1-2M NaCl. The micropipette was positioned on the surface of layer 2/3 and responses to single pulse (0.2 ms duration, 1.5x threshold) stimulation were recorded at a number of closely spaced locations (across layer 2/3) in order to obtain a spatial profile of the activity evoked by single site stimulation at the layer VI/WM border. At each location a series of 10 single pulses were delivered (ISI of 10 seconds) and responses were averaged. Recordings were sampled at 20 kHz, amplified and bandpass filtered (10-300 Hz) before being stored and analyzed (pClamp 6.0; Axon Instruments). Typical field potential recordings reflect both subthreshold and spiking activity of local neurons and contain elements of presynaptic and postsynaptic excitation.

CHAPTER THREE: SI Response to Changes in Stimulus Amplitude

Background

The way in which stimulus intensity is represented in primary somatosensory cortex has remained an intriguing question in the study of cortical correlates of perception. Although there have been numerous studies of somatosensory cortical response to changes in stimulus intensity, few have focused on the population response of the cortex with regard to this subject. Thus, a dearth of information about the cortical network response to changes in stimulus intensity exists – current knowledge of the subject depends predominantly on reconstruction of predictions of the cortical response from afferent recordings (Werner and Mountcastle 1965; Johnson 1974; Connor et al. 1990; Whitsel et al. 2000; Guclu and Bolanowski 2002) and single unit cortical recordings (Mountcastle et al. 1963; Simons 1978). Very few studies have examined the population response of the somatosensory cortex to varying stimulus intensity at resolution sufficient to provide details of cortical response that would provide information necessary to increase understanding about the primary somatosensory network dynamics involved in processing stimuli of different intensities.

A number of studies have examined the population response with imaging techniques such as fMRI (functional Magnetic Resonance Imaging) (Arthurs et al. 2000; Backes et al. 2000; Nelson et al. 2004) and MEG (MagnetoEncephaloGraphy) (Iguchi et al. 2002; Torquati et al. 2002). In general, results from these studies have reported that increases in the intensity of the evoked signal as well as increases in the activated volume

of cortex could be correlated with increases in stimulus intensity. These studies predicted that amplitude could be coded for by not only the average firing rates but also by the total aggregate of responding neurons. However, although each of these imaging techniques uses measures which are indirectly related to neuronal activity, the resolution is limited in two important ways. First, it is difficult to determine the nature of the neuronal activity being imaged (whether or not it is excitatory or inhibitory) and second, fMRI and MEG studies have limited spatial resolution, which is typically on the order of $\sim 1\text{mm}^2$ (Arthurs et al. 2000; Backes et al. 2000; Iguchi et al. 2002; Torquati et al. 2002; Nelson et al. 2004).

Recently, Chen and colleagues used the intrinsic signal to demonstrate that a proportionally greater response (magnitude) is evoked in SI cortex of squirrel monkeys as the amplitude (as measured by force) of a flutter stimulus is increased (Chen et al. 2003). However, the primary focus of their report was that the response to simultaneous stimulation of multiple adjacent sites on the skin produced a smaller, more intense region of cortical activation than would be normally predicted by summation of the two, and their findings did not detail the effects of amplitude on the dynamics of the population response to a flutter stimulus at a single locus on the skin. In this report, we extend the aforementioned work by imaging the optical intrinsic signal (OIS) evoked in primary somatosensory cortex (SI) of squirrel monkeys to a range of amplitudes of flutter stimulation. Our results suggest that large amplitude stimuli evoke patterns of proportionally higher absorbance, which although more intense, do not occupy a larger cortical territory than responses evoked by smaller amplitude stimuli. These spatially constrained regions of evoked activity are surrounded by regions of decreased absorbance

suggesting the presence of an inhibitory zone which may contribute to the cortical processing of stronger stimuli.

Analytical Methods

Imaging and Stimulus Protocol

In each of five experiments, the OIS evoked in SI by cutaneous flutter (25 Hz) stimuli on the thenar region of the forelimb was recorded. The flutter stimulus was delivered at 50, 100, 200 and 400 μ m and was interleaved in order to prevent conditioning of the response. Images of the exposed anterior parietal and surrounding cortical surface were acquired 200 ms before stimulus onset (“reference images”) and continuously thereafter for 22 s after stimulus onset (“poststimulus images”) at a rate of one image every second. Exposure time was 200 ms.

Spatial Histogram

Difference images acquired from the time of stimulus onset to 5 seconds after stimulus offset were summed and their activity characterized using linear segmentation. The activity was measured along a line through the region of interest in 200 x 40 μ m bins and plotted as a function of their distance along the line. Such segmented analysis typically produces a Gaussian profile of absorbance values with the local maximum corresponding to the center of the ROI.

Correlation Maps

Correlation maps were constructed for comparison of spatial characteristics of the OIS response. This method of analysis has been previously described in detail (Tommerdahl et al. 2002). Briefly, maps were constructed by choosing a reference region within the imaged field and computing the intensity correlation r_{ij} between the

reflectance value of each pixel (i, j) and the average reflectance value within the reference region over the time from stimulus onset to stimulus offset. The region selected as the reference was defined by a boxel ($\pi \text{ mm}^2$ area) centered on the region of interest (ROI). Each pixel (i, j) on the correlation map is represented by a coefficient of determination r^2_{ij} ($-1 < r^2 < 1$; - 1 indicates negative correlation; + 1 indicates positive). The statistical significance of each of the correlations was tested with an independent samples t-test.

Results

Figure 3.1 illustrates typical examples of the intrinsic signal detected in SI of three different subjects (A-C) in the absence of stimulation (control), and during low ($50\mu\text{m}$) versus high ($400\mu\text{m}$) amplitude stimulation. Each image shown in Figure 3.1 represents the sum of frames taken from the time of stimulus onset to 5 seconds after stimulus offset (frames 1-16). Areas of high absorbance are indicated by dark patches within each image; regions of high absorbance in each case correspond to the SI locus that represents the stimulated site on the skin. In each of the three subjects the increase in absorbance within the region of interest (ROI) in SI detected under the $400\mu\text{m}$ condition was larger than that measured under the $50\mu\text{m}$ condition. Moreover, in each subject the increase in absorbance appears more evenly distributed and less diffuse throughout the ROI under the $400\mu\text{m}$ condition.

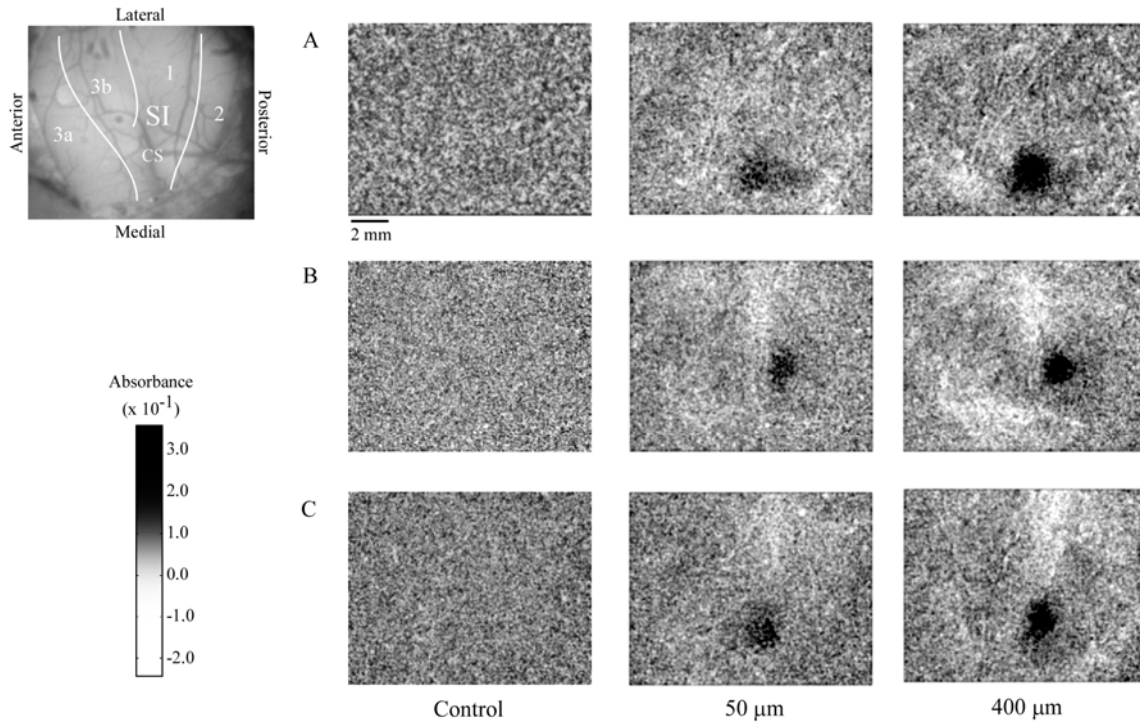


Figure 3.1. OIS response to low vs. high amplitude stimulation. Paired OIS images taken from three experiments (A, B, C). All images are anatomically oriented as shown in top left green filter image; location of central sulcus (CS) as well as cytoarchitectonic boundaries are drawn in and relevant cortical areas (1, 2, 3a, 3b) are labeled. Images were obtained by averaging across 10 experimental trials and then summing frames taken from the time of stimulus onset to 5 seconds after stimulus offset to better show regions of activation indicated by dark pixels (gray-scale bar at bottom left). The left column represents responses measured at the 50 μm stimulus amplitude while the right column shows the same respective experiment with a stimulus amplitude of 400 μm .

Spatial histograms were constructed in order to allow identification of the boundaries of the SI regions that underwent an increase in absorbance in response to skin flutter stimulation. Figure 3.2 illustrates the average results obtained from all experiments ($n=5$) as well as the methodology used to evaluate the spatial extent of the stimulus-evoked activation. In each experiment, the image was segmented along a line 6 mm long and approximately centered on the area of increased absorbance, as shown in

the top panel. Pixels along the line were binned (bin size 40 x 200 μm) and absorbance values averaged and plotted as a function of distance along the line. The plots demonstrate that at all amplitudes of stimulation, the spatial extent of the region of above-background absorbance (ie. absorbance values larger than control) is similar and at every stimulus amplitude occupies a circular-shaped territory in SI between 1.8 – 2.24 mm in diameter. The ROI (to be used for further analysis) was therefore defined as the region displaying above background levels of absorbance within the activated region of SI.

Figure 3.3 demonstrates the method used to evaluate the time course of the stimulus-evoked SI absorbance change in one exemplary subject. Panel A shows an image of the cortical surface which highlights the cortical vasculature. Panels B&C demonstrate the OIS responses evoked by the low (50 μm) and high (400 μm) stimulus amplitudes respectively. The ROI is the circular territory enclosed by the dashed white lines. Absorbance values within the ROI were averaged for each amplitude of stimulation and plotted as a function of time. The time course of the absorbance values measured between 1 and 22 sec after stimulus onset is plotted for each of the stimulus conditions, and in the absence of stimulation (“control”). Arrows along x-axis of plots at bottom left of Figure 3.3 indicate stimulus onset (1 sec) and stimulus offset (11 sec), and reveal how absorbance increased with increasing amplitude of stimulation. For each stimulus amplitude absorbance is maximal during stimulus offset.

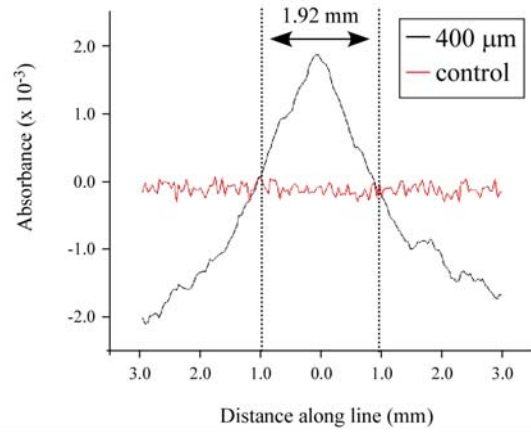
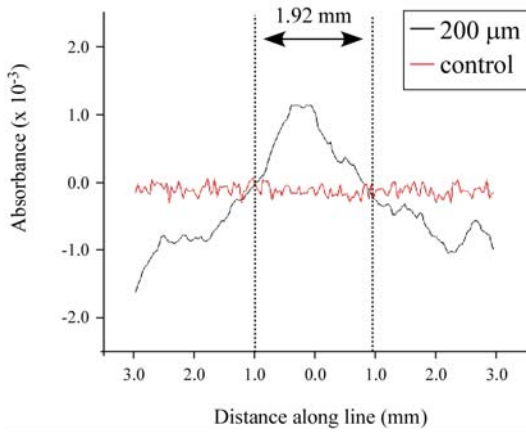
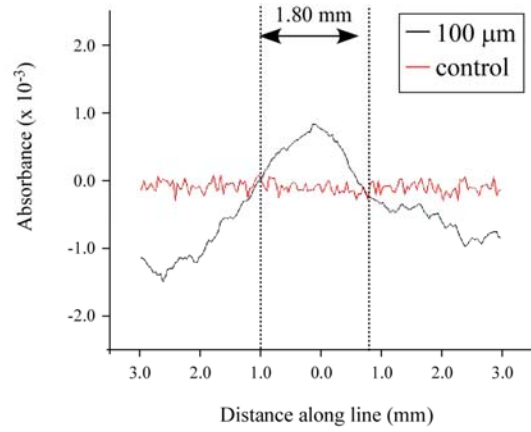
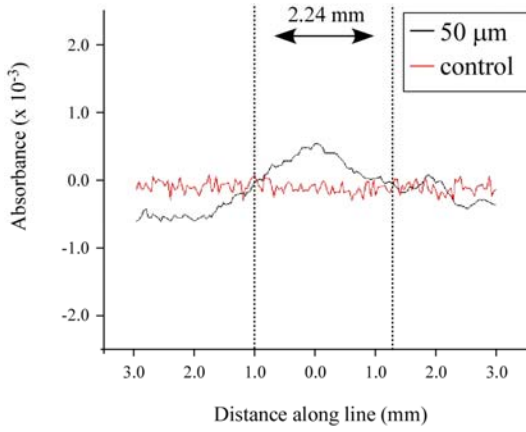
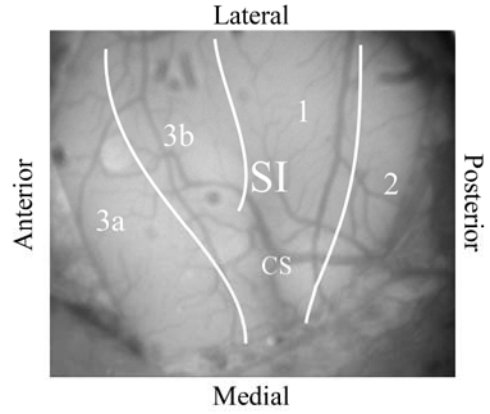
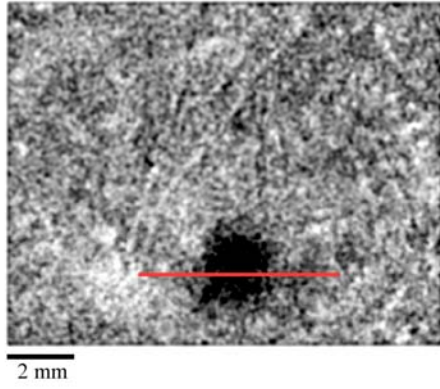


Figure 3.2. Spatial histograms of activity at different amplitudes. Absorbances were measured at each amplitude along the red line shown in the OIS image at top left. Anatomical orientation for the image is shown in the green filter image shown to the right; location of central sulcus (CS) as well as cytoarchitectonic boundaries are drawn in and relevant cortical areas (1, 2, 3a, 3b) are labeled. Each plotted value represents an average of pixels spanning 200 μm above and below the line and a distance of 40 μm along the line (total bin size was 40 x 400 μm). The control condition is plotted on each graph to indicate levels of above and below background absorbance. Dashed lines on plots indicate where stimulus evoked activity crosses background absorbance levels (indicating the boundaries of above background absorbance). Histograms indicate no significant change in cortical territory displaying above background absorbance with respect to stimulus amplitude.

The analytical approach illustrated in Figure 3.3 was performed on the data obtained from all subjects ($n=5$) and the resulting absorbance plots were averaged (Figure 3.4). All data were normalized prior to averaging. Similar to Figure 3.3, the plots in Figure 3.4 demonstrate that SI absorbance increases with increasing stimulus amplitude. To quantify this relationship a measure of $\Delta\text{Absorbance}_{\text{evoked}}$ was used. $\Delta\text{Absorbance}_{\text{evoked}}$ was defined as the difference between the absorbance measured at 1 sec (prior to stimulus onset) and 11 sec (point of stimulus offset) - shown in the plot at the bottom of Figure 3.4. The plot of $\Delta\text{Absorbance}_{\text{evoked}}$ vs. amplitude is well described (coefficient of determination $R^2=0.9921$) by the linear function (solid line) $\Delta\text{Absorbance}_{\text{evoked}} = (4 \times 10^{-6}) * d + 0.0005$. This type of analysis, however, gives little or no information about the spatial properties of the response.

Radial histograms were constructed to better visualize the spatiotemporal relationship of the OIS response at different amplitudes. The radial histograms shown in Figure 3.5 are representative time-space plots of the data obtained at each amplitude.

From the ROI center (as determined by spatial histogram analysis), average absorbance values were determined for the pixels within concentric rings located at progressively larger

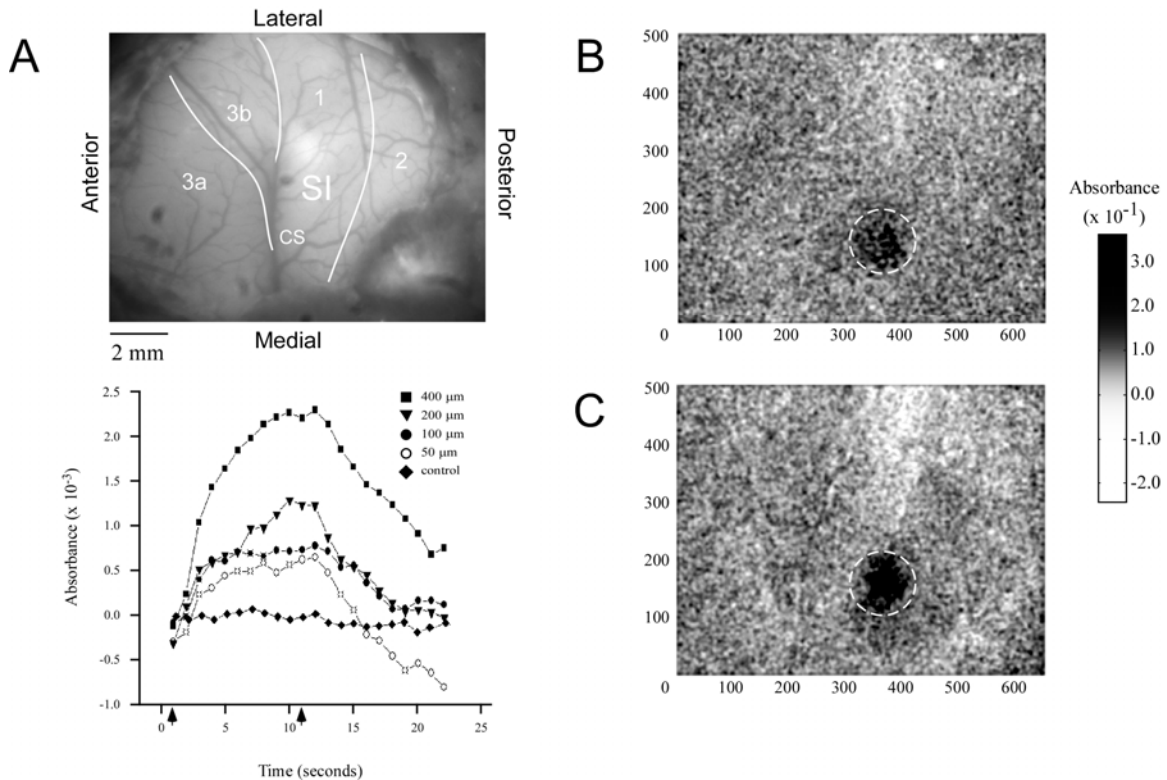
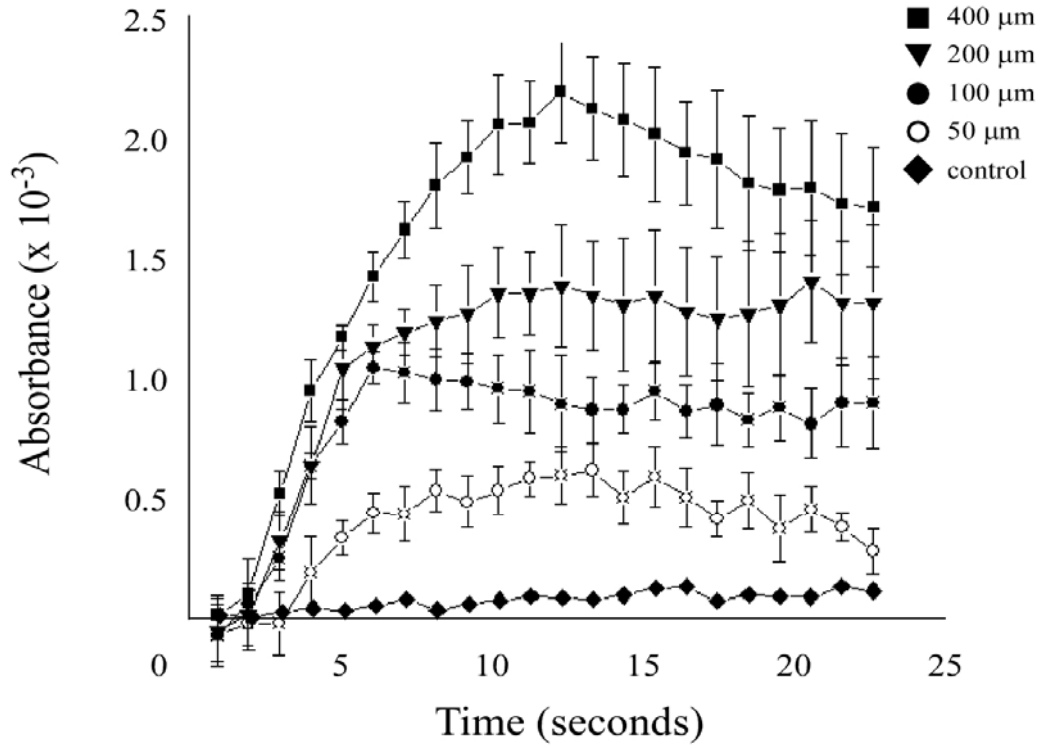


Figure 3.3. Absorbance time course and anatomical registration in SI. A) Green filter image of SI cortex in vivo, used for anatomical registration of OIS images. Location of central sulcus (CS) as well as cytoarchitectonic boundaries are drawn in and relevant cortical areas (1, 2, 3a, 3b) are labeled. B&C) Resulting OIS image obtained from averaging across 10 experimental trials and then summing frames taken from the time of stimulus onset to 5 seconds after stimulus offset: B) at stimulus amplitude 50 μm, C) at 400 μm. Absorbance values are indicated by gray-scale bar at right. Dashed circles enclose the ROI within SI. Bottom left) Graph of the averaged optical response measured within the ROI. Arrows indicate time of stimulus onset (1s) and stimulus offset (11s). Measurements were made at each amplitude and plotted as a function of time.

distances from the center at each frame acquired. Absorbance values are color coded (red areas indicate high absorbance; blue areas indicate low absorbance) and plotted as a function of time and radial distance from the center of the ROI. Figure 3.5 demonstrates that the major differences that exist in the SI global responses to different amplitudes of stimulation are differences in the magnitude of absorbance, but not in the spatial properties of the absorbance pattern (this also is apparent in the spatial histogram analysis of Figure 3.2). As would be expected based on the absorbance curves shown in Figures 3-3 & 3-4, higher stimulus amplitudes evoked a more intense and discrete region of increased absorbance than did the lower amplitudes. Interestingly, one of the more robust differences between low- and high-amplitude stimulation, is the magnitude of decreasing absorbance detected in the territory that surrounds the region in which absorbance increases. This response is most pronounced under the 400 μ m condition where it can be seen to occur much sooner after stimulus onset at radial distances as small as 1.5mm from the ROI center. Spatially, the regions of above- and below-background absorbance are nearly the same at each stimulus amplitude, with the above-background portion extending nearly 1mm away in all directions from the center of activity, whereas the below-background portion of the response comprises a ring beginning at a radial distance of 1.5mm from the ROI center and extending out beyond the area that was analyzed.

A



B

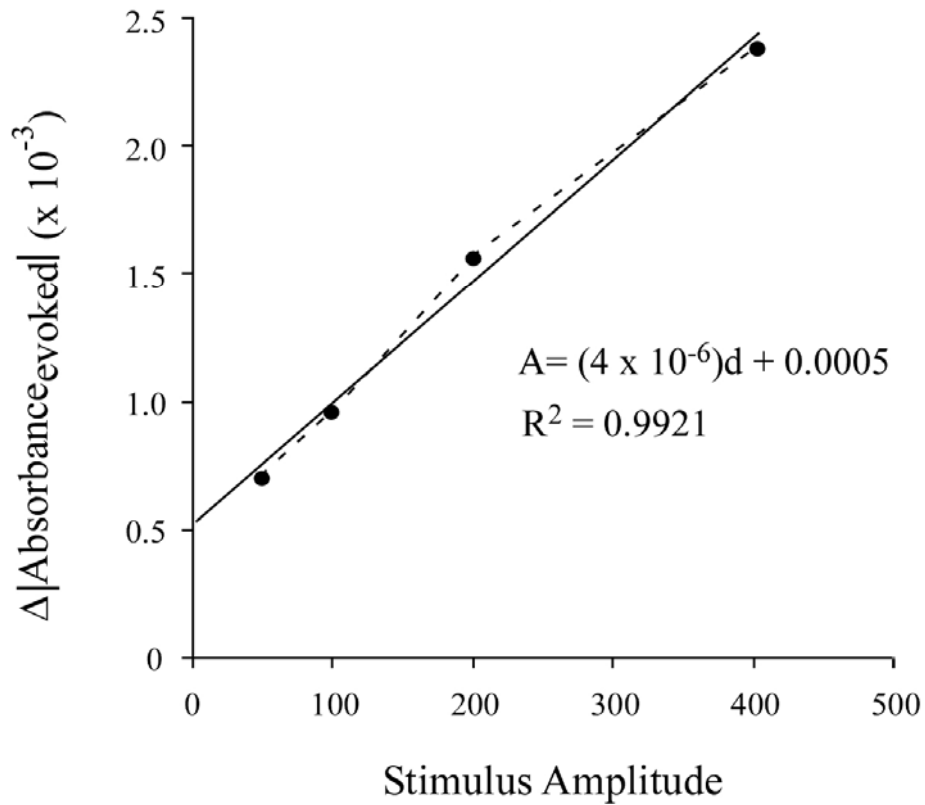


Figure 3.4. Time course of absorbance change across all subjects (n=5). (Top) Plots of average absorbance and standard deviation. All data was normalized prior to being averaged. Plotted absorbances were measured within the ROI which was defined as all pixels within a 1mm radius of the center of activation which was defined empirically. Control conditions in which no stimulus was administered are plotted simultaneously for comparison to test conditions. (Bottom) Plot of $\Delta\text{Absorbance}_{\text{evoked}}$ which was defined as the change in absorbance measured from frame 1 (prior to stimulus onset) to frame 11 (point of stimulus offset). The plot is fit with a linear function (solid line) described by the equation $A = (4 \times 10^{-6})d + 0.0005$ where A is absorbance and d is stimulus amplitude (displacement). Coefficient of determination for the linear regression (R^2) is also shown.

Using similar techniques to those we used to analyze above-background activity in the ROI (as in Figures 3-2 & 3-3), regions outside the designated ROI were examined to determine whether a similar amplitude-dependency could be established for the time courses of the below-background absorbance observed in the surround. Figure 3.6 shows plots constructed from averaging the absorbance values in pixels lying 1.5 – 2 mm away from the center of the ROI. Data were normalized and then averaged across experiments (n=5). It is apparent that the time courses at different amplitudes of stimulation are different with respect to the stimulus timing, (compared with above background levels of activity, all of which show maximum absorbance at the point of stimulus offset). Consequently, a different measure was adopted to quantify this relationship: In this case $\Delta\text{Absorbance}_{\text{max}}$ was defined as the difference between the minimum absorbance and the maximum absorbance value obtained at any point during the recording. Interestingly, the relationship between stimulus amplitude and $\Delta\text{Absorbance}_{\text{max}}$ in the surround is not linear (Figure 3.6b). Instead, each of the higher stimulus amplitudes employed (100-400 μm) evoked a very similar level of below-background absorbance. The sole difference

between each of the curves shown in 3-6a is the time required to reach the peak of the decrease in absorbance. That is, as amplitude is increased from 100 to 400 μm the point of minimum absorbance was attained earlier in time. This same result also is apparent in Figure 3.4.

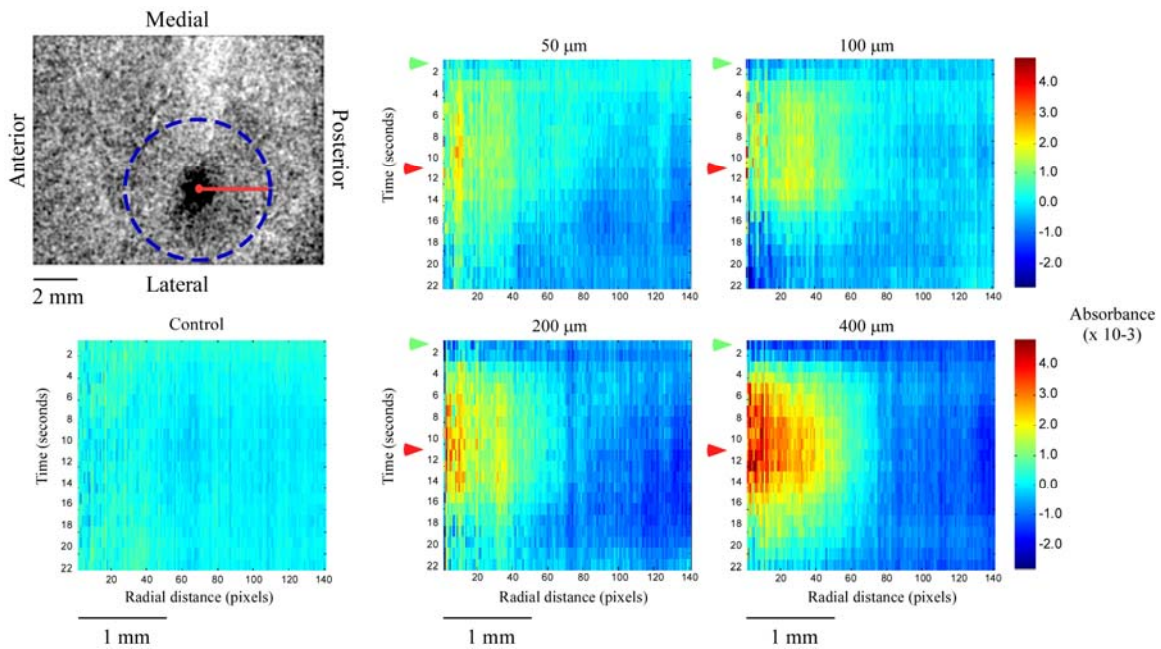


Figure 3.5. Radial time space plots. Radial histograms were performed on OIS data at all stimulus amplitudes. Radii were measured from the center of activation chosen empirically and held constant over each amplitude as demonstrated by panel at top-left. The dashed blue line is the maximum radial distance used in the maps shown. The schematic at bottom left indicates the anatomical orientation of the cortex in the OIS image above. Absorbance values in maps shown represent an average at each radial distance for each second in the recording. Green arrows indicate stimulus onset (1s) while red arrows indicate stimulus offset (11s). All graphs were normalized over the spectral range of the entire data set.

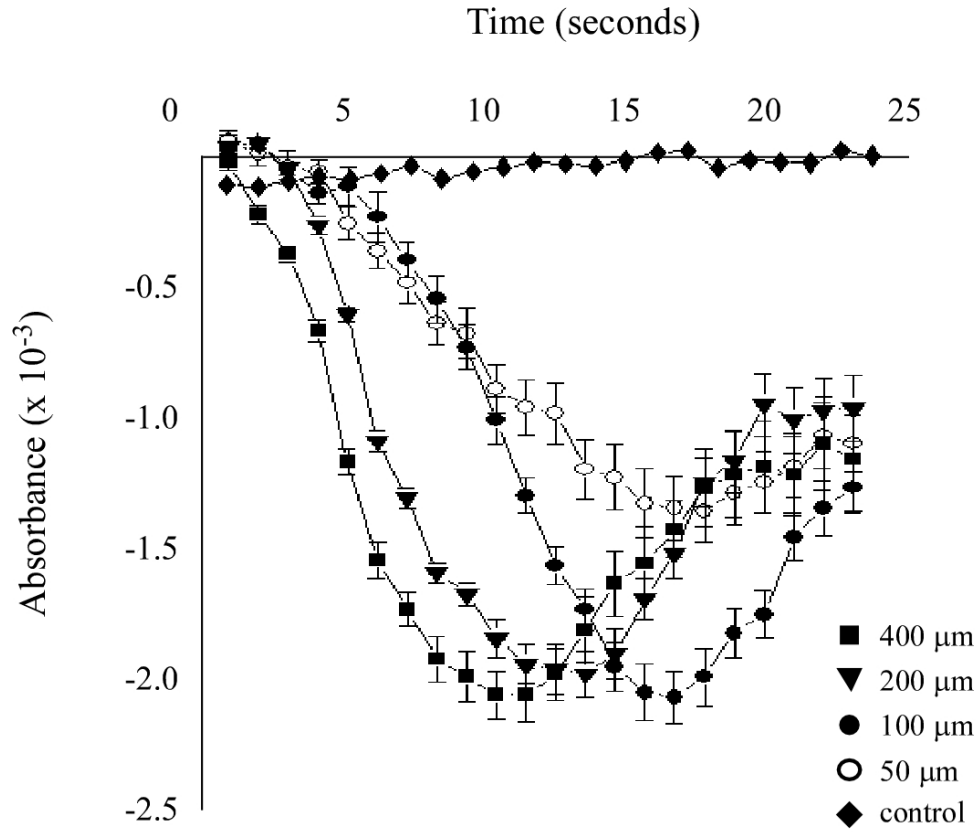
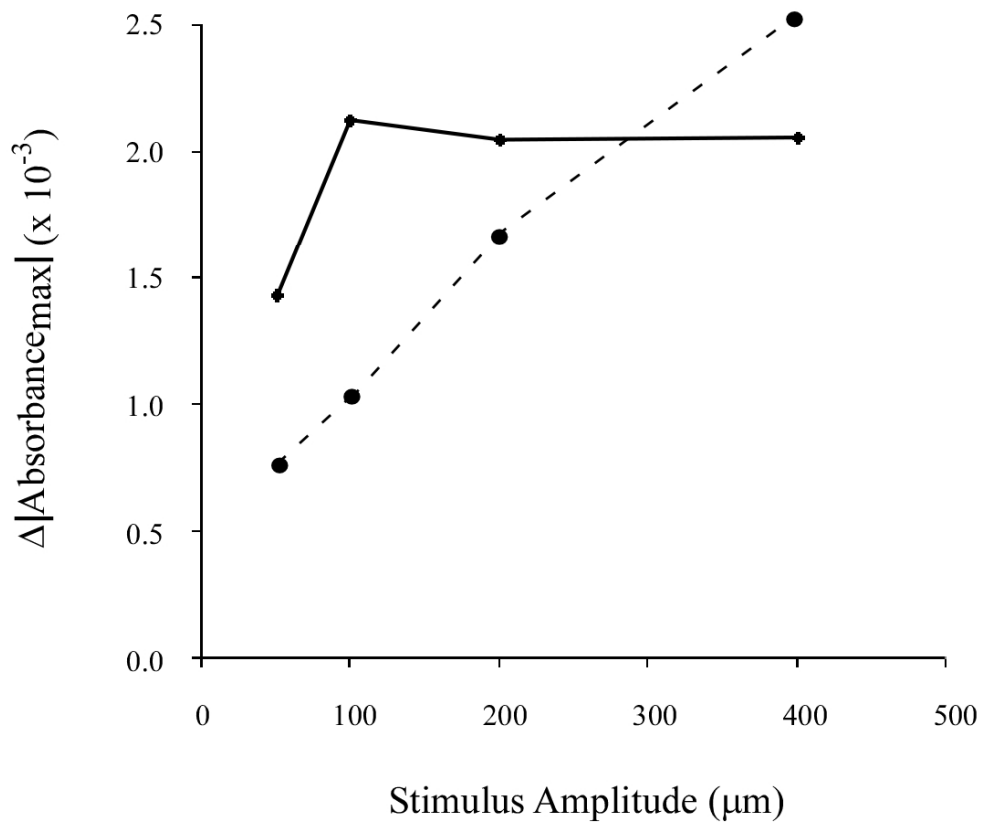
A**B**

Figure 3.6. Absorbance trends surrounding the ROI across five experiments. (Top) Plots of absorbance and standard deviation averaged across all experiments (n=5). Plotted absorbances were measured at radial distances between 1 and 1.5mm away from the center of activation (defined earlier). (Bottom) Plot of the maximal change in absorbance (absolute value) as a function of stimulus amplitude. The linear trend, obtained from averaged absorbances, measured at the ROI (dashed line from figure 3) has been plotted alongside to demonstrate the significant differences between the two regions.

Correlation maps were constructed to further characterize the spatial properties of the SI response to 25 Hz flutter. A correlation map compares every pixel in the image with the signal referenced from the ROI, and assigns a coefficient of determination (r^2) to the location of the pixel being compared. This gives a fairly good approximation of the signal at all locations in the image. Since there is no significant difference in the spatial properties between stimuli at intermediate amplitudes (as demonstrated by radial and spatial histograms) only the 50 and 400 μ m amplitudes will be compared with this technique. Figure 3.7 shows correlation maps of the OIS responses to stimulus amplitudes of 50 and 400 μ m (Top panels). The bottom panels of the figure show the input signal (solid dark red line) used for correlation of each pixel in the map, and the negative (opposite) of the input signal (dotted blue line). A coefficient of determination of +1 (although it never appears in the map) indicates that a pixel's time course perfectly matches the input signal while a coefficient of determination of -1 indicates that pixel's time course perfectly matches the opposite of the input signal (dotted blue line). At 50 μ m the correlation map (color-coded image) shows that the correlation is weak and more dispersed within the ROI in area 3b. At the highest amplitude, however, there is a

pronounced and well-defined positive correlation within the ROI that is more evenly distributed throughout the ROI. A large region of negatively correlated activity (corresponding to strong below background activity) surrounds the ROI in the high-amplitude map.

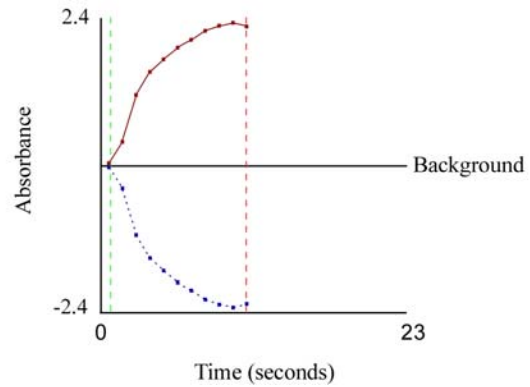
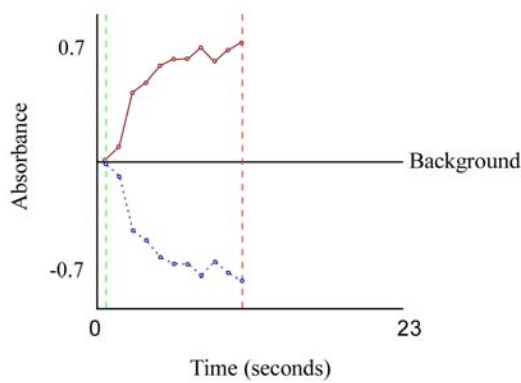
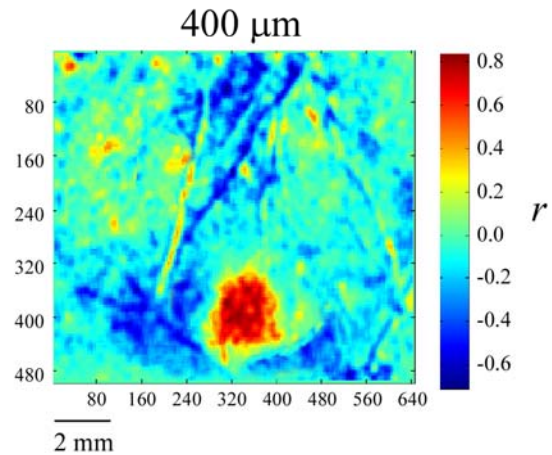
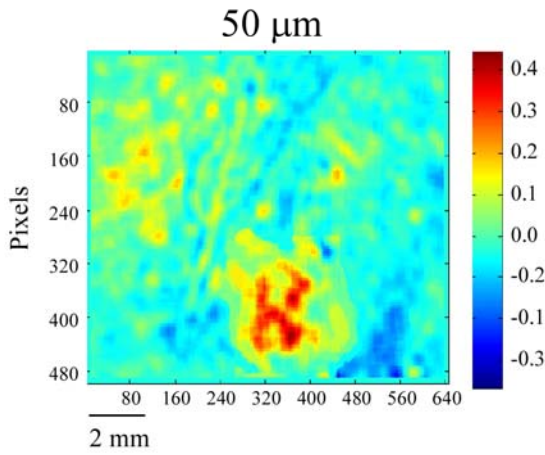
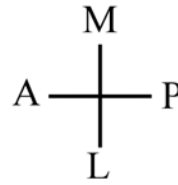
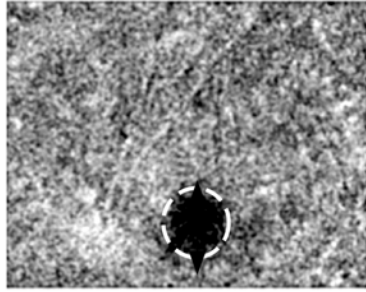


Figure 3.7. Correlation maps for stimulus amplitudes of 50 (left) and 400 (right) microns. The entire field of view is correlated with the selected ROI (shown in OIS image at top-left encircled by dashed line). The schematic at top-right indicates the anatomical orientation of the OIS image as well as all maps: A-anterior, M-medial, P-posterior, L-lateral. Color bars show correlation coefficient values for each map. The correlated signal, obtained from averaging of absorbance values within the ROI at each frame, is shown under each map. Only the portion of the signal enclosed within the dashed lines (corresponding to the stimulus duration, green-on, red-off) is correlated. A correlation of +1 would correspond to the signal shown in dark red while a correlation of -1 would correspond to the signal in dark blue.

To examine the spatial dynamics of the SI response in more detail we examined the patterns of activity generated by low- and high-amplitude stimulation in a 16mm^2 (4×4) area centered around the ROI. Figure 3.8 demonstrates the patterns of activity evoked at three time intervals during the delivery of the stimulus. The 3D surface plots show activity measured within the boxel indicated by the dashed box in the image at the top. In each 3D plot absorbance is plotted in two-dimensional space and is indicated by two measures: height of the peak along the z-axis (as shown in the schematic at the top right), and the color (indicated by the color bar to the right of each row of 3D plots). These data make it apparent that after a short period of stimulation (1 sec) the activity pattern is very similar for the different amplitudes. That is, at this early time interval both patterns are diffuse and occupy much of the ROI. However as stimulus duration increases, the pattern of increased absorbance evoked by high-amplitude stimulation tends to become restricted to the center of the ROI and within this region becomes homogeneous. Standard deviation was used to measure the variability within the ROI at low and high amplitudes. At 10s after stimulus onset, standard deviations for low- and

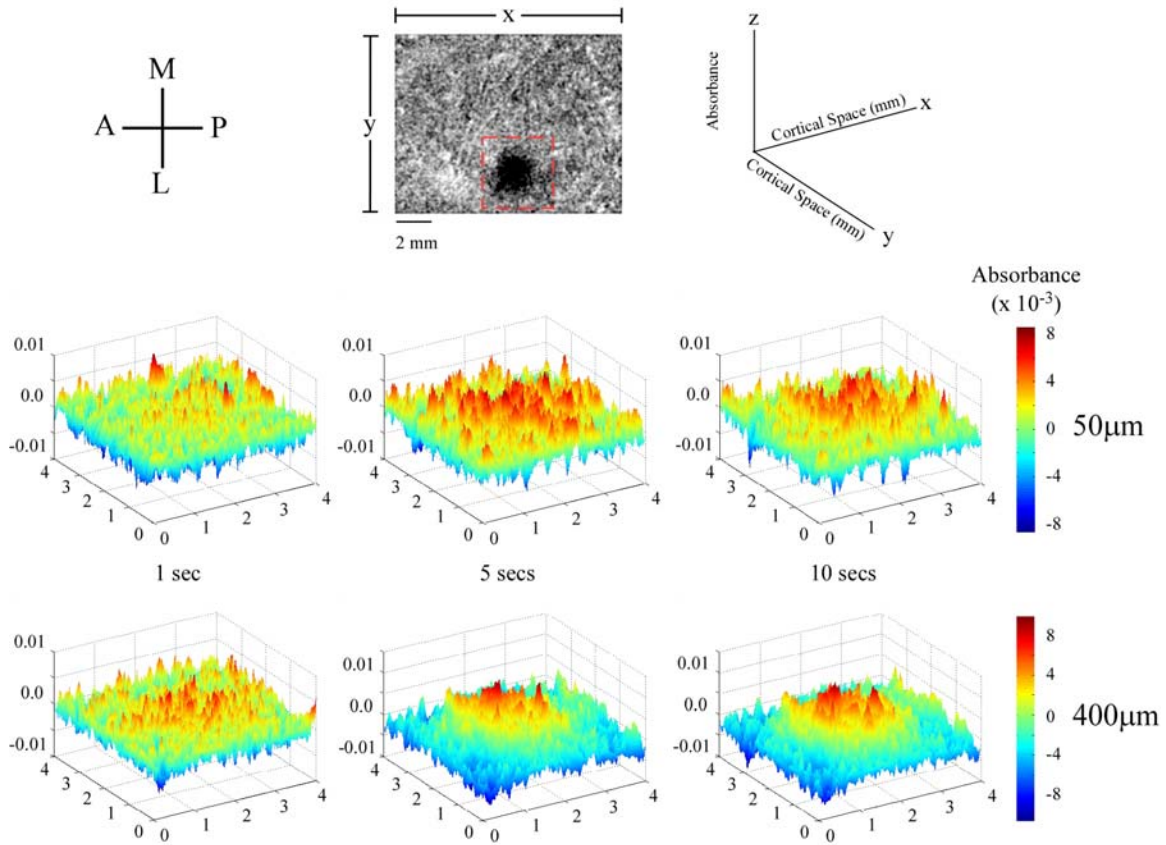


Figure 3.8. Spatial plots of activity evoked by low (50µm) and high (400µm) amplitudes of stimulation. The schematic at the top-left indicates the anatomical orientation of the cortex: A-anterior, M-medial, P-posterior, L-lateral. Absorbances were measured within the voxel shown in the top-middle panel. The schematic (top-right) shows how each frame is spatially represented with respect to the voxel of interest. Both stimulus amplitudes are mapped 1, 5 and 10 seconds after the onset of the stimulus. Absorbance values at each pixel (x,y location) are represented two fold both by their height along the z-axis and by their color. Each stimulus amplitude displays similar dimensions of activated cortical space at each frame. However within the activated area the pattern of activated pixels displays significant dynamics over time as does the activity in the surrounding regions.

high-amplitude surface plots were 0.1415 and 0.1166 respectively. Average standard deviation across all sets of maps (n=5) differs very little from these values (0.1448 at low amplitude vs. 0.1201 at high amplitude). In addition, at 5 and 10s after onset of high-

amplitude (but not low-amplitude) stimulation the territory surrounding the ROI becomes dominated by below-background changes in absorbance.

Discussion

This series of experiments evaluated the global response of contralateral SI cortex to different amplitudes of flutter stimulation by imaging the optical intrinsic signal (OIS). The OIS indirectly reflects both cortical neuronal spike discharge activity and the local, subthreshold changes in neuronal membrane potential evoked by sensory stimulation (MacVicar and Hochman 1991; Holthoff and Witte 1996; Kohn et al. 2000). As a result, the observed tendency for absorbance in the same localized region of area 3b to increase with increasing stimulus amplitude (Figures 3-3 & 3-4) most likely is due to the amplitude-dependence of the average firing rate of neurons in the same region (Whitsel et al. 2003). An increase in SI absorbance in response to an increase in vibrotactile stimulus intensity has been reported previously by Chen et al (Chen et al. 2003). The observed increase in the stimulus-evoked SI OIS that accompanies increases in stimulus amplitude is well described by a linear function.

One important distinction between previous work done using the OIS and the present study is the use of infrared light for illumination during acquisition of the OIS. The OIS obtained using infrared light has been shown to be highly correlated with light scattering effects that accompany astrocyte swelling subsequent to the clearance of extracellular K^+ and neurotransmitter (Holthoff and Witte 1996; Kohn et al. 2000; Lee et al. 2005) and local increases in blood volume (Frostig et al. 1990; Ba et al. 2002). Although the OIS at this wavelength may be influenced by changes in hemoglobin concentration and oxygenation, it is likely that contributions from these factors are minor

compared to the contributions of light scattering effects (Ba et al. 2002). Additionally, OIS imaging using near-infrared illumination not only minimizes the contributions of artifacts introduced by changes in the vasculature (which can dominate the OIS at lower wavelengths) (Frostig et al. 1990), but the time course of the OIS detected at shorter wavelengths (600 nm) is markedly different (shorter) than the protracted OIS observed in this study (Frostig et al. 1990; Kohn et al. 2000; Chen et al. 2003).

Previous studies from our laboratory have reported that the SI optical response evoked by an extended period (>1 sec) of flutter stimulation not only consists of an increase in absorbance in the region that receives its input from the skin site that was stimulated, but also decreases in absorbance (frequently to levels well below-background) that occur in the surrounding cortex (Tommerdahl et al. 2002). The present study demonstrates that the below-background component of the SI optical response to flutter stimulation is particularly evident at large stimulus amplitudes (figures 3-5, 3-7 & 3-8). However, unlike the increase in absorbance evoked by flutter, the relationship between the magnitude of the stimulus-evoked decrease in absorbance and stimulus amplitude is not satisfactorily described by a linear function. Indeed, the results shown in Figure 3.6 suggest that this component of the optical response to skin flutter (the decrease in absorbance) is either absent or extremely small at small stimulus amplitudes, but once stimulus amplitude exceeds an intensity sufficient to evoke it, it then remains maximal or near-maximal even though amplitude is further increased across a wide range of values. Interestingly, the stimulus-evoked decrease in absorbance that occurs in the surround of the SI activation pattern appears later in time than the increases in absorbance (within the

ROI); in addition, as amplitude is increased it tends to develop at a progressively earlier time after stimulus onset.

The correlation maps shown in Figure 3.7 provide a comprehensive overview of the time course of absorbance at each location in the image. The optical signal at each pixel is cross-correlated with a known input signal. In this case, it is the average absorbance measured within the ROI. The assigned coefficient of determination indicates the degree of similarity between a pixel's time course of absorbance and the input signal. Therefore pixels with a large positive correlation undergo increases in absorbance very similar to the input signal, while pixels with a large negative correlation undergo a decrease in absorbance which more closely resembles the opposite (negative) of the input signal. Figure 3.8 suggests that at high amplitudes of stimulation the ROI in SI becomes more homogeneously activated with longer stimulus duration. Some evidence for this is indicated by the large discrepancy (between low- and high-amplitude surface plots) in the standard deviations measured within the ROI. Further studies are required to investigate absorbance distribution and patterning within the ROI.

Examination of spatial histograms (Figure 3.2) and the maps in Figures 3-5 & 3-7 also reveal that the size of the SI region that undergoes an increase in absorbance does not increase with increasing stimulus amplitude, but rather remains relatively constant. Regardless of stimulus amplitude, the activated cortical region appears circular in shape and occupies an area approximately 2mm in diameter. Within the ROI average absorbance increases progressively with increasing stimulus duration. The dimensions of the SI region activated by flutter stimulation observed in this study contrast sharply with results presented in previous studies which demonstrated activation within a 1mm region

in diameter (Shoham and Grinvald 2001; Chen et al. 2003). One possible explanation for this discrepancy is the level and type of general anesthesia used in the different studies. Previous studies have reported that anesthetics (e.g. ketamine) which block NMDA receptors or enhance GABA_A receptor mediated inhibition (barbiturates), significantly reduce the dimensions of the receptive field of individual SI neurons; actions that would reduce the size of the responding SI neuronal population (McKenna et al. 1982). Chen et al. previously reported similar (~2mm) sized regions of activation in response to flutter stimulation of the digit tips in squirrel monkey anesthetized with isoflurane, as well as showing in the same report that use of pentothal anesthetic confined the response to a much smaller (~1mm) region (Chen et al. 2001).

It has been suggested that the amplitude of skin flutter stimulation is coded by both the number of activated SI neurons as well as by their level of spike discharge activity (Johnson 1974). This suggestion is based largely in part on the fact that larger-amplitude stimuli, through transduction of the laterally-transmitted mechanical wave produced by sinusoidal skin displacement, recruit larger numbers of RA afferents and therefore lead to a spatially more widely distributed pattern of afferent input to SI cortex. Combined metabolic tracer and neurophysiological studies have shown that the initial response to a repetitive tactile stimulus occupies an extremely large cortical territory. As the repetitive mechanical stimulation is continued, however, the response is quickly sculpted by cortical inhibitory mechanisms, leading to an activity pattern that becomes confined to a relatively restricted region in SI (Juliano and Whitsel 1987; Whitsel et al. 1989; Tommerdahl and Whitsel 1996a). The results obtained in the present study and results previously reported by other researchers, lead us to suggest that stimulus

amplitude contributes importantly to the shaping (via lateral inhibitory mechanisms) of the SI response to protracted skin flutter.

Conclusions

This study investigated the global response of SI cortex to flutter stimulation of the skin using the OIS. An increase of the amplitude of the flutter stimulus was associated with an increase in absorbance within the region of SI cortex that receives its input from the stimulated skin field. The relationship between the maximal change in absorbance and stimulus amplitude is well characterized by a linear function within the range of amplitudes studied. Measurement of the spatial extent of the activated SI region showed that higher amplitudes of stimulation do not produce a more extensive region of SI activation. Instead, as amplitude is increased, while average peak absorbance within the same ~ 2mm diameter SI region increases with amplitude of stimulation, and at the same time the region of surrounding cortex undergoes a prominent decrease (frequently to levels well below background) in absorbance. Further studies are required to establish the relationship between the effect of different amplitudes of skin flutter stimulation on SI absorbance and SI neuroelectrical activity.

CHAPTER FOUR: The Effects of Bilateral Stimulation

Background

The activity evoked by tactile stimulation of the skin mechanoreceptors projects primarily to thalamocortical neurons in the middle laminae of primary somatosensory cortex (SI) in the contralateral hemisphere. Traditionally, the impact of ipsilateral input on contralateral SI has been trivialized. However, imaging and neurophysiological studies (in monkeys, (Iwamura et al. 2002; Lipton et al. 2006) and in humans, (Allison et al. 1989a; Korvenoja et al. 1995; Nihashi et al. 2005; Hlushchuk and Hari 2006)) described modifications of SI (specifically area 3b) activity in response to input evoked by either mechanical stimulation of an ipsilateral skin site or electrical stimulation of an ipsilateral peripheral nerve.

The concept of SI as a processor of tactile information arising exclusively from the contralateral body surface has coexisted with the idea that fusion of tactile information from contralateral and ipsilateral sites occurs at an early stage of cortical information processing. This chapter characterizes the effects of 25 Hz vibrotactile (“flutter”) stimulation of the ipsilateral thenar eminence on the SI response to an identical stimulus applied to the contralateral thenar eminence. The results suggest that the spatiointensive characteristics of the SI response to contralateral stimulation are significantly modulated by the addition of an ipsilateral input to the skin. Furthermore the results provide insight into the possible mechanisms of the observed response modification to bilateral stimulation.

Methods

Stimulus Protocols

Sinusoidal vertical skin displacement stimulation (25 Hz, 200 μm , stimulus duration 5sec, interstimulus interval 60sec - “skin flutter”) was delivered to the thenar eminence of both forelimbs in squirrel monkeys, and to the central pads of the forelimbs in cats, using two servo-controlled transducers (Cantek Enterprises, Canonsburg, PA). The probe of each stimulator was advanced so that in the absence of stimulation the probe of each stimulator delivered a static indentation (500 μm) to the skin. Skin contact was detected and signaled by the force transducer and readout circuitry of each servo-controller. The flutter stimuli were delivered (1) independently to each member of a pair of mirror-symmetric ipsilateral and contralateral skin sites, and (2) simultaneously to the two sites (bilateral stimulation). Contralateral, bilateral, and ipsilateral stimuli were interleaved on a trial by trial basis. The sinusoidal contralateral and ipsilateral components of each bilateral flutter stimulus always were in-phase and synchronized so that the two stimuli started and stopped at the same time.

Cluster Analysis

Cluster plots were generated by considering the maximally responding (top 10%) pixels in response to contralateral and ipsilateral stimulation as two separate samples. In each plot the activity of a single pixel is plotted as a function of its (normalized) evoked absorbance by ipsilateral stimulation (x-axis) and contralateral stimulation (y-axis). Thus, pixels which respond equally strongly to stimulation of either hand will be located along the diagonal, while pixels which display a differentially stronger response to stimulation of one hand or the other will be located closer to the appropriate axis. Cluster

analysis was used in Figure 4.7 to demonstrate the relative preference of anterior or posterior SII to stimulation of the ipsilateral or contralateral stimulation respectively.

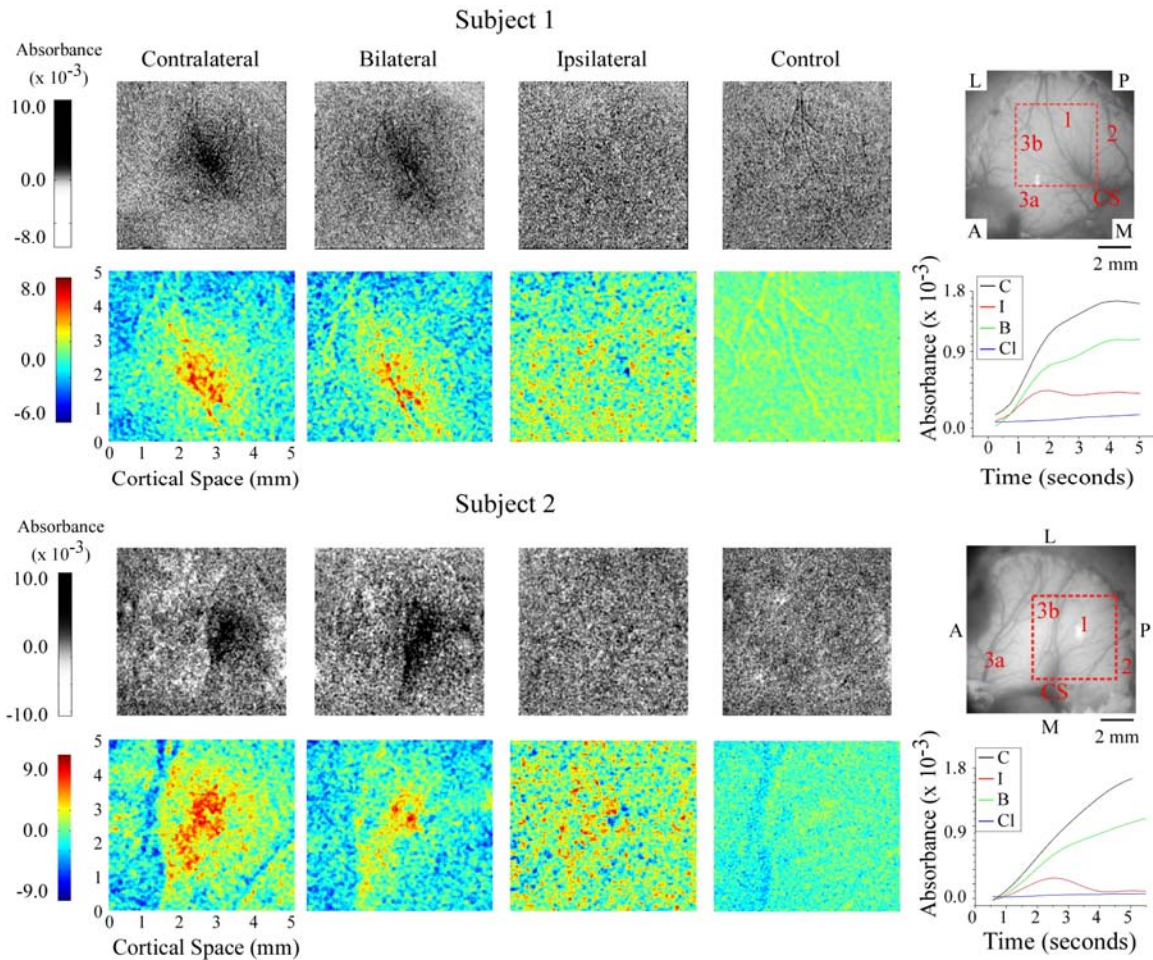
Results

Squirrel Monkey SI

The response of SI in the right hemisphere to vibrotactile stimulation of the thenar eminence on each hand was studied in 5 squirrel monkeys. The goal in each experiment/subject was to assess the influence, if any, of ipsilateral stimulation on the response evoked from the mirror-symmetric contralateral skin site.

The patterns of absorbance change recorded in the hand representational region of SI in 2 of the 5 subjects are shown in Figure 4.1. The grayscale average difference images in the top and 3rd rows of Figure 4.1 show not only the response of the SI hand region to each of the three conditions of skin flutter stimulation (i.e., “contralateral, bilateral, ipsilateral”), but also the spatiointensive pattern of absorbance values recorded in the no-stimulus controls in the same SI region. Visual inspection of these grayscale images reveal that in both exemplary subjects (1) the magnitude of the response to contralateral flutter greatly exceeds the response to flutter stimulation of the mirror-symmetric ipsilateral skin site alone, whereas (2) although differences between the responses to contralateral vs. bilateral skin flutter can be discerned, they are relatively slight.

Color maps of the responding region within each average difference image (ROI; the 5 x 5 mm region centered on the maximal response evoked by the contralateral stimulus – outlined in red in the image of the cortical surface shown at right of the top and 3rd rows in Figure 4.1) demonstrate more clearly the differences between the responses of SI of each subject to the 3 conditions of skin flutter stimulation. First,



bilateral stimulation evokes a weaker and spatially less extensive response than that evoked by contralateral skin flutter. Second, although the response to ipsilateral flutter is

Figure 4.1. OIS response evoked by flutter stimulation of the thenar pad in two subjects. 1^{st} & 3^{rd} Row: Average difference images evoked by contralateral, bilateral, and ipsilateral stimuli and the no-stimulus control condition. All images within a subject group are oriented as indicated in the green filter image at the right; P (posterior), A (anterior), M (medial) and L (lateral). 2^{nd} & 4^{th} row: Magnified view of selected ROI (identified in image at far right of 1^{st} & 3^{rd} row) from difference images for each subject. Absorbance time courses are plotted and color-coded for each stimulus condition at far right; time courses were calculated within a 2 x 2mm area centered on the maximally responding region.

located in the same SI region that responds to contralateral flutter, the spatial distribution

of absorbance values evoked by the ipsilateral stimulus is distinctly different from the responses (i) evoked by stimulation of the contralateral site and (ii) obtained in the absence of stimulation (the no-stimulus condition) – i.e., in each subject ipsilateral flutter evoked a unique and spatially inhomogeneous pattern of absorbance values within the ROI. For both subjects shown in Figure 4.1 the average across-ROI increase in absorbance evoked by ipsilateral flutter is substantially smaller than that evoked by contralateral flutter, although it is also evident that at numerous loci within the ROI the absorbance values attained during ipsilateral skin flutter exceed by far the values measured at the same locations in the absence of stimulation.

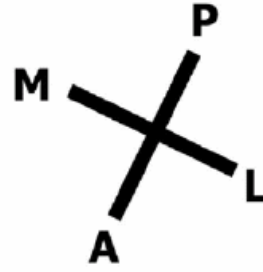
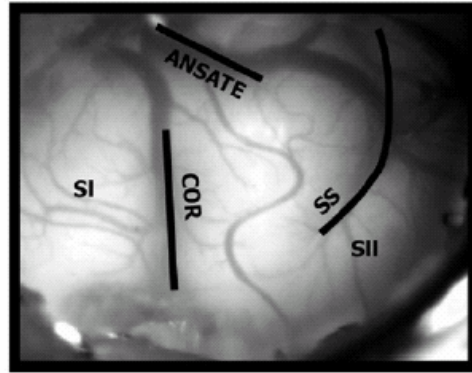
The plots of absorbance time course shown at the right of Figure 4.1 (2nd and 4th rows from top) show absorbance values at successive time intervals averaged within the 4mm² region that responded maximally to contralateral stimulation; see Simons et al., 2005 for methodological details). Such plots quantitatively confirm the impression (gained from visual inspection of the grayscale difference images) that the response in SI of each subject to bilateral skin flutter was substantially weaker than the response to contralateral flutter. In addition, the plots demonstrate that the SI responses (absorbance increases) to contralateral vs. bilateral skin flutter follow a very similar time course.

Cat SI

Similar results were found in the cat which offers the unique advantage of allowing simultaneous imaging of SI and SII (second somatosensory cortex). The responses to contralateral only, ipsilateral only and bilateral stimulation are shown in Figure 4.2. Also shown is an image of the exposed cortex used for anatomical orientation and to demonstrate locations of SI and SII using known anatomical markers. The

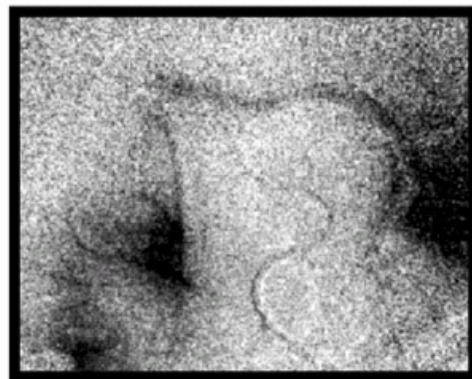
difference images in panels B-D indicate that although a response is evoked in SI during contralateral only and bilateral stimulation, no response is visible in SI during ipsilateral only stimulation. However, the exposed region of SII displays activity in response to all three stimulus conditions.

A



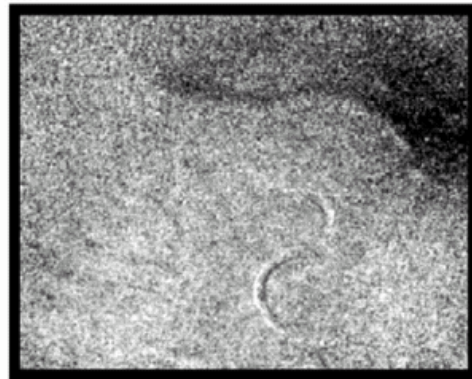
2 mm

B



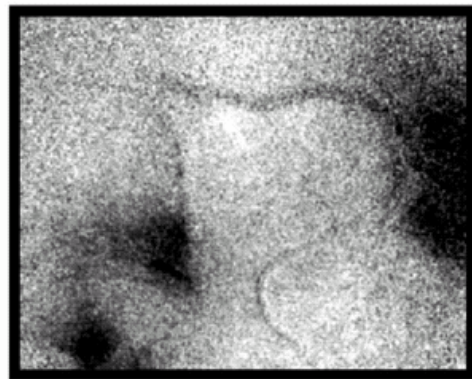
Contralateral
25 Hz

C



Ipsilateral
25 Hz

D



Bilateral
25 Hz

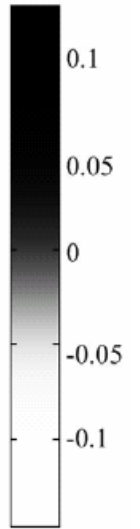


Figure 4.2. Optical responses recorded in cat SI and SII to 25 Hz vibrotactile stimulation of the forepaws. **A)** View of the cortical surface, showing the vascular pattern and coronal (COR), ansate (ANS), and suprasylvian (SS) sulci. Exposed regions of SI and SII are labeled. *Below:* Averaged absorbance images for responses evoked by **B)** contralateral, **C)** ipsilateral and **D)** bilateral stimuli. Difference images were generated by subtracting a single pre-stimulus (reference) image from each corresponding post-stimulus image and subsequently dividing by the reference image ($\Delta A/A$). Stimulus locations are indicated by figurines. Scale bar is 2 mm. Orientation of images indicated by P (posterior), A (anterior), M (medial) and L (lateral) axes.

Figure 4.3 compares the stimulus evoked response of SI to contralateral vs. bilateral stimulation at 5 seconds after stimulus onset. The top left panel indicates the orientation and location of the sampled region of interest (ROI) in SI. Also visible is the SII response located posterior and lateral relative to the maximally responding region in SI. The surface plots show the absorbance values at each location in the imaged field (absorbance values are indicated both by height along the z-axis and by color). Consistent with the results observed in SI of squirrel monkey, the response evoked by ipsilateral stimulation is near-background (or nonexistent), whereas the responses to contralateral and bilateral stimulation are localized and robust. Close visual inspection of these surface plots also reveals that the magnitude of the SI response evoked by contralateral stimulation is greater than the response evoked by bilateral stimulation.

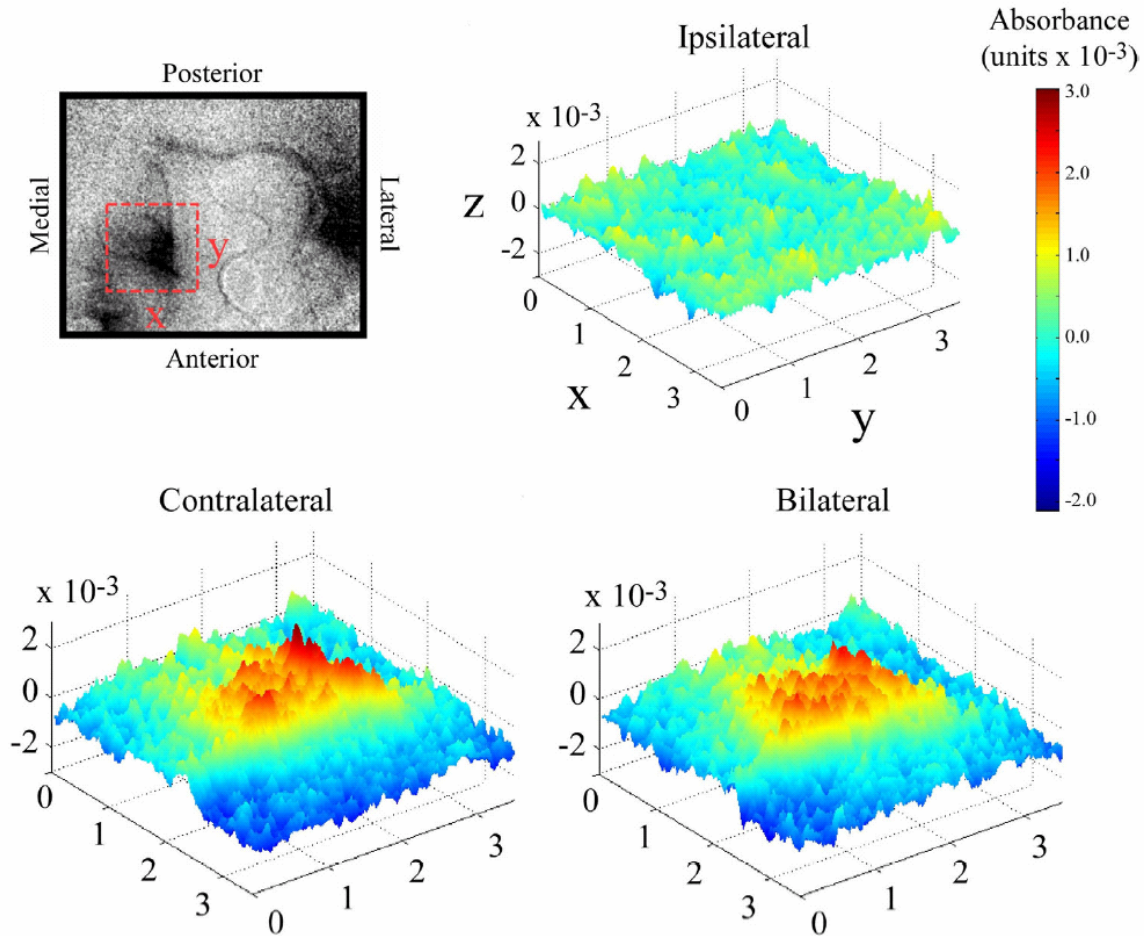


Figure 4.3. Surface plots of absorbance evoked in SI by contralateral, ipsilateral, and bilateral stimulation. Data displayed is a subset of the data displayed in Figure 1. Region of interest is indicated by the dashed box shown in the OIS image (top left). Orientation of the ROI is indicated by X (medial-lateral) and Y (anterior-posterior) labels on the dashed box and axes (in ipsilateral map). Cortical space along X and Y axes is measured in mm. Z axis is absorbance which is represented by both the height of the graphic as well as the color indicated by the color bar to the right. Surface plots represent absorbance values within the ROI at 5 seconds after stimulus onset and demonstrate that the 1) response in SI to ipsilateral stimulation is small or nonexistent and, 2) magnitude of evoked absorbance in response to contralateral stimulation is slightly larger than the response evoked by bilateral stimulation.

Figure 4.4 displays the time course of the absorbance change in two subjects within the ROI

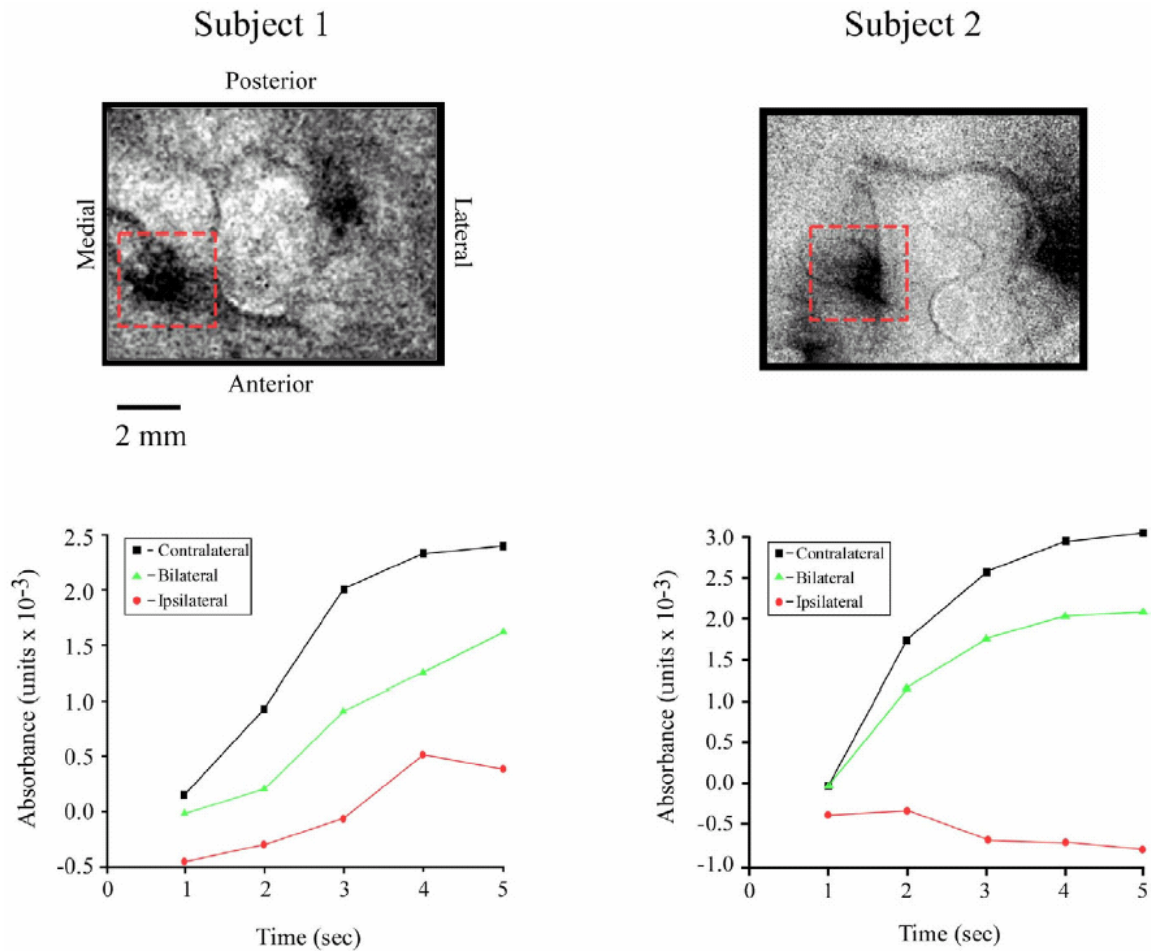


Figure 4.4. Time course of the absorbance change within the region of interest (ROI) in SI. *Top:* Dashed box on difference images indicates dimensions and orientation of ROI in SI used for analysis. Orientation and scales are identical in both subjects. Stimulus duration was 5 seconds; stimulus onset was at time 0 s. *Bottom:* Absorbance values within the ROI were averaged and plotted as a function of time for each stimulus condition. In both subjects contralateral stimulation evokes the largest change in absorbance, while ipsilateral stimulation evokes only a weak change in absorbance. Bilateral stimulation evokes an absorbance change that is less than that evoked by a contralateral stimulus.

in SI to the three stimulus conditions. As in the squirrel monkey the largest increase in absorbance is evoked by the contralateral only stimulus, while bilateral stimulation evokes a somewhat smaller absorbance increase. No reliable increase in absorbance was observable within the ROI in response to stimulation of the ipsilateral skin site alone.

Comparison of the averaged normalized absorbance values at 5 seconds (post-stimulus) for each condition is shown in Figure 4.5. The data indicate that the bilateral response is on average 28% smaller than the contralateral only response ($p < 0.01$). The fact that a response is observed in SII in response to all three stimulus conditions is interesting and may play a role in the response reduction that occurs during bilateral stimulation.

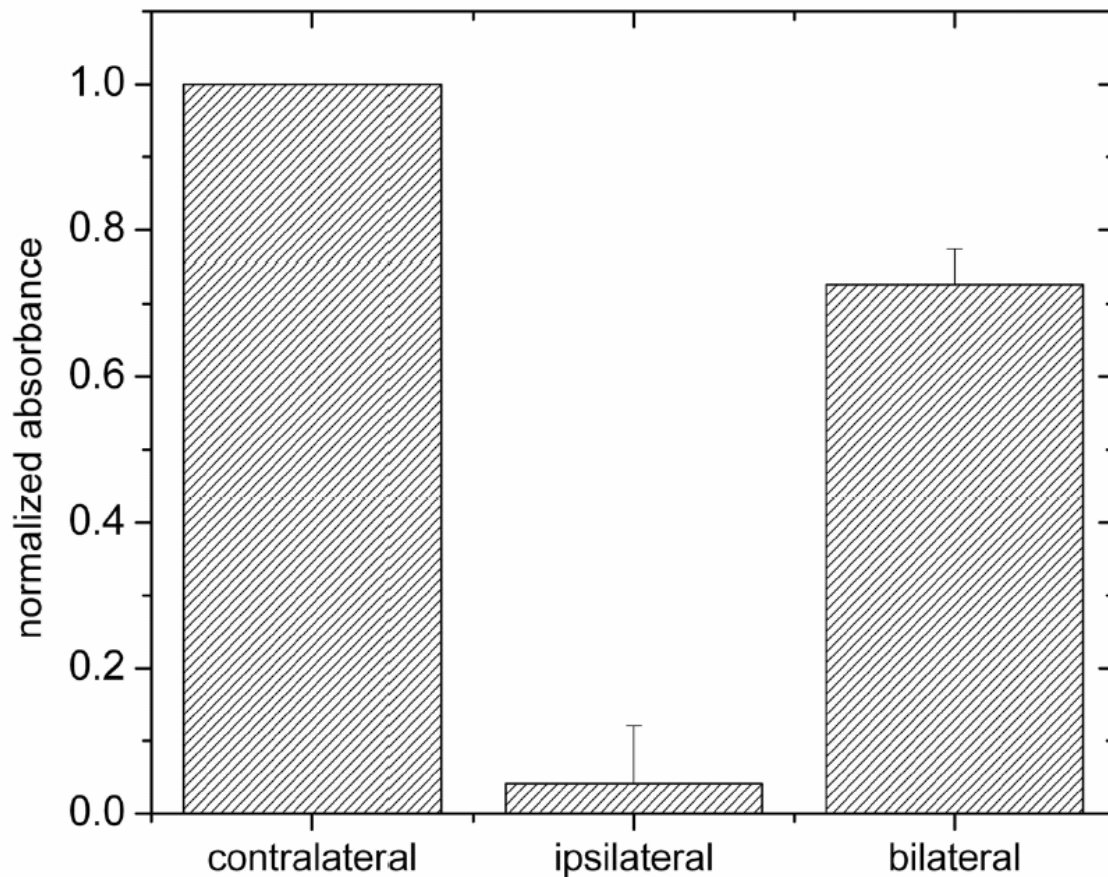


Figure 4.5. Comparison of averaged normalized absorbance values ($n = 5$) evoked under 3 different stimulus conditions. Peak absorbance values were normalized to those obtained from the contralateral stimulus condition (thus, standard error bar for the contralateral condition is zero) and were obtained at 5 sec after stimulus onset of a 5 sec flutter stimulus. The contralateral stimulus consistently evoked the greatest change in absorbance, while the ipsilateral stimulus evoked the weakest. The response evoked by bilateral stimulation was always less than the response evoked by the contralateral stimulus. One way ANOVA revealed that the ratio of the bilateral response evoked to the contralateral response evoked in SI was between 0.51 and 0.92 (99% confidence interval).

Cat SII

Figure 4.6 shows the OIS responses evoked in SII of two exemplary subjects by contralateral, ipsilateral, and bilateral central pad stimulation. Visual inspection of the images for the three stimulus conditions in each subject shows that: (1) the optical response to contralateral stimulation occurs in a region more posterior in SII than does the response to ipsilateral stimulation; (2) the SII optical response to bilateral stimulation occupies both the anterior and posterior regions that responded to independent stimulation of the contralateral and ipsilateral central pads; and (3) the optical response to ipsilateral stimulation does not evoke a large absorbance change in SI.

To directly compare the time course of the response of the anterior and posterior regions of SII to the three stimulus conditions, we determined the time course of the absorbance changes in each region under each stimulus condition (Figure 4.7). The plots in Figure 4.7 show that in each subject and under each stimulus condition, the magnitude of the absorbance change evoked in either the posterior or anterior region of SII by ipsilateral stimulation was less than that evoked in the same region by contralateral or bilateral stimulation. Moreover, in both subjects, the magnitude of the response of the

posterior region to bilateral stimulation was greater than that evoked by contralateral

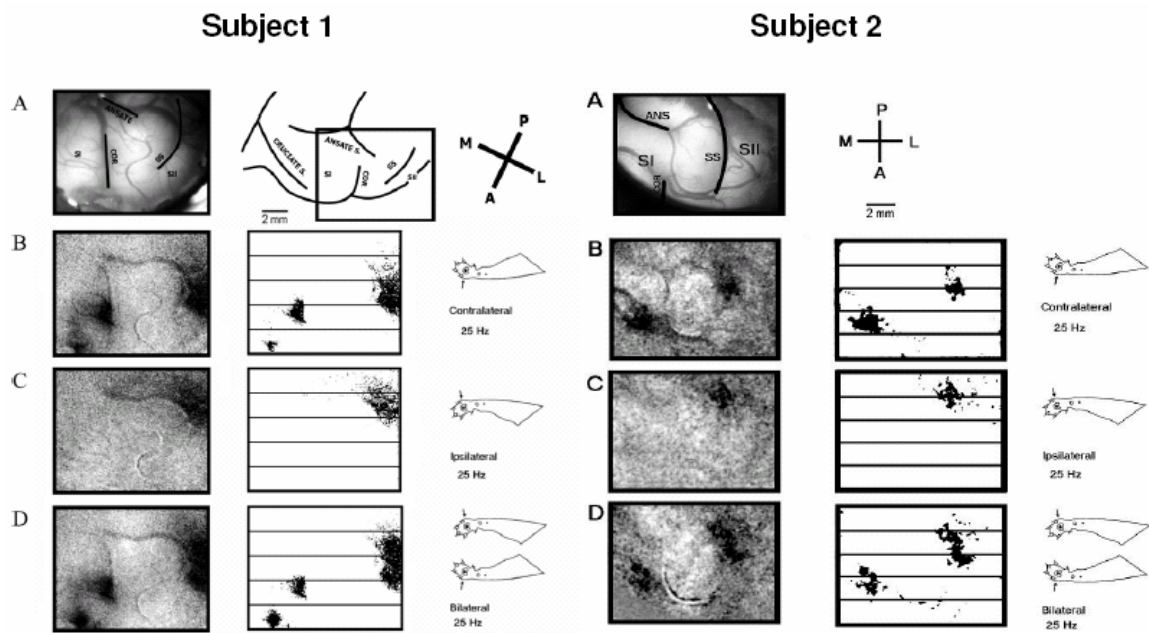


Figure 4.6. Optical responses in cat SI and SII to 25 Hz vibrotactile stimulation of the central pad in 2 subjects. **A.** View of the cortical surface, showing the vascular pattern and coronal (COR), ansate (ANS), and suprasylvian (SS) sulci. Exposed portions of SI and SII are labeled. *Left column of Subject 1&2:* Averaged difference images for responses evoked by **(B)** contralateral, **(C)** ipsilateral and **(D)** bilateral stimuli. *Right column of Subject 1&2:* Thresholded images of responses evoked by each mode of stimulation. Horizontal grid lines facilitate comparison of the position of loci of the evoked responses and are spaced 2 mm apart. Stimulus locations are indicated by figurines. Note that in both subjects, ipsilateral stimulation evokes a response posterior to the response evoked by contralateral stimulation. Scale bar is 2 mm. Orientation of images indicated by P (posterior), A (anterior), M (medial) and L (lateral) axes.

stimulation, whereas in the anterior region of SII, the magnitude of the response evoked by bilateral stimulation is either less than or approximately equal to the response evoked by contralateral stimulation.

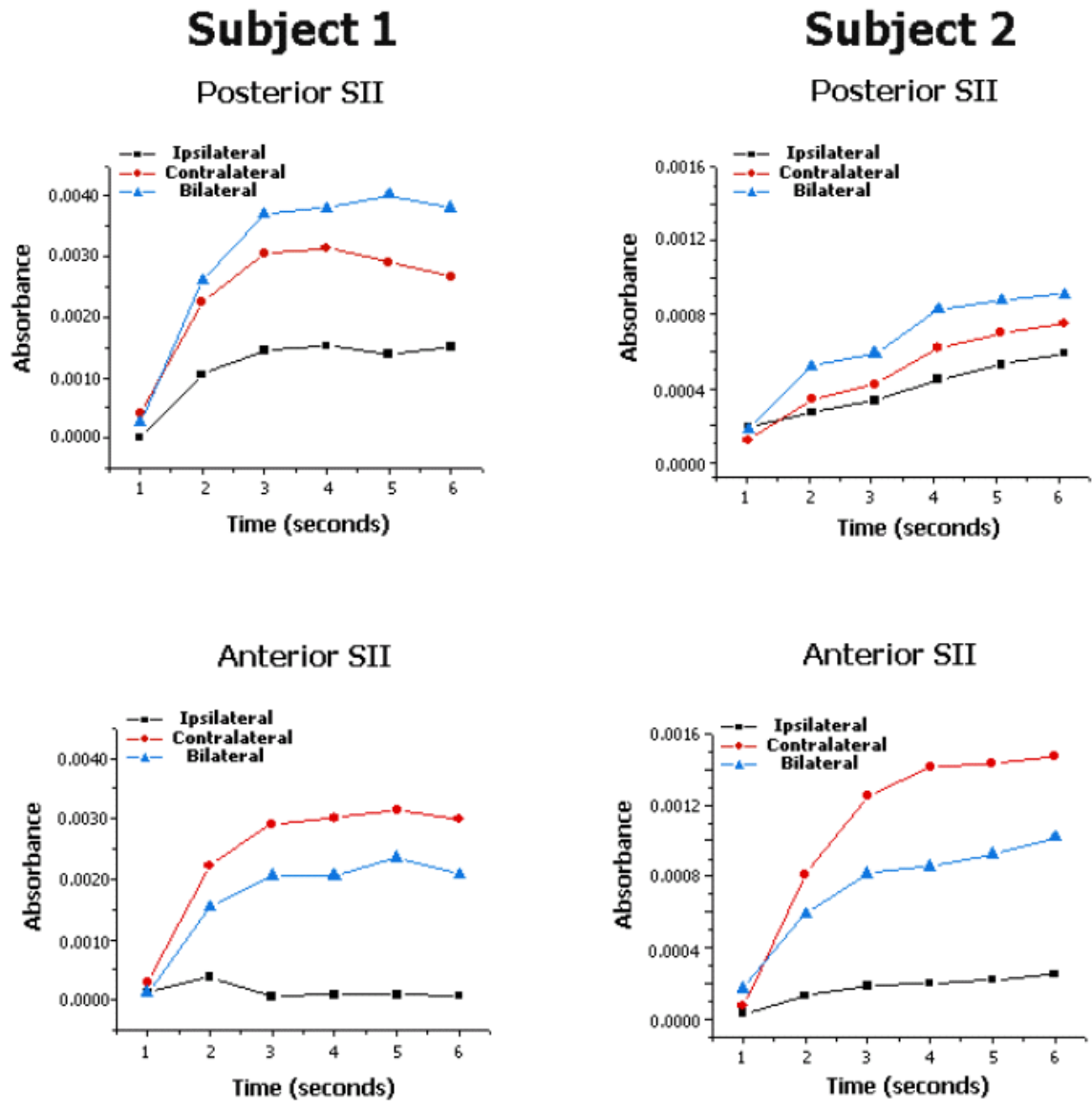
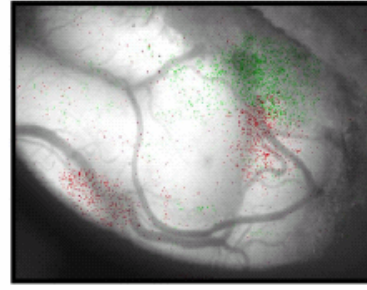
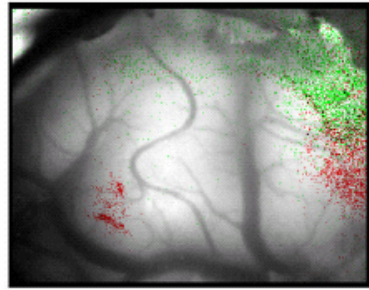


Figure 4.7. Time course of the absorbance change in the anterior and posterior SII cortical regions evoked by flutter stimulation of the central pad in 2 subjects. (A) *Top Panels:* Time course of absorbance values from the posterior SII region obtained with ipsilateral, contralateral, and bilateral stimulation. (B) *Bottom Panels:* Time course obtained from the anterior SII region during ipsilateral, contralateral, and bilateral stimulation.

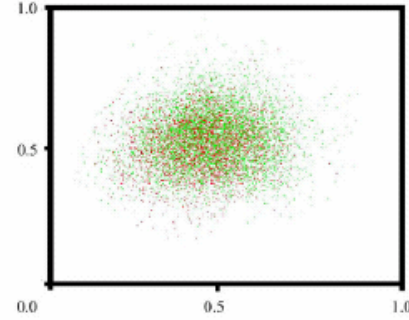
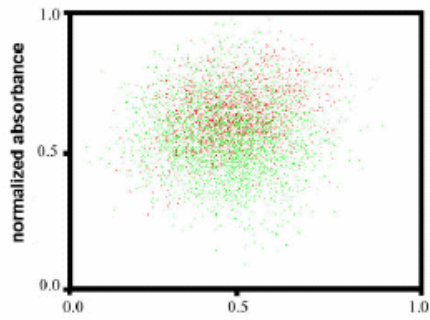
Cluster analysis was used to directly compare the response of SII to the different conditions of ipsilateral and contralateral stimulation. The results of cluster analysis are

Subject 1

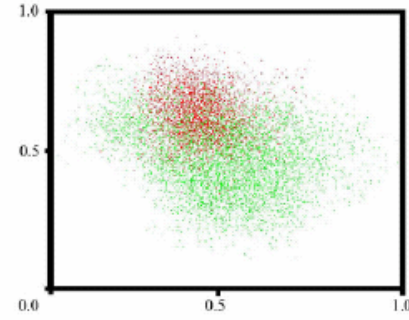
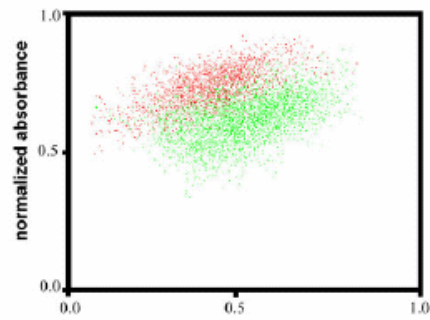
Subject 2



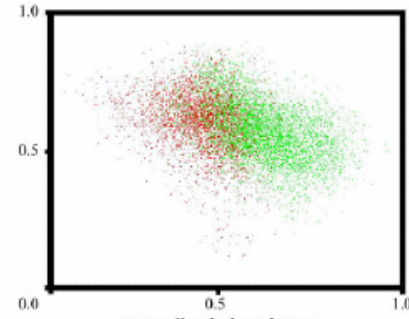
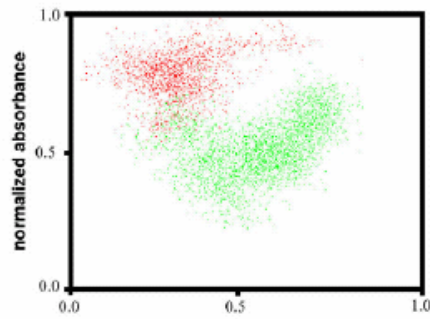
contralateral response



t = 1 sec



t = 2 sec



t = 5 sec

normalized absorbance

normalized absorbance

ipsilateral response

Figure 4.8. Cluster plots of ipsilateral vs. contralateral response of 2 subjects. For each cluster plot, values of individual pixels are plotted as a function of the response measured at that pixel to the ipsilateral stimulus (horizontal axis) vs. the response measured at that locus evoked by the contralateral stimulus (vertical axis). Colors depict the pixels that maximally responded to ipsilateral (green) and contralateral (red) stimulation. Cluster separation follows the same trend as the time course shown in Figure 4.7. After 5 seconds, the activity of the responding population has diverged into two distinct clusters. Reference images at top are at same orientation as the reference images in Figure 4.6.

shown in Figure 4.8. Two sets of pixels were chosen and depending on whether they were maximally activated (top 10%) by i) contralateral or ii) ipsilateral stimulation. The two samples were plotted together (but remain visibly distinguishable based on color; red – contralateral, green - ipsilateral) and each pixel was plotted as a function of its evoked absorbance to ipsilateral stimulation and contralateral stimulation. The clusters reveal a distinct differentiation in the population of SII neurons to the different stimulus conditions. Furthermore, it appears that this could be a time dependent process, as there is little difference in the behavior of the pixels localized to the SII region in the early stages of the response ($t=1$ sec); separation in the two populations becomes more evident after 2 seconds, and there are two distinct clusters formed 5 seconds after stimulus onset. It should be emphasized that this type of analysis does not necessarily reflect spatial differences in the responses of two different stimulus conditions, but rather, it reveals whether or not different members of a set respond differently to different stimulus conditions.

Discussion

Much of the current literature reflects the long-held idea that mechanical stimulation of the skin of the hand has either no, or a negligible, influence on neurons in

areas 3b and 1 of the SI hand representational region in the ipsilateral hemisphere. The findings reported in this study are incompatible with the widely accepted idea that areas 3b and 1 in the SI hand region are insensitive to mechanical events on the ipsilateral hand. First, they provide unambiguous evidence that a skin flutter stimulus to an ipsilateral skin site evokes a statistically significant optical response (absorbance increase) within the same SI territory that in prior combined OIS-neurophysiological studies (Shoham and Grinvald 2001; Whitsel et al. 2001; Tommerdahl et al. 2002; Whitsel et al. 2003) was shown to undergo increased single neuron spike discharge activity in response to flutter stimulation of the contralateral hand. Second, our experiments demonstrate that simultaneous bilateral stimulation of both the ipsilateral and contralateral hand sites evokes an SI response significantly smaller and spatially less coherent than the response evoked in the same SI region by stimulation of only a site on the contralateral hand – a finding that strongly suggests that input from the ipsilateral hand can modify the ability of SI to process information about the status of mechanoreceptors in the skin of the contralateral hand.

The above-described modulatory effect of ipsilateral input on the SI response to stimulation of the contralateral hand, together with (1) reports by others of neurons with ipsilateral receptive fields in SI of non-human primates (see (Iwamura et al. 2002) for review), (2) demonstrations of short-latency activation of human SI in response to electrical stimulation of the ipsilateral median nerve (Allison et al. 1989a; Allison et al. 1989b; Allison et al. 1992; Korvenoja et al. 1995; Nihashi et al. 2005), and (3) the recent discovery that unilaterally applied flutter stimulation of the hand evokes short-latency neuromagnetic activity in both the contralateral and ipsilateral SI of conscious humans

(Tan et al. 2004) demonstrates not only that the SI hand representational region receives substantial ipsilateral input but, in addition, shows that ipsilateral input evoked by gentle mechanical skin stimulation can alter the SI response to contralateral flutter stimulation.

Insofar as the perceptual meaning of our finding that ipsilateral input alters the SI hand region's optical response to skin flutter is concerned, observations reported in published human psychophysical studies are highly suggestive – those observations clearly indicate that input from a skin region on one hand can significantly alter one's perception of a tactile stimulus to the opposite hand. Importantly, while some of the published psychophysical findings indicate that concurrent input from mirror-symmetric sites on the two hands can enhance tactile perceptual performance above that obtained with unilateral stimulation, other studies indicate that tactile input from the two hands can lead to perceptual performance inferior to that observed when the stimulus is applied unilaterally. As examples of the former, (i) Lappin and Foulke (1973) observed that when a subject scans the pattern using two fingers on opposite hands, braille cell perception improves over that achieved unilaterally; (ii) Craig (Craig 1985) reported that a subject's ability to correctly identify a split tactile pattern (dot array) is substantially greater when the two halves of the pattern are presented simultaneously to two fingers on opposite hands (relative to the performance achieved when the two halves are delivered to two fingers - neighboring or non-neighboring - on the same hand); and (iii) Essick and Whitsel found that human subjects' accuracy of perceived direction of tactile motion on the hands improves greatly over that obtained with unilateral stimulation when the bilateral stimuli (the sites on the 2 hands were mirror-symmetric) move across the 2 sites at the same time, in the same direction, and at the same velocity. Essick and Whitsel also

reported that whenever the physical properties of the brushing stimulus applied to one hand differed in some way (e.g., in direction, velocity, relative timing) from those of the stimulus to the opposite hand, the subject's ability to accurately report direction of bilaterally applied stimulus motion declined, often reaching performance levels well below those achieved when each moving stimulus was applied unilaterally (Essick and Whitsel 1988). Furthermore, a recent human psychophysical study found that vibrotactile stimulation of an unattended hand reduces tactile spatial acuity (as measured using a 2-point discrimination paradigm) on the attended hand by as much as 35% (Tannan et al. 2005b). That same study also found that two-point discrimination improves substantially when a small-amplitude high-frequency vibration is superimposed on both of the probes used to present the two-point stimulus, but worsens during the delivery of high-frequency stimulation of the mirror-symmetric site on the opposite hand. Taken together, these observations strongly suggest that multiple factors (e.g., positional, temporal, and modal correspondence between the two stimuli) may determine the sign and magnitude of the influence of input from one hand on how a stimulus to the other hand is perceived.

How does input that arises in the mechanoreceptors of the skin of the ipsilateral hand access the SI hand region? While the available evidence does not enable this question to be answered definitively, the observations obtained in multiple neuroanatomical tracing studies (for review see Jones 1986) make it clear that the modulatory influence exerted on the SI hand representational region evoked by stimulation of the ipsilateral hand is not mediated directly via interhemispheric connections that cross the midline in the corpus callosum. Indeed, the fact that a distinguishing feature of the SI hand area is its *lack* of direct interhemispheric

connections forces the conclusion that the modulatory influence on SI of ipsilateral hand stimulation detected in the present study is mediated by a 2-stage path: a route that initially involves the extensive interhemispheric (callosal) connections that directly link higher-level (integrative) areas in the two hemispheres, and subsequently involves intrahemispheric connections from those higher-level areas to the SI hand region in the same hemisphere. The studies described earlier in this chapter which used cats as subjects, made simultaneous observations of activity evoked in SI and SII under conditions of ipsilateral, contralateral, and bilateral mechanical skin stimulation very similar to those reported in this paper (Tommerdahl et al. 2005b; Tommerdahl et al. 2005d). The data obtained in that study indicated that while different regions of SII were activated under the different conditions of stimulation, there was significant correlation (both positive and negative) between the stimulus-evoked activities in SII and SI, and the sign of the correlation was stimulus-dependent. Thus, there is indirect evidence that SII, which receives extensive interhemispheric projections, may be the source of the modulatory influence that is exerted on SI during stimulation of the ipsilateral hand.

The evidence presented in this chapter leads us to suggest that although the distal limb regions of SI are relatively acallosal, this should not (as is frequently done) be interpreted to indicate that these SI regions are free of influences arising from the ipsilateral body. The extraordinary ability of primates to use the two hands cooperatively to explore and discriminate the features of tactile objects shows not only that fusion of sensory input from both hands occurs within the CNS, but that it underlies essential behaviors. With this in mind, the absence of direct callosal connections should not be viewed to indicate that SI does not receive significant influences from the ipsilateral

body. Instead, absence of callosal connections in the distal limb regions of SI may be a reflection of (1) the extraordinary flexibility/mobility of the primate hands (i.e., the ability to substantially alter the positional relationships between distal forelimb skin regions in the accomplishment of tactile object exploration and feature extraction – in contrast, the positional relationship between skin regions on opposite sides of the midline at the level of the proximal limbs/trunk is relatively fixed), and (2) the need for the participation of higher-level cortical areas in fusing the elaborate time-, position-, and modality-dependent somatosensory experiences gained via bimanual tactile exploration.

CHAPTER FIVE: SI Response to Changes in Stimulus Duration

Background

In a previous chapter, we reported that varying the amplitude of a 25 Hz vibrotactile (“flutter”) stimulus on the forelimb of the skin did not significantly alter the spatial extent of the responding population in SI (Simons et al. 2005). Rather, at all amplitudes, the dimensions of the cortical response were spatially constrained and were surrounded by a region of decreased absorbance. It was suggested that these regions of decreased absorbance were attributed to stimulus-evoked surround inhibition that originated from stimulus-dependent activity in SI. Although the stimulus-evoked above-background activity increased with increasing stimulus amplitudes, the below-background activity observed in the surround did *not* change concurrently with stimulus amplitude. These results led us to conclude that a feature of the stimulus other than amplitude could play a more prominent role in the establishment of the below-background surround field. Based on previous studies in which we made observations of the differences in response to short vs. long stimuli, we postulated that one determinant of the spatially restricted SI response to vibrotactile stimuli was the dependency of the inhibitory surround on the duration of the stimulus.

Comparison of 2DG experiments and receptive field mapping experiments gave the first evidence of a time-dependent process involved in the formation of somatosensory cortical activity patterns (Whitsel and Juliano 1984; Juliano and Whitsel

1987; Tommerdahl 1989). Discrepancies in the results of these experiments conducted with contrasting methodologies led to the investigation into the response of SI cortex to repetitive stimulation, and the possible role that cortical dynamics played in SI pattern formation. These studies (Diamond et al. 1986; Whitsel and Kelly 1988; Whitsel et al. 1989) revealed that the initial cortical response to a tactile stimulus is not the selective activation of a relatively few, highly tuned neurons, but rather a complex spatio-intensive pattern of activity involving very large numbers of neurons. With repetitive stimulation, this extensive and less differentiated initial activity pattern becomes rapidly sculpted by a dynamic cortical inhibitory mechanism into a more stimulus-specific spatiotemporal pattern. Thus, in a time-dependent manner, the somatosensory cortex appears to generate a unique and statistically reliable response (a spatiointensive activity pattern) out of the activity of extremely large numbers of broadly-tuned, individually unreliable elements.

The goal of this study was to characterize the SI response evoked by different durations of vibrotactile stimulation in order to test the hypothesis that stimulus duration plays a prominent role in the funneling of the spatiointensive pattern of response. The results reported in this paper demonstrate that brief (0.5sec) stimulus durations do not evoke regions of decreased cortical absorbance which are observed in the surround in response to longer duration stimuli (1-5 sec). Regions of decreased absorbance were previously described as contributing to the improvements in spatial contrast of the cortical activity patterns evoked by increasing stimulus amplitudes.

Methods

Stimulus Protocol

Stimulus protocols were delivered in blocks of 100 trials (typically 20 trials per stimulus condition). All flutter stimuli (25 Hz) were 200 μ m and were delivered to the glabrous skin of the contralateral forelimb with a vertical displacement stimulator (Cortical Metrics; Chapel Hill, NC). Four stimulus durations were tested (0.5, 1.0, 2.0, and 5.0s) and interleaved with an intertrial interval of 60s. A no-stimulus control condition was also interleaved with experimental test conditions.

Response Recovery

Due to the technical demands encountered in the acquisition and analysis of imaging data there are inevitably tradeoffs between temporal and spatial resolution. The focus of this report was the spatial sharpening of the response and we thus opted to maximize spatial resolution over a shorter (10 second) interval which maximized the temporal resolution immediately before and after stimulus delivery. As such, recovery back to pre-stimulus levels was not observed for responses to five second stimuli. Cannestra et al. reported that optical responses to 3.5 & 10 second stimuli show intervals of reduced responsivity of 7.0 & 8.0 seconds respectively which could be attributable to incomplete recovery (Cannestra et al.). It is worth noting that while the absolute time necessary for recovery to five second stimulation is not observable in the time course plots presented here that all responses were recovered to pre-stimulus levels within the 60 second ISI used between stimuli which is evidenced by the consistent lack of response observed in the no-stimulus control trials.

Determination of ROI

Stimulation of a discrete skin site evokes increases in neuronal activity and thus increases in the measured optical signal in regions of varying size and dimensions

depending on the stimulated skin site. The region of cortical territory which displays an evoked increase in the OIS in response to a given stimulus in this report is called the region of interest (ROI). The ROI was defined for each stimulus location using the following procedure. Evoked responses to five second stimulation were summed over the duration of the stimulus. The maximally responding region was segmented along its anterior/posterior axis and absorbance was measured in $40 \times 200 \mu\text{m}$ bins along the line. Segmentation through the maximally responding region typically reveals a Gaussian-like distribution of absorbance values, which steadily decrease (usually to below baseline values) as distance from the maximal response is increased. Borders of the ROI were defined by the edges of regions of increased absorbance which in the case of thenar stimulation is consistently characterized by a circular region of ~ 2 mm diameter as indicated by the dashed circle in Figure 5.2.

Correlational Methodology

Correlation maps are typically used to characterize the spatiotemporal properties of the OIS response. Maps were constructed by choosing a reference region within the imaged field and computing the intensity correlation r_{ij} between the slope of the (average) absorbance time course in a 4×4 pixel moving window at location (i, j) and the slope of the time course within a reference region over the interval between stimulus onset and the time of peak response. The region selected as the reference was defined by a boxel ($\pi \text{ mm}^2$ area) centered on the region of interest (ROI). Each pixel (i, j) on the correlation map is represented by a correlation coefficient r_{ij} ($-1 < r < 1$). Since the slope of the response within the ROI (used for correlation) is strongly positive, positive coefficients

indicate locations where absorbance increases during this interval, while negative coefficients indicate likely locations of decreased absorbance.

Radial Histograms

Radial histograms were generated (results shown in Figure 5.5) by averaging absorbance values of all pixels lying at an equal radial distance from the maximally responding center. All equidistant pixels were averaged over one second of the maximal response (as determined by time course within the ROI), independently for each duration. Prior to averaging across subjects, plots were normalized according to peak absorbance. Error bars represent the across subjects standard deviation after normalization. Every fifth error bar is shown.

Surround Anisotropy Plots (SAPs)

Surround anisotropy plots (Figure 5.6) were generated by measuring the average absorbance in ten degree (36 total measurements) segments within a ring located between 1.5 and 2.5 mm outside of the center of the ROI over the one second interval during which the response was maximal. The region used to obtain an estimate of absorbance in the surround was identified as the territory of greatest below-background activity in radial histograms. Absorbance values were represented with vectors indicating both the intensity (vector length), and the location of the evoked absorbance. All vector lengths were normalized to the maximum vector length for the 5.0 second stimulus condition. Note that since vectors are normalized to the largest decrease in absorbance (negative values), vectors that are negative indicate an increase in absorbance. The longest vectors within a plot thus indicate locations of strongest suppression (decreased absorbance).

Results

Figure 5.1 shows the OIS difference images evoked in SI of the contralateral hemisphere for two subjects in response to five different stimulus conditions (four stimulus and the no-stimulus control conditions). As stimulus duration was increased, the maximum absorbance increase evoked in SI of each subject became progressively more intense, and the borders of the ROI became visibly sharper.

Characterization of the temporal response within the maximally activated region

The time course of the absorbance change was computed for stimulus-evoked responses differing only in duration and is plotted in Figure 5.2. The responses evoked by 0.5, 1.0, and 2.0 second stimuli displayed delayed responses typical of the intrinsic signal, with the peak of the response occurring at approximately 2-3 seconds after stimulus onset, followed by the decay of the response to below-baseline levels between 5-6 seconds after stimulus offset. In striking contrast, the time course of the absorbance change evoked by 5.0 second flutter stimulation corresponded much more closely to the timing of the flutter stimulus – i.e., with 5sec stimulation the response steadily increased during stimulus delivery and then decreased progressively after stimulus offset, although full recovery to pre-stimulus levels was not observed in the ten second period during which data were acquired.

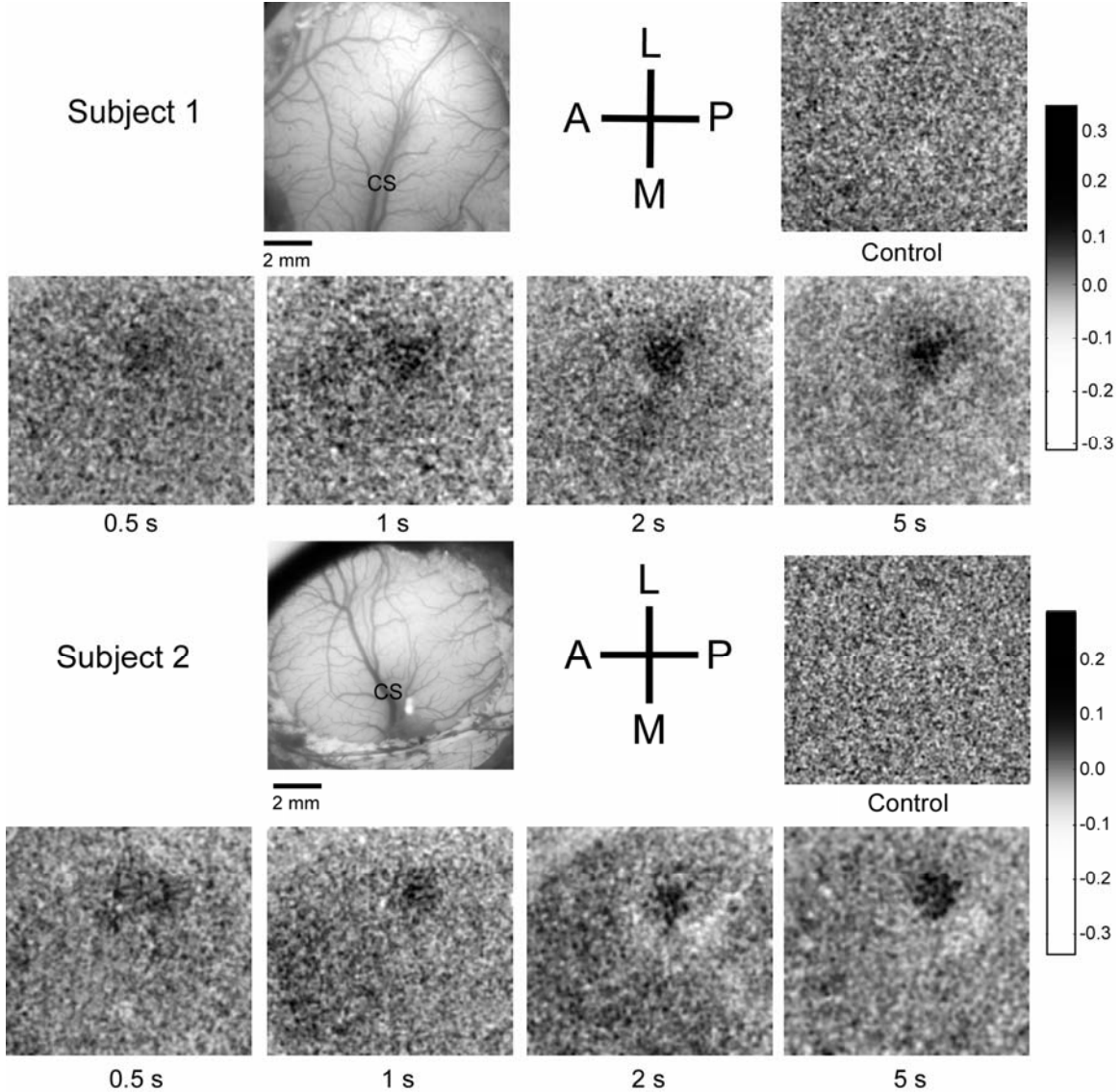


Figure 5.1. Difference images evoked by stimulation of the contralateral thenar pad in two exemplary subjects. Reference images show vasculature and location of the central sulcus (CS) on the cortical surface. Anatomical orientation is indicated by the crosshair schematic to the right. Difference images were generated by summing all images acquired over the duration of the response. Responses to 0.5, 1.0, 2.0, and 5.0 second stimuli as well as a no-stimulus control (summed over the same interval as the 5.0 second stimulus) are shown. Images have been spatially filtered using an averaging filter with a three pixel kernel size for easier visual identification of regions of activation.

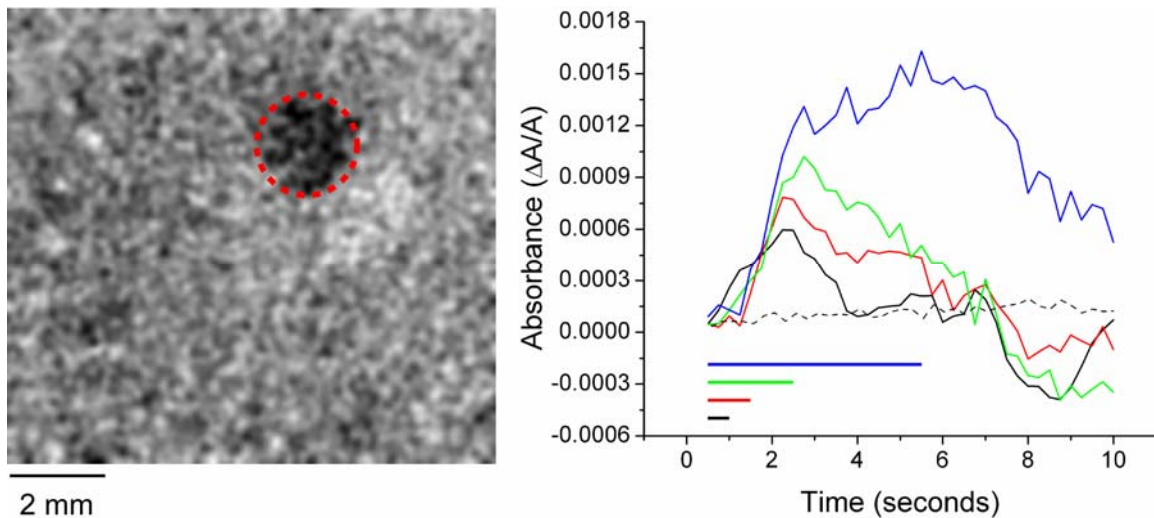


Figure 5.2. Absorbance time course in one subject. *Left:* Difference image of the response to five second stimulation from Figure 1. The ROI was defined as the 2 mm diameter circular region shown by the red dashed circle. *Right:* Pixels lying within the ROI were averaged for each frame and plotted as a function of time. Stimulus timing is indicated by the lines under the plots which are matched with the time course of the same color (0.5s-black, 1.0s-red, 2.0s-green, 5.0s-blue). The no-stimulus control (dashed black line) is plotted for comparison to test conditions.

The across-experiment (n=5) average time course within the ROI under each duration of flutter stimulation is shown in Figure 5.3. Plots were normalized with regard to the magnitude of peak absorbance in the 5.0 second response prior to averaging. The time

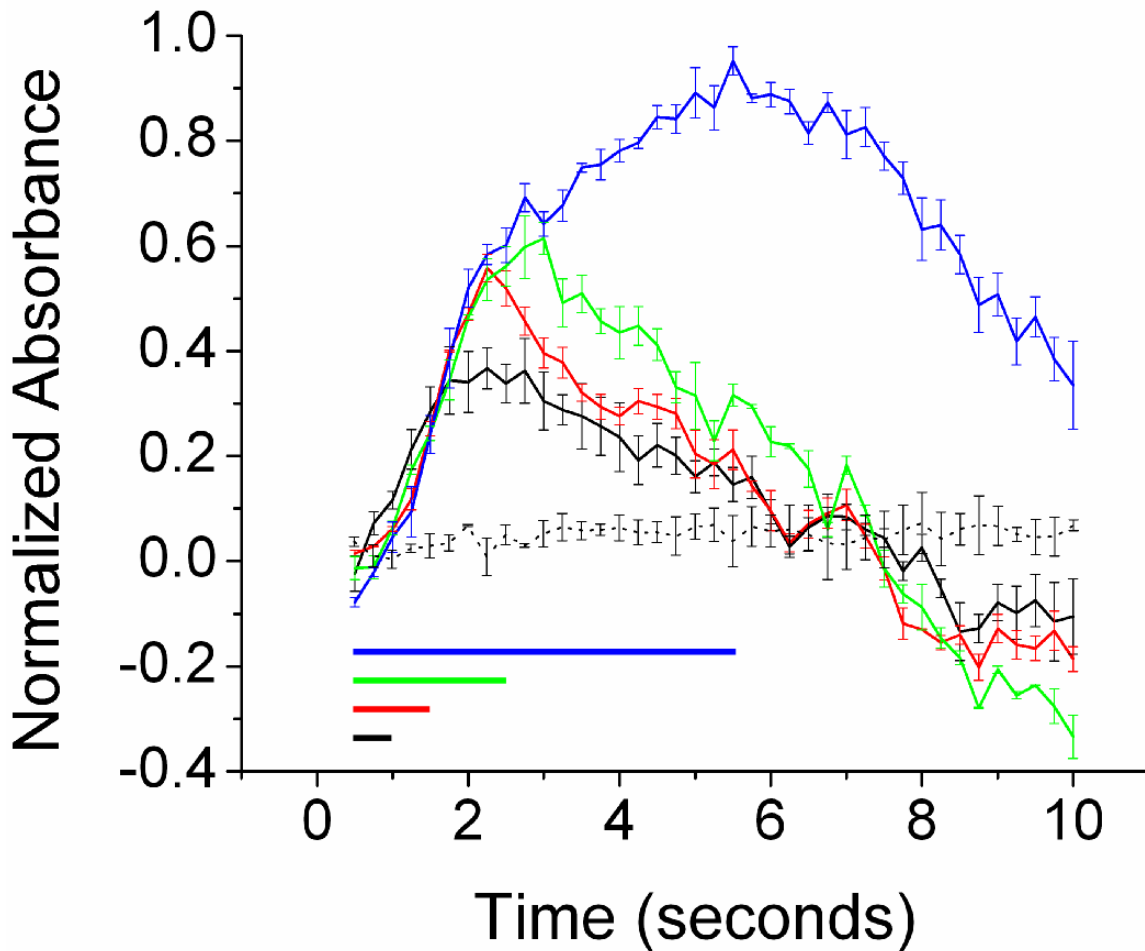


Figure 5.3. Across-subjects absorbance time course. The method of time course analysis from Figure 5.2 was performed on all subjects ($n=5$), and the resulting plots were normalized (according to peak absorbance) and averaged. Stimulus timing is indicated by the lines under the plots which are matched with the time course of the same color (0.5s-black, 1.0s-red, 2.0s-green, 5.0s-blue). The no-stimulus control (dashed black line) is plotted for comparison to test conditions. Error bars represent the between subjects standard deviation after normalization.

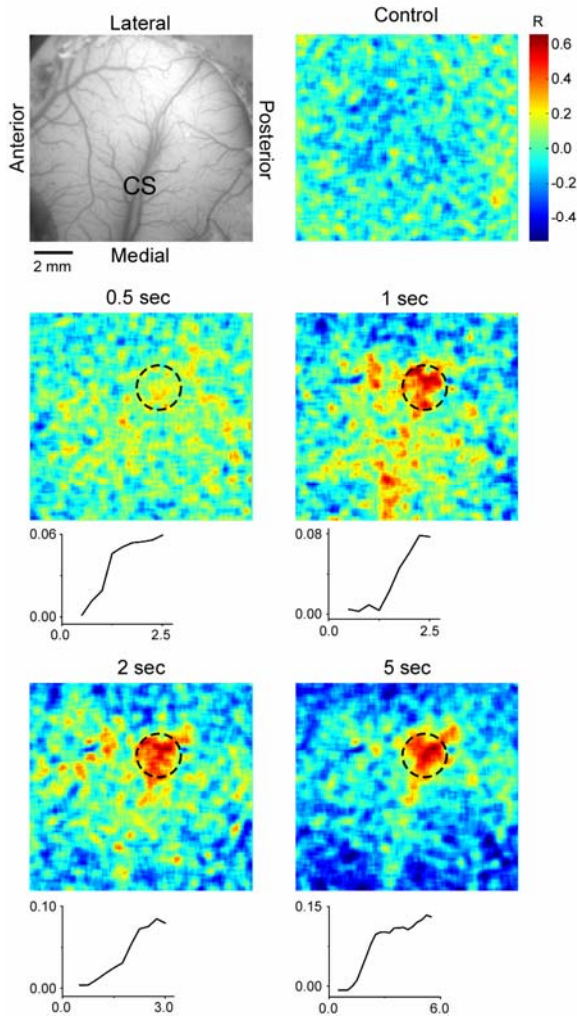
course of the responses to 0.5, 1.0 and 2.0 second stimuli are clearly distinguishable from the time course of the response to 5.0 second stimulation. More specifically, the responses evoked by the 0.5, 1.0, 2.0 second stimuli consist of an absorbance increase that corresponds closely with stimulus onset followed (after stimulus offset) by a relatively slower absorbance decrease. Similarly, the response to 5.0 second stimulation

shows an initially rapid absorbance increase, followed by a slower absorbance increase that begins approximately 3 seconds after stimulus onset (i.e., 2 seconds prior to stimulus off). Decay of the stimulus-evoked increase in absorbance occurred on a very similar time course for the 0.5, 1.0, and 2.0 second stimuli, and for these stimulus durations recovery to pre-stimulus levels occurred at nearly the same time in all subjects. Additionally, the responses to the 0.5, 1.0, and 2.0 sec stimuli included a decrease of absorbance to below-baseline values that became increasingly larger in magnitude as stimulus duration was increased. Similar to the data shown in Figure 2 (obtained from a single subject), the recovery of absorbance to pre-stimulus levels was significantly slower to 5.0 second flutter stimulation than at all shorter stimulus durations; in fact, for no subject did the absorbance increase measured in response to 5.0 second stimulation recover to baseline values during the ten second period during which data were acquired.

Changes in degree of correlated activity with increasing stimulus duration

Correlation maps provide an estimate of the stimulus-evoked increase or decrease in absorbance at every location in the image, and thus enable in-depth examination of the spatiotemporal properties of the SI response to stimulation. Figure 5.4 shows a correlation map for each of the stimulus durations used in two subjects. The maps for the 0.5 second stimulus condition reveal large and spatially diffuse patterns of positively correlated activity which extend beyond the indicated ROI. Furthermore, the maps of the response to the half-second stimulus reveal that both in the vicinity of the ROI, and in the surrounding regions, both the positive and negative correlation coefficients are small. Conversely, the maps computed for the responses to 1.0, 2.0, and 5.0 second stimuli

Subject 1



Subject 2

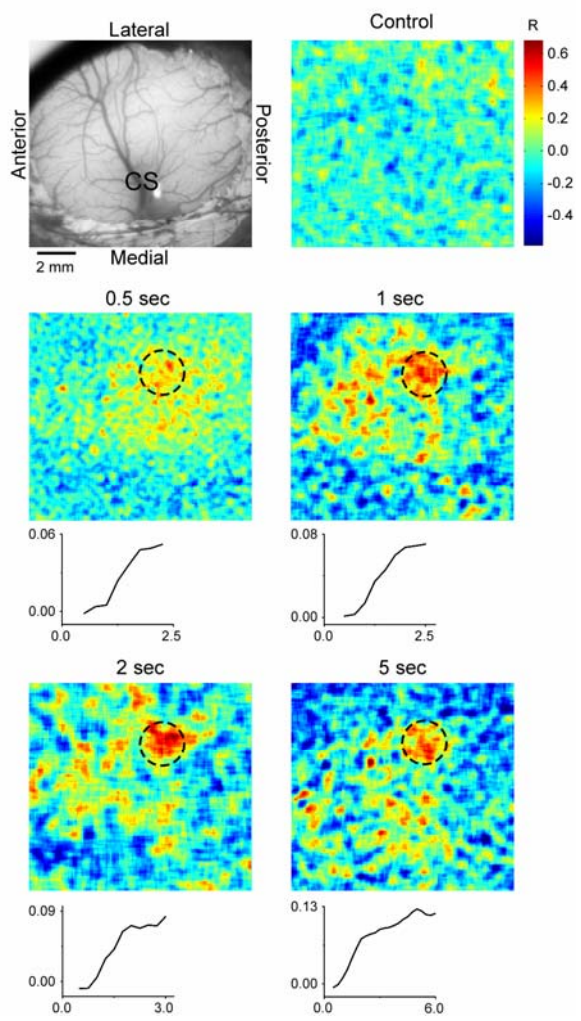


Figure 5.4. Maps of correlated activity in two exemplary subjects. The image of the exposed cortex at top left of each subject shows surface vasculature and anatomical orientation of SI. Correlation maps compare the slope of the average time course in a (4 x 4 pixel) moving window to the slope of the known time course of the ROI (2mm diameter region of maximal activity indicated by the dashed circle) over the interval from stimulus onset to peak response, and assign a coefficient to show the degree of correlation. The input signal used for correlation is shown below its respective map; with absorbance scaled according to %change from baseline (y-axis) and time in seconds (x-axis). Pixels displaying positive coefficients have time courses with positive slope (increased absorbance), while pixels displaying negative coefficients have time courses with negative slope (decreased absorbance). Control conditions show a lack of correlated activity in the absence of stimulation. All maps, within a subject group, have been scaled to the same color map to facilitate comparison.

display patterns of positively correlated activity within the ROI with significantly higher correlation coefficients (note color bar scale in Figure 5.4). The regions surrounding the ROI in these maps consistently display negatively correlated activity which, while observed only rarely in the response to 0.5 second stimulation, is present in increasing amounts in response to 1.0, 2.0 or 5.0 second stimulation. The negatively correlated activity in the surrounding regions indicates locations of stimulus-evoked decreases in absorbance.

Effects of stimulus duration on spatial extent

The average across-subject (n=5) radial histograms in Figure 5.5 demonstrate that increasing stimulus duration evoked increasingly higher absorbance in regions most proximal to the maximally responding central region (the ROI) and progressively less absorbance, often below pre-stimulus levels (zero), in the surround. Interestingly, 0.5 second stimulation evokes a broad, albeit weak, absorbance increase over the entire 3mm radius of the imaged region.

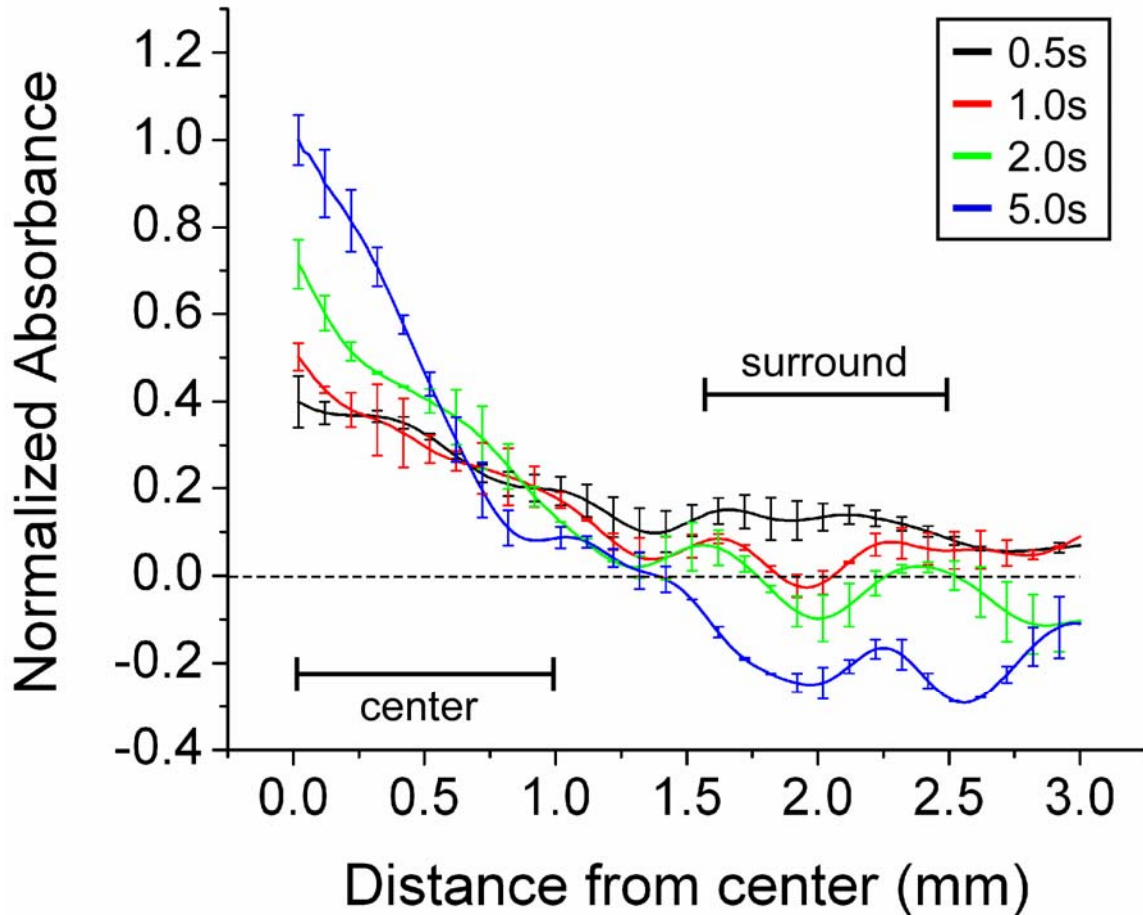
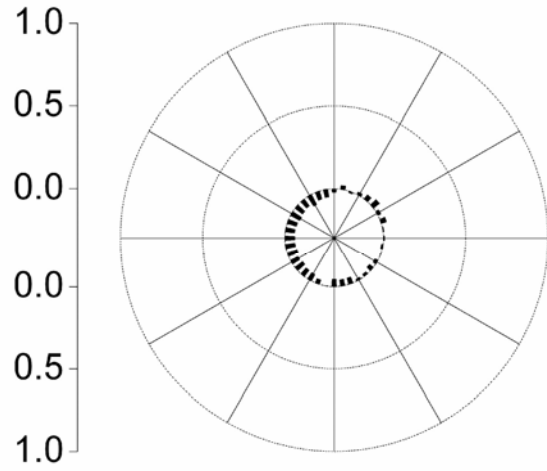
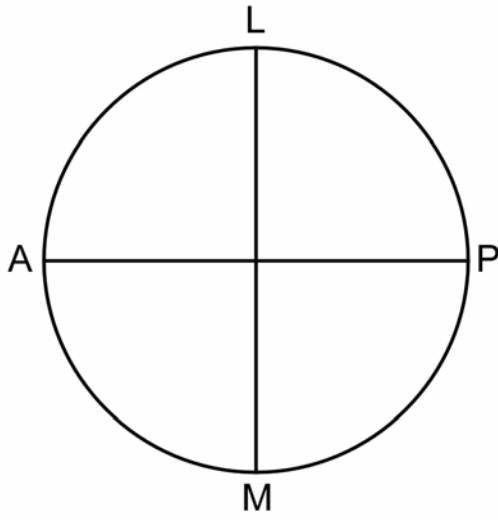


Figure 5.5. Radial absorbance trends across subjects (n=5). Using radial binning, absorbance values were averaged over one second of the maximal response to each stimulus duration (determined using time course) in all subjects. Responses were normalized according to peak absorbance of the five second response and averaged. Error bars show the between subjects standard error. As stimulus duration is increased, absorbance increases at distances near the center of the maximally responding region, and decreases in surrounding regions. Regions defined as center and surround are indicated on the plot (“center” = 0 - 1mm; “surround” = 1.5 - 2.5mm).

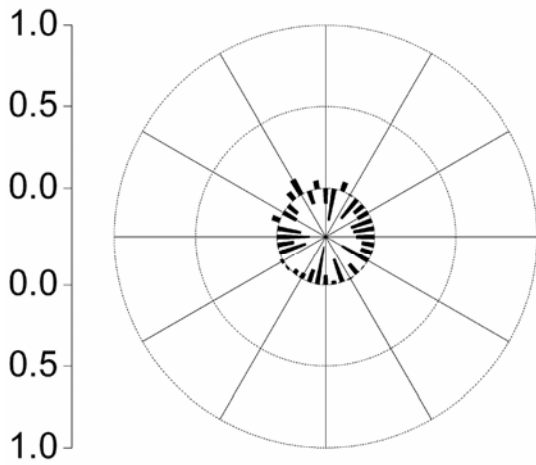
Anisotropy in magnitude of surround suppression

Although radial binning provides an overview of the spatial profile of the evoked response, and characterizes the approximate contrast between the center and the surround, it provides few details about the spatial distribution of the response within the

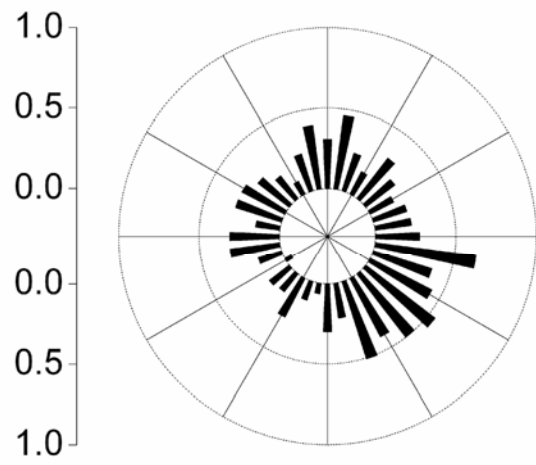
surround. To more precisely identify the locations in SI of strongest suppression (below baseline absorbance decrease) a new method of analysis was developed (“Surround Anisotropy Plot” or SAP; see Methods). SAPs use vectors to indicate the magnitude (represented by vector length), and anatomical location (represented by the orientation of the vector) of the evoked absorbance changes in regions of the surround located between 1.5 – 2.5mm from the ROI center. Note that because the response in the surround is negative for the 5.0 second stimulus duration (used for normalization), vectors showing positive values indicate an absorbance decrease while negative vectors indicate an absorbance increase. Figure 5.6 shows SAPs for one subject computed for each stimulus duration. The plots demonstrate that the average magnitude of suppression in surrounding regions increases with increasing stimulus duration. In addition to the increase in overall magnitude, the SAPs in Figure 5.6 strongly suggest that the locations in SI of the stimulus-evoked suppression are different at different stimulus durations, although at all durations it consistently was largest in a location posterior and medial to the maximally activated region (ROI), and consistently smaller in a location lateral to the ROI.



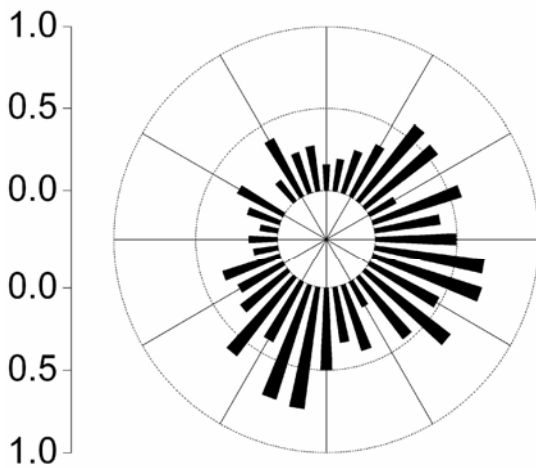
Control



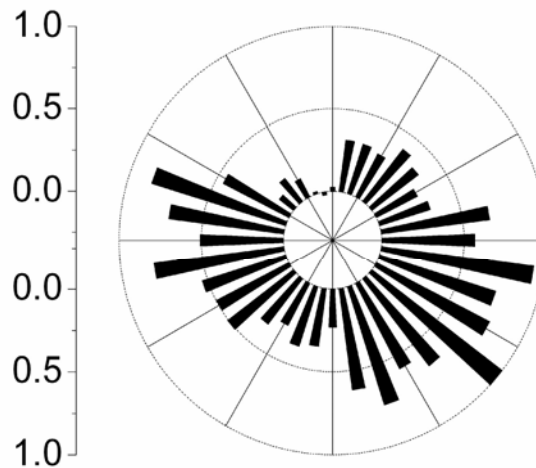
0.5 sec



1 sec



2 sec



5 sec

Figure 5.6. Surround Anisotropy Plots (SAPs) for one exemplary subject. Plots indicate directions of largest suppression (absorbance decrease) for each stimulus duration. Anatomical orientation of plots is indicated by the schematic at the top left (posterior = 0°, lateral = 90°, etc.). Absorbance was averaged in ten-degree increments at distances between 1.5 and 2.5mm outside of the ROI center (as per Figure 5) over a one second interval of the maximal response. Each measurement is plotted as a vector displaying magnitude (indicated by the vector length) and direction of the absorbance change in the surround. All vectors were normalized to the minimum value obtained (in the surround) in response to 5.0 second stimulation, thus vectors with positive values indicate negative absorbance.

Characterization of the temporal response in the surround

The SAPs of Figure 5.6 clearly show that the magnitude of the absorbance decrease in the surround is largest immediately medial and posterior to the region maximally activated by flutter stimulation of the contralateral thenar. The absorbance time course was calculated for the posterior/medial surround (the red shaded region) shown in the difference image at the left of Figure 5.7. Time courses were normalized by peak absorbance within the maximally responding ROI to 5.0 second stimulation and then averaged across all subjects (n=5). Consistent with the maps of correlated activity, the 0.5 second stimulus produces a modest increase in absorbance in this region and does not decrease below baseline. In contrast, 1.0, 2.0, and 5.0 second stimulation each evoked decreases in absorbance, and the magnitude and rate of decay of those decreases varied systematically with increasing duration. The magnitude of the stimulus-evoked absorbance decrease became progressively larger with increasing stimulus duration; and while the average response evoked by either 1.0 or 2.0 second stimulation did not significantly decrease below baseline during stimulus delivery, the response evoked by

5.0 second stimulation decreased substantially during the stimulus.

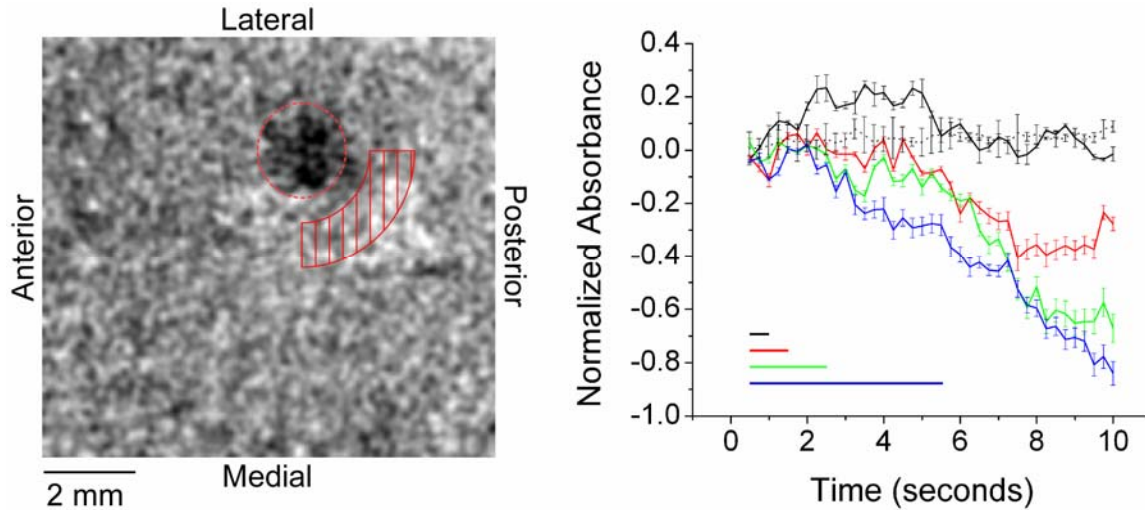


Figure 5.7. Time course in medial/posterior region of surround. Time course of the absorbance change in the surround was computed in the regions of the largest absorbance decrease, as indicated by SAPs in Figure 6. *Left*) Difference image of response to 5.0 second stimulation from Figure 1. Absorbance was averaged within the medial/posterior surround located 1.5 - 2.5mm outside of the maximally responding center (red shaded region). *Right*) Absorbance time course of this region was computed in all subjects and over all durations tested. Stimulus timing is indicated by the lines under the plots which are matched with the time course of the same color (0.5s-black, 1.0s-red, 2.0s-green, 5.0s-blue). The no-stimulus control (dashed black line) is plotted for comparison to test conditions. Plots were normalized according to peak absorbance (within the ROI), and averaged. Error bars represent the across-subjects standard deviation after normalization.

Perhaps the most striking observation was that the decrease in absorbance evoked in the surround region by different durations of stimulation persisted for significantly different times; and for the 2.0 and 5.0 second durations there was little or no recovery towards pre-stimulus activity levels within the 10 seconds during which data were acquired.

Stimulus site specific suppression

To determine whether the distribution of surround suppression within SI is sensitive to changes in stimulus site, the responses evoked (in the same subject) by 5.0

second flutter stimulation of the tip of digit two (D2) and of the thenar eminence were compared. The OIS responses and SAPs obtained in response to flutter stimulation delivered to each site are shown in Figure 5.8. As before, radial binning was used to identify the boundaries of regions of increased and decreased absorbance for stimulation of D2 (not shown). Although strong SI suppression in a posterior/medial location was obtained using each stimulus condition, an additional strong suppression at an anterior location was evident with thenar stimulation but this component of the response was much weaker with stimulation of D2. Additionally, stimulation of D2 evoked a stronger suppression in a location lateral to the ROI than was detected in the same location in response to thenar stimulation. Regions of strongest suppression are visible in the difference images provided under each plot in Figure 5.8 – in these images suppressed regions appear as white patches located medial and posterior to the maximally responding region.

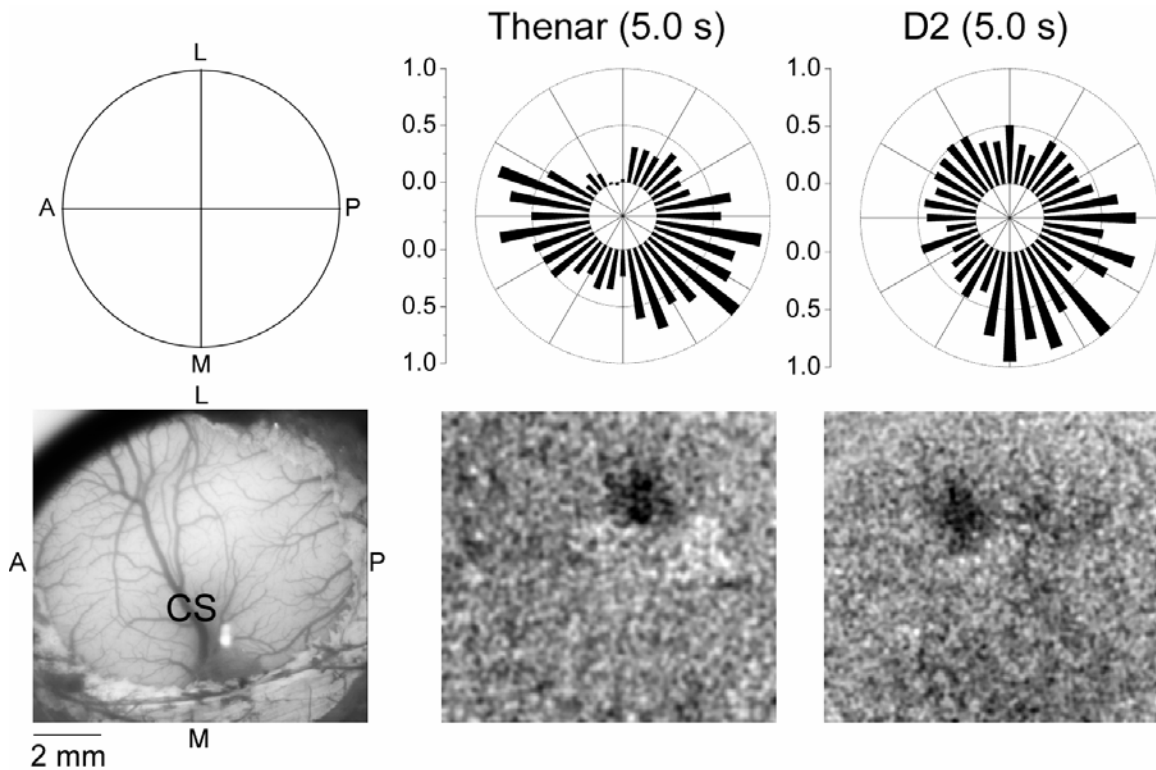


Figure 5.8. Surround Anisotropy Plots (SAPs) for two different stimulus sites in the same subject. Plots were computed for the response evoked by 5.0 second stimulation of the thenar eminence and tip of digit two in the same subject. *Top/Left*) Anatomical orientation is indicated on the image of the exposed cortical surface. *Top/Right*) Schematic showing anatomical orientation of SAPs. *Top/Middle*) The SAP of 5.0 second thenar stimulation from Figure 5.6 is shown for comparison. *Bottom/Middle*) OIS response to 5.0 second thenar stimulation from Figure 5.1. *Top/Right*) SAP of 5.0 second stimulation of the tip of digit two. *Bottom/Right*) OIS response to 5.0 second D2 stimulation.

Our observations that (1) the distribution of surround suppression evoked in SI by stimulation of a skin site is non-uniform, and (2) this distribution alters when the site of skin stimulation is changed, raise the possibility that the location of stimulus-evoked SI suppression is functionally relevant. Although precise identification of the topographic identity of the suppressed SI sites requires that detailed receptive field maps be obtained from each subject and under each stimulus condition, this was not done in this set of

experiments. Nevertheless, a first approximation of the topographic identity of the SI region(s) suppressed during flutter stimulation was made by co-registration of the optical images (images showing the locations of both the maximal absorbance increase and maximal suppression) with published receptive field maps of the SI forelimb region in squirrel monkey (Sur et al. 1982).

To this end, SAPs were computed for 5.0 second flutter stimuli delivered to eight different skin sites on the forelimb (using the data obtained in multiple experiments). In most cases, SAPs generated in this way (Figure 5.9) indicate that the direction of strongest suppression consistently is located posterior/medial to the maximally responding SI region. This preliminary approach to comparison of the optical response of SI and SI topographic organization strongly suggests that stimulation of the digit tips evokes strong suppression of the anterior parietal representation of the corresponding interdigital pads; while conversely, stimulation of either the thenar or interdigital pads (specifically ID 1 and 2) evokes a strong suppression within those SI regions that represent the corresponding digit tips.

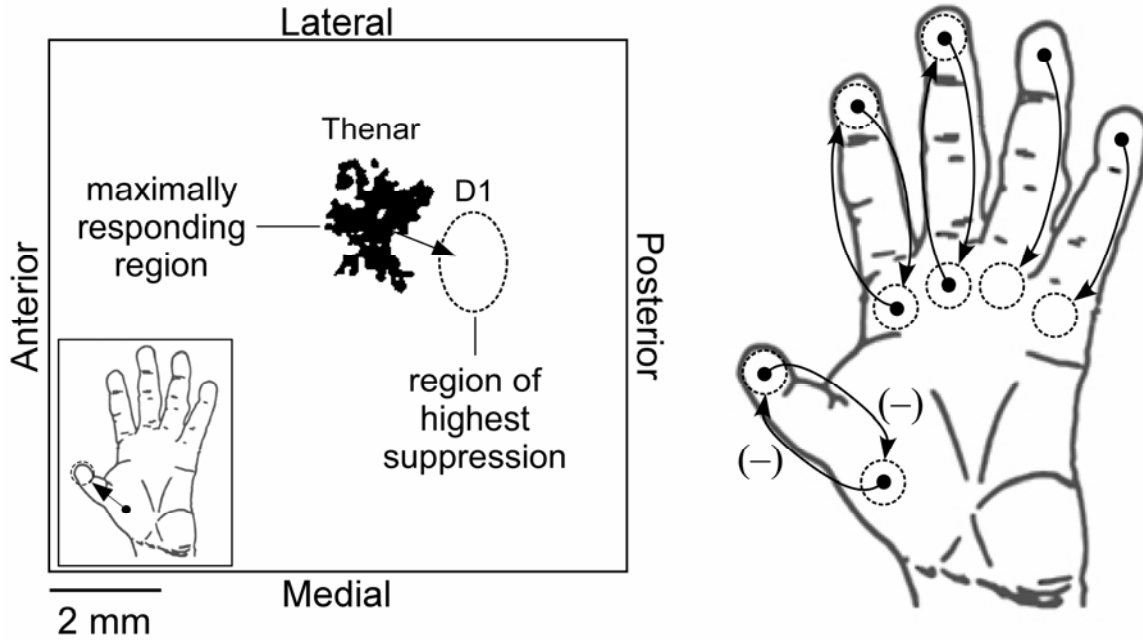


Figure 5.9. Corresponding skin sites to locations of strongest suppression. Illustration at the left summarizes the method used to estimate the skin sites represented by locations of suppression. Shown in the box is the thresholded ($\geq 90\%$ of maximum) response to 5.0 second thenar stimulation. The arrow that points posterior/medial from the maximally responding region indicates the region (as identified by the SAP) of strongest suppression which, based on estimates, corresponds to cortical locations representing digit 1, as shown on the hand at the lower left inset. The schematic at the right shows the location of eight different stimulus sites that were examined on the hand. Arrows point to predicted skin sites, enclosed by dashed circles, corresponding to locations of strongest suppression for each stimulus location. Stimulation of a digit tips appears to evoke strongest suppression in regions representing the corresponding interdigital pad, while stimulation of an interdigital pad evokes strongest suppression in region representing the tip of the corresponding digit.

Discussion

The results of this study demonstrate that: **1)** a minimal duration of skin flutter stimulation, $\geq 0.5s$ and $\leq 1.0s$; is required to evoke a pattern of SI activity characterized by a $\sim 2mm$ diameter sized region of increased activity, surrounded by one or more

regions in which activity is suppressed to below-baseline levels; **2)** increasing the duration of a flutter stimulus, within the range 0.5 – 5.0 seconds, evokes i) a progressively larger absorbance increase within the cortical territory that receives its principal input from the stimulated skin site and ii) a decrease in absorbance that increases in magnitude with increasing stimulus duration in one or more surrounding regions; **3)** the pattern of decreased absorbance evoked by longer duration (≥ 1.0 s) stimuli in the region that surrounds the maximally activated region is non-uniform, with the region undergoing the strongest suppression most often located anterior and/or posterior to the maximally activated region. While the relationship between stimulus duration and the patterns of SI response observed in this study may differ somewhat depending on stimulus intensity, the findings indicate that when the stimuli are clearly suprathreshold, such as those used in this study, stimulus duration plays a critical role in the establishment of the response suppression that occurs consistently in regions that surround the region of SI that responds maximally to skin flutter.

Prolonged stimulation reduces the spatial extent of the responding population

Multiple animal studies have demonstrated that repetitive stimulation is reliably accompanied by reductions in neuronal responsiveness at both peripheral and central levels of the somatosensory nervous system. For example, such stimulation is accompanied by a sustained decrease in the responsiveness of skin mechanoreceptors located in the vicinity of the stimulated skin region (Bensmaia et al. 2005), a long-lasting depression of the responsiveness of neurons in the cuneate nucleus of the brainstem ipsilateral to the stimulus site (OMara et al. 1988), a decrease in the thalamic and cortical neuron firing rate (Chung et al. 2002), and a persistent reduction in the spatial extent of the SI region that responds

to mechanical stimulation of a discrete skin site (Juliano et al. 1981; Juliano et al. 1983). This time-dependent spatial funneling of the responding SI cortical neuronal population has been widely reported (Kleinfeld and Delaney 1996; Derdikman et al. 2003; Wirth and Luscher 2004; Simons et al. 2005). Kleinfeld and Delaney reported that a single train of stimulation evoked an increase in activity in an extensive region of barrel cortex but with repetitive stimulation the size of the responding region was significantly decreased (Kleinfeld and Delaney 1996). Single unit studies and imaging studies using voltage sensitive dyes likewise have demonstrated that excitation in the responding neuronal population is accompanied by the development of a surrounding field of inhibition (Brumberg et al. 1996; Derdikman et al. 2003; Wirth and Luscher 2004; Foeller et al. 2005). Similarly, imaging studies which have used the optical intrinsic signal (OIS) have demonstrated that prolonged stimulation of a discrete skin site evokes regions of highly increased absorbance within the SI region representing the stimulated skin site, coupled with surrounding regions of sharply decreased absorbance (Tommerdahl and Whitsel 1996a; Moore et al. 1999; Tommerdahl et al. 1999a; Simons et al. 2005). Regions of decreased absorbance (increased reflectance) such as those reported in this study are widely believed to be indicative of decreases in neuronal spike discharge activity, (Grinvald 1985; Grinvald et al. 1991; Grinvald et al. 1991) possibly resulting from stimulus-evoked inhibition at these locations.

Stimulus site-specific SI suppression

The anisotropy in the distribution of suppression in the surrounding regions of SI leads us to suggest that this feature of the SI population response contributes importantly to sensorimotor function. Anisotropy in the distribution of surround inhibition has been

previously reported in single unit recordings obtained from the barrel cortex of the rat – e.g., Brumberg et al. reported that locations of strongest inhibition are aligned in a manner consistent with the anatomical orientation of the barrel field (Brumberg et al. 1996). The caudomedial orientation of this inhibition, relative to regions of excitatory activity, was subsequently confirmed by imaging studies using voltage sensitive dyes (Derdikman et al. 2003). In the present study suppression of the SI intrinsic optical response was strongest at locations oriented in a highly specific way relative to the maximally responding region in SI. Furthermore, the distributions of these regions of suppression are stimulus site specific and thus provide more evidence that this suppression may be functionally significant.

Functional implications

Vierck and colleagues have demonstrated that absolute tactile localization in behaving monkeys was better along the proximodistal axis than the mediolateral axis of the distal forelimb (Vierck Jr. et al. 1988). If the perceptual ability to spatially localize a stimulus is a reflection of SI's ability to spatially discriminate stimuli at adjacent skin sites, then the findings of Vierck et al (1988) would be in accord with the idea that stimulus-evoked inhibition acts to preferentially enhance the spatial separation of the SI responses to stimuli delivered to skin sites arranged along the proximodistal axis of the hand. Consistent with this prediction is the present study's demonstration that flutter stimulation of a skin site evokes a strong below-baseline suppression of activity in SI territories that (based on comparison of our images of the stimulus-evoked OIS with published maps of SI topographic organization) represent skin sites displaced along the proximodistal axis of the hand. The observation that the areas of strongest suppression

occur along the anterior/posterior axis of SI also identifies a plausible functional role for the high density interareal connections reported by Burton and Fabri (Burton and Fabri 1995). The results of the present study support the idea that neuroanatomical connections that link columns in neighboring, but somatotopically distinct regions arranged in the anteroposterior dimension of SI play a crucial role in tactile acuity (Vierck Jr. et al. 1988).

The characteristic temporal development of the spatially patterned response of SI cortex to the long-duration tactile stimuli employed in the experiments of the present study is of interest because it lead us to predict that if perceptual localization is based on activity in the contralateral SI, a prolonged (e.g., 5 sec) tactile stimulus should enable significantly better performance than that measured when the stimulus is brief (0.5 sec). For example, our experiments have shown that (1) delivery of a five second vibrotactile stimulus to the skin evokes an SI response that includes a persisting, suppressive component which occurs in the a region of SI that surrounds the maximally activated region – a component which presumably would inhibit the SI response to a stimulus applied concurrently or subsequently to the skin region represented by neurons in that region of SI; and (2) brief (0.5 second) stimuli fail to evoke such a suppressive component. The results reported in a recent psychophysical study are in fundamental agreement with these predictions. That study observed the impact of a 0.5 vs. 5.0 second adapting stimulus on a subject's ability to spatially localize a subsequent tactile stimulus. All subjects demonstrated nearly a two-fold improvement in spatial discrimination with a 5.0 second adapting stimulus (Tannan and Tommerdahl 2006). These recently published psychophysical results, in combination with the findings of this study, suggest that the

slow-to-develop but persistent suppressive responses observed in regions surrounding the maximally activated region of SI may underlie the recently observed (Tannan et al. 2006) adaptation-mediated improvements in the capacity of human subjects to localize the skin site contacted by a vibrotactile stimulus.

In primates the hand is the primary means not only for tactile exploration of the environment, but also for voluntary manipulation of the environment. One example is a task involving grip requiring not only the coordination of hand and digit movement, but also the continuous incorporation of sensory feedback. We propose that the site-specific SI suppression we have observed to accompany multi-second vibrotactile stimulation shapes the SI response to the inputs it receives from the multiple skin sites on the hand (e.g., the digit tips and corresponding interdigital pads) contacted either simultaneously or in rapid succession during tactile exploration and object manipulation. Further studies are needed to electrophysiologically confirm the presence and specificity of the stimulus evoked inhibition inferred by the imaging results reported in this paper, and to examine the impact of multi-site stimulation on the spatiotemporal patterned SI response to mechanical stimulation of the skin.

CHAPTER SIX: In Vitro Examination of Pericolumnar Excitability

Background

In the neocortex horizontal connections, that is connections within a given cortical lamina and across multiple columns, are essential for intracortical communication and may profoundly impact its activity. While only a small proportion of these connections may synapse on inhibitory interneurons (~20%), this relatively small population can dominate lateral excitability generating strong inhibition.

The role of GABAergic inhibition in the developed cortex is diverse and still poorly understood. It serves multiple functions in the shaping of neuroelectrical activity including the temporal fine tuning of spiking activity of neurons located within the same cortical column, the synchronization of spike trains in large neuronal populations, and the spatial sharpening of the spread of excitation tangential to the pial surface via the suppression of subthreshold excitatory inputs (commonly known as inhibitory sharpening of receptive fields)(Ling and Benardo 1995; Kyriazi et al. 1996; Salin and Prince 1996; Foeller et al. 2005). In the somatosensory cortex precise localization of a stimulus on the skin may be reflected by the degree of spatial discriminative capacity in the cortex; in other words the minimum amount of cortical space necessary for distinguishing between an active cortical column and an inactive one. Several studies have established that the spread of excitation within the rat sensory/barrel field is anisotropic, exhibiting a larger tangential spread within rather than across a barrel row (Kyriazi et al. 1998; Derdikman

et al. 2003; Petersen et al. 2003). Fewer studies have examined the function of GABAergic inhibition in relationship to this anisotropic spread and its potential impact on cortical discriminative capacity. The in vivo imaging experiments discussed in chapter five demonstrated that the distribution of suppression possesses an anterior/posterior bias which could be based on the functional connectivity of multiple areas in the cortical map. This result indicated the possibility that lateral inhibition was more pronounced in a manner consistent with the proximal/distal axis of the body representation in SI; although direct measurement of inhibition is not currently demonstrable using OIS imaging.

To examine the anisotropic spread of cortical activation and the role of GABA in establishing it; we studied the cortical activity, using optical intrinsic signal (OIS) imaging, evoked by repetitive stimulation of layer V/VI in rat sensorimotor cortical slices which were sectioned in the coronal and sagittal planes. Recordings of local field potential were also made under multiple pharmacological conditions to determine the contribution of the fast acting inhibitory channel GABA_A to these patterns of cortical activation. Results indicate that under control conditions slices cut in the coronal plane display a narrower spread of cortical activity that is at least in part due to a stronger influence of GABAergic inhibitory conductance in these sections; an effect which is blocked by the GABA_A antagonist bicuculline methiodide.

Analytical Methods

See chapter 3 for description of spatial histogram technique.

Results

The spread of activation in cortical layers 2/3 evoked by electrical stimulation in layer 5/6 was measured in sensorimotor cortical slices cut in the coronal and sagittal planes. Figure 6.1 shows optical intrinsic signal (OIS) images of the activity evoked in each type of slice during control conditions in which the slice was perfused with normal artificial cerebral spinal fluid (ACSF), and subsequently with ACSF containing the GABA_A antagonist bicuculline methiodide (BMI). Electrical stimulation of lower cortical layers typically evokes patterns of activity which are columnar in shape (i.e. similar distributions of increased transmittance are observed at each cortical lamina). Visual examination of the patterns of activity evoked during control conditions reveals that the horizontal spread of increased transmittance appears smaller in the coronal slice when compared with that of the sagittal slice. Conversely, images of the evoked activity in each slice after perfusion with BMI display both an increased intensity and an increase in the horizontal spread across each cortical layer.

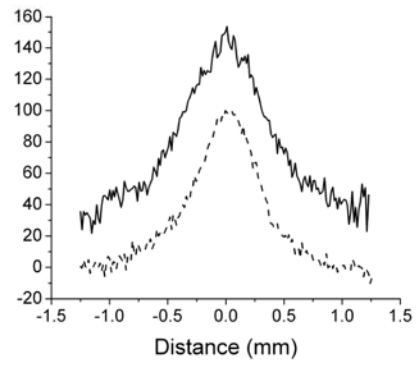
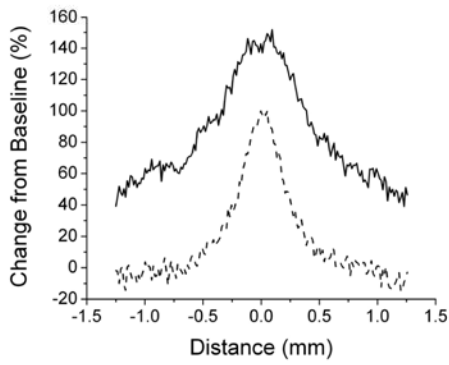
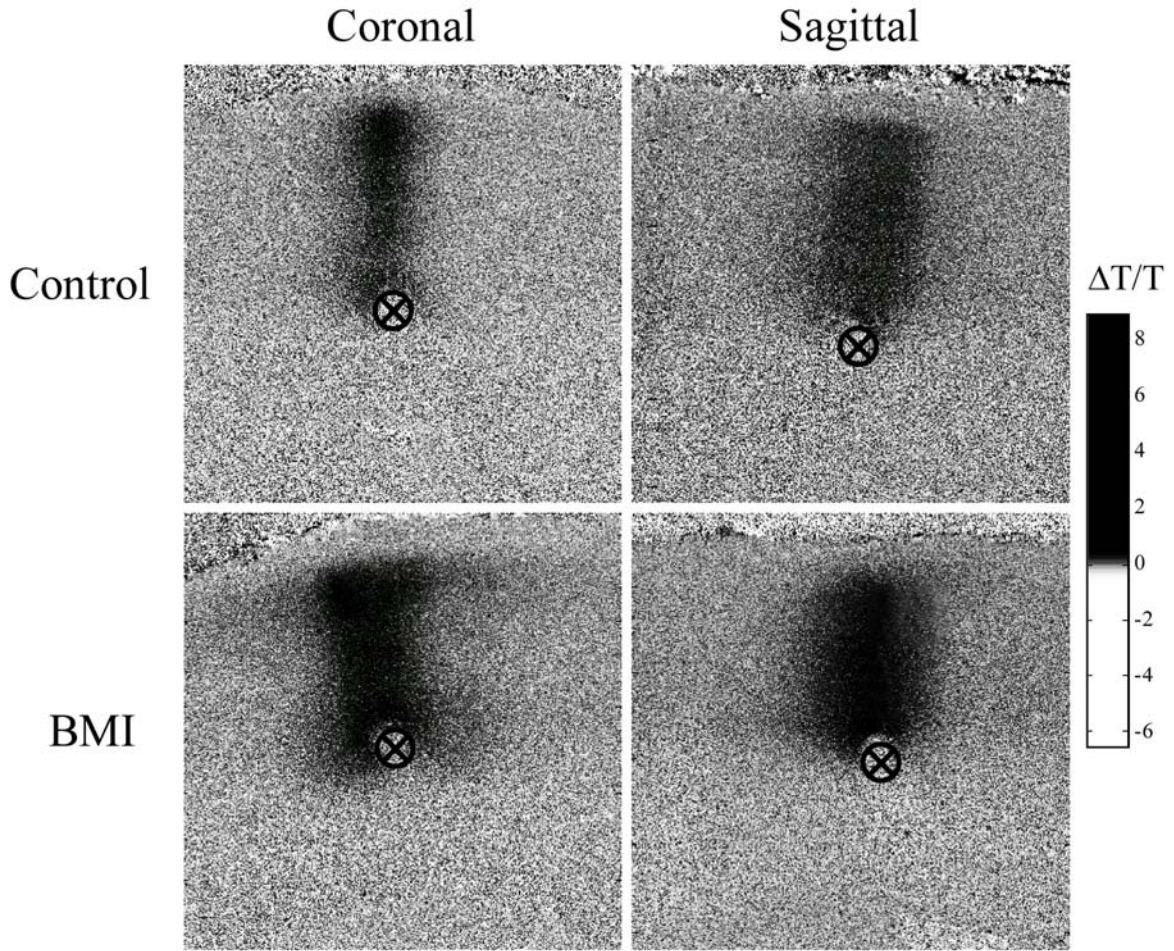


Figure 6.1. OIS images in sensorimotor cortical slices during perfusion with normal ACSF and after application of 2 μ mol bicuculline methiodide (BMI). Each image represents the sum of all difference images acquired during the interval from stimulus onset to 5 seconds after stimulus offset. Location of the stimulus electrode is indicated by the circled x in each image. Scale bar is 1mm. Activity profiles plotted at figure bottom show the distribution of transmittance along a 2.5mm span across upper cortical layers 2/3. All transmittance values were plotted as a function of their % change from baseline and normalized to the peak transmittance value obtained during control conditions.

Since a large number of lateral connections (known to significantly effect the horizontal spread of activity) exist in the upper cortical layers 2/3, we assessed the distribution of activity in each slice and in each experimental condition across these cortical layers. Plots of the normalized transmittance distribution across layer 2/3 indicate that the spread of activity during control conditions is consistently narrower in coronal sections when compared with sagittal sections. Furthermore, the application of BMI evokes increases in the OIS at every location across layer 2/3 in both types of slice. Since the transmittance distribution is essentially Gaussian in each case, the full width half maximum (FWHM) can be used as a measure of the spread of activity across layer 2/3 and are 378 and 574 μ m during control conditions for the coronal and sagittal sections respectively and 1041(coronal) and 952 μ m (sagittal) after the application of BMI. Thus the transmittance distributions across layer 2/3 demonstrate that blockage of fast inhibitory current has a much larger impact on the lateral spread of activity in the coronal slice. Consequently, it is possible that the narrower distribution observed in the coronal slice during control conditions is a reflection of the stronger recruitment of lateral inhibition in this plane, however it is also possible that differences in the distribution of activity are due to differences in the lateral extent and efficacy of excitatory connections.

To test this possibility we next examined the impact of applying the NMDA receptor antagonist D-2-amino-5-phosphonopentanoate (D-AP5) on the horizontal spread of the OIS.

Figure 6.2 shows the effects of NMDA block on the intrinsic signal evoked in the coronal and sagittal slice. Comparison of the difference image for each type of slice during control conditions with its respective image after the addition of D-AP5 reveals a large decrease in the intensity of the intrinsic signal in the maximally activated regions, however little difference is visually perceptible in the spatial characteristics of each response. The transmittance distribution across layer 2/3 was computed in the same manner as in Figure 6.1 and is plotted underneath the difference images for each type of slice. Distributions in both types of slices indeed demonstrate a smaller transmittance increase within the stimulated column, on average ~60% of control levels, however as distance from the maximally activated center increases the effect of D-AP5 becomes less significant. The FWHM (normalized to the maximum of control peak transmittance) values under NMDA block decreased to 322 and 350 μ m for coronal and sagittal slices respectively. Since the magnitude of the OIS was not uniformly affected across layer 2/3 caution should be used when interpreting the relative change in the values of the FWHM. For example, although the magnitude of the transmittance change near the center of the responding region was reduced to ~60% of its control value the transmittance change in more remote locations of layer 2/3 was nearly identical to control levels; therefore although the strength of the response is relatively unchanged at these locations the FWHM will show a significant reduction due to the change in maximal response. Figure

6.3 summarizes the effects of GABA_A and NMDA block on the intrinsic signal distribution in layer 2/3 in each type of slice.

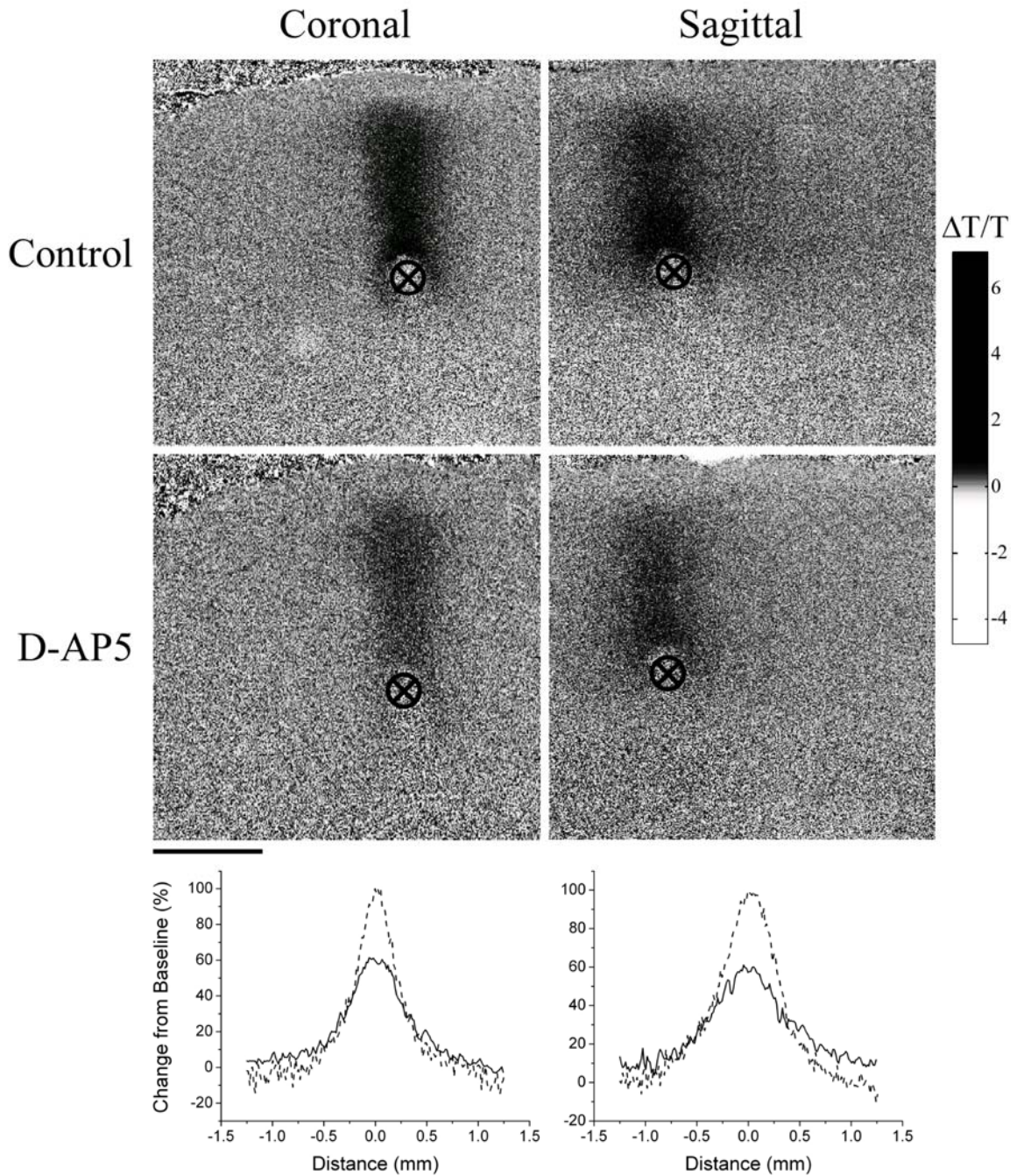


Figure 6.2. OIS images in cortical slices before and after perfusion with the NMDA antagonist D-AP5. Images and distributions were computed using the same methods as Figure 6.1. Scale bar is 1mm.

The plot at the top left of Figure 6.3 demonstrates that GABA_A block with BMI increased the layer 2/3 response in both types of slices and at all distances. This increase in response was larger in the coronal slice at nearly all locations; a result which is more clearly shown in the plot at the top right which plots the difference between the two distributions (coronal – sagittal). BMI had a greater impact on the response across layer 2/3 in the coronal slice when compared with the sagittal slice and this difference was greatest at distances between 250 and 500 μ m outside of center. Even at distances >1mm the change in response magnitude in coronal slices exceeded that of the sagittal slice by more than 10%. The difference between the responses measured after NMDA block by D-AP5 (from control responses) are plotted in the bottom left panel of Figure 6.3. Unlike GABA block, NMDA block produced very similar effects on the distribution of activity in layer 2/3 in coronal and sagittal slices. Responses near to the center were maximally affected and were similarly reduced in both types of slices by ~40%. NMDA block had a much smaller effect on responses outside of the stimulated center, and was minimal as distance from the center approaches ~350 μ m. The difference between the effects of NMDA block on coronal and sagittal slices is plotted at the bottom right of Figure 6.3 and demonstrates that D-AP5 had similar effects (change was within 5% of each other) on the responses in both types of slices at the center and at distances >0.5mm. Hence, while the effects of GABA_A block at locations in layer 2/3 which were laterally remote to the responding column were quite large and demonstrated significant differences between the coronal and sagittal sections, the effects of NMDA block in these locations were equally negligible in both types of slices. This result implies that GABA_A inhibition may be more critically important in determining the lateral spread of activity in layer 2/3 and

thus could also be responsible for the differences in activity distribution observed in coronal and sagittal slices during control conditions.

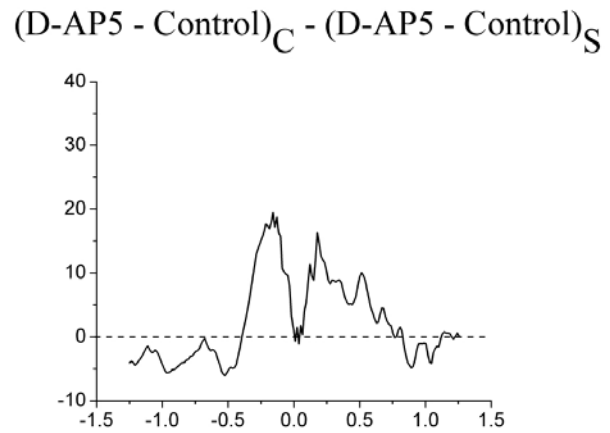
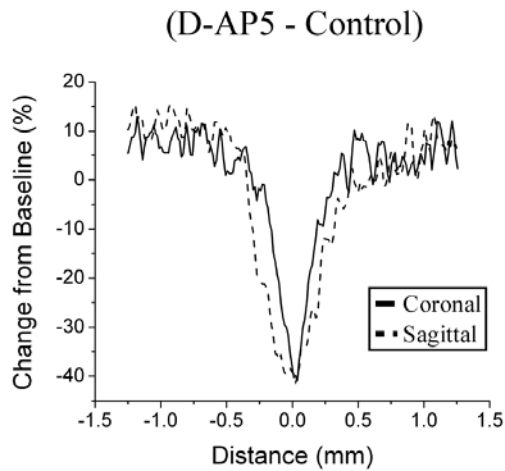
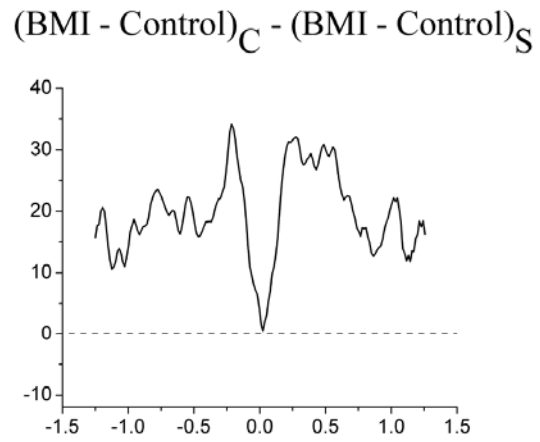
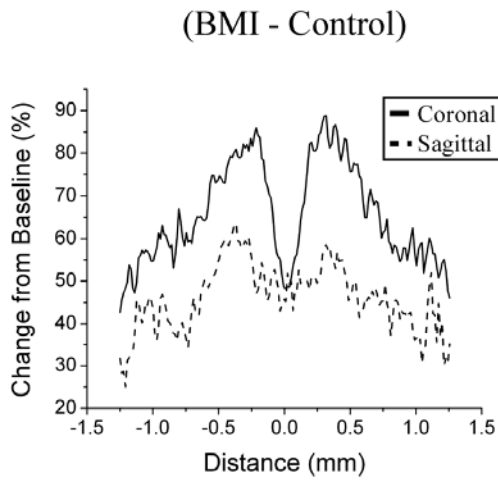
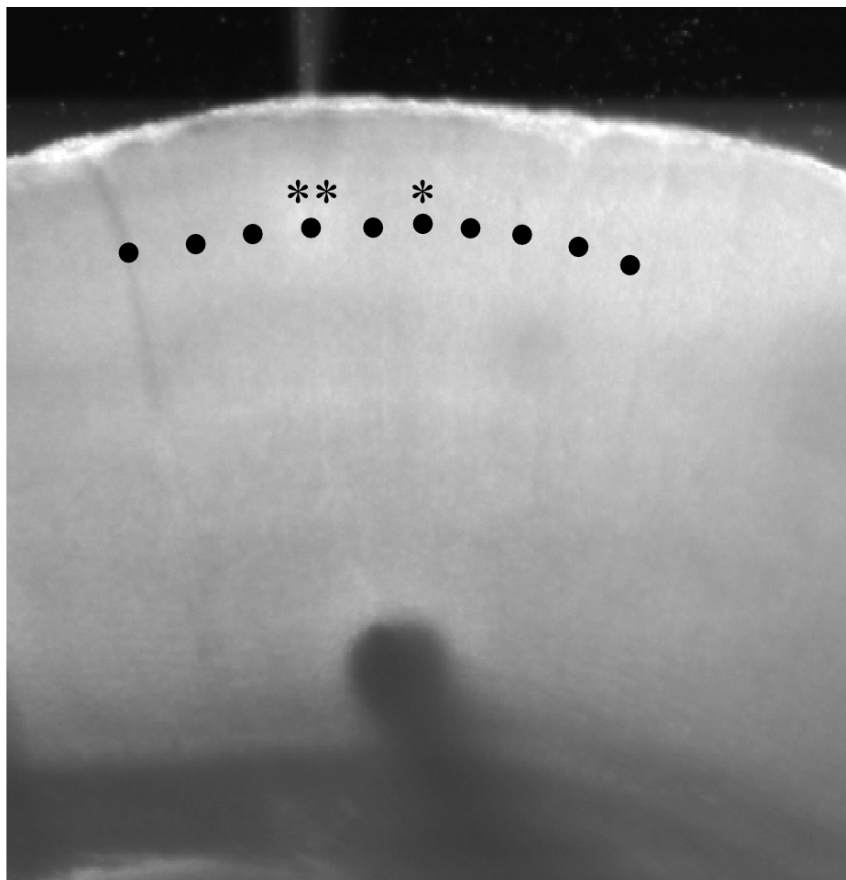


Figure 6.3. Differential effects of GABA_A block with BMI and NMDA block with D-AP5 on the distribution of activity in layer 2/3. *Left*) Effect of each pharmacological manipulation in both types of slice. Plots were computed by subtracting the transmittance distribution measured during control conditions from the distribution measured after subsequent pharmacological block with BMI (top) or D-AP5 (bottom). Thus baseline (zero) indicates locations where pharmacological block had no effect on neuronal response. *Right*) Differential effect of each drug on the coronal vs. sagittal slice. Plots were computed by subtracting the sagittal distribution from the respective graph to the left from the coronal distribution in the same graph. Therefore baseline (zero) indicates locations where the effect of pharmacologic block was equal in both types of slice.

The results of Figures 6-1 – 6-3 suggest that the spread of electrical activity evoked in layer 2/3 by stimulation of layer 5/6 is more strongly attenuated in coronal slices when compared with sagittal slices and that this attenuation is at least in part due to the impact of the fast inhibitory channel GABA_A. Measurements of local field potential (LFP) evoked by single pulse stimulation were made at a number of closely spaced sites across layer 2/3 in both types of slices; distance between recording sites varied but was always between 0.100 and 0.200mm. Figure 6.4 shows the locations of recordings made across layer 2/3 in one exemplary (coronal) slice. Traces of LFP below the image display the average responses (n=10) recorded from two discrete sites in single slices of each type in normal ACSF (Control) and after application of 2μmol BMI, and 50μmol D-AP5. Peak response magnitude was typically largest within the stimulated column (location determined using the previously obtained OIS response) corresponding to traces labeled *. As distance from the center of the stimulated column increases peak response magnitude decreases in both the coronal and sagittal slices, however the response

magnitude is more strongly attenuated in the case of coronal slices. This can be seen by comparing the responses recorded at sites located $\sim 500\mu\text{m}$ outside of the stimulated column center (labeled **). Traces of LFP recorded from the same slices at near identical locations after the application of $2\ \mu\text{mol}$ BMI demonstrate an increase in peak magnitude at each recording location and in both types of slices, and although the peak LFP decreases with increasing distance from the stimulated column the magnitude of decrease in both planes appears similar. This contrasts strongly with the evoked potential measured at the same locations under control conditions in which traces recorded in coronal slices appear much more strongly attenuated. Additionally, LFP measured under GABA_A block with BMI demonstrated a smaller lag between pre and post-synaptic elements of the evoked potential (i.e. a decrease in time between the two phases of the positive potential). In a similar manner the LFP was measured across layer 2/3 after NMDA block with D-AP5. Under this condition the peak magnitude of the LFP was not significantly affected, although a small reduction was observed at sites within the stimulated column.



1 mm

C *

C **

S *

S **

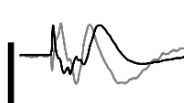
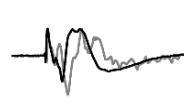
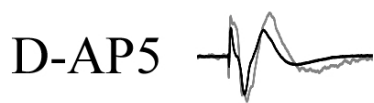
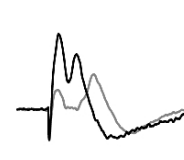
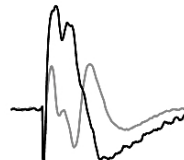
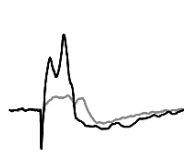


Figure 6.4. Recordings of local field potential across layer 2/3. Image of cortical surface indicates locations of LFP recording in one exemplary coronal slice (electrode can be seen approaching from top at location **). Traces displayed under image show recordings made in exemplary slices of each type during control conditions (gray trace) and pharmacological block (black traces) at two locations. C*) coronal slice at stimulated column center, C**) coronal slice ~ 0.5mm from stimulated column center, S*) sagittal slice at stimulated column center, S**) sagittal slice ~ 0.5mm from stimulated column center. Scale bar at bottom right indicates magnitude (10mV vertical) and time (50ms) of all displayed traces.

Comparing the LFP distribution across slices can be technically challenging, since obtaining recordings made at identical locations across layer II/III in multiple slices is problematic; therefore in order to characterize the LFP distribution, measurements were normalized according to the (same slice) peak evoked potential and binned in four discrete regions according to their distance from the center of the maximal optical response. Those four regions are: 0.0 - 100 μ m the maximally responding center, 100 - 300 μ m corresponding to the locations of the FWHM, 300 - 500 μ m, and distances > 500 μ m. Plots of normalized peak evoked potential are shown in Figure 6.5. Clear differences between the coronal and sagittal slices are apparent during control conditions; more specifically the distribution of LFP is more strongly attenuated with increasing distance in coronal slices. Differences in the population averages of normalized evoked potential were tested using an independent samples t-test and were statistically significant ($p < 0.05$) at distances of 300 - 500 μ m and > 500 μ m, but not at distances of 0-100 μ m and 100-300 μ m. Plots of the normalized peak evoked potential following the application of BMI indicate that the LFP distribution in both types of slices is very similar under conditions of GABA_A block, and at no distance across layer 2/3 are the differences

between coronal and sagittal slices statistically significant ($p < 0.05$) although a large increase in magnitude of response is observed at all distances. Similarly, following NMDA block with D-AP5, no statistically significant difference was observed between the distributions of peak evoked potential in coronal and sagittal slices. The fact that the distributions of LFP were nearly the same in both types of slices after both pharmacological manipulations suggests that the impact of each manipulation was not equal in both types of slices. For example, the distribution of LFP following GABA_A block suggests that the relative effects of BMI on the coronal slice were larger (because peak response was increased in both types of slices, but more so in coronal slices). Conversely, since the peak evoked potential was decreased in response to NMDA block this suggests that the effect of D-AP5 may have been larger in the sagittal slice. Coupled with the results of the intrinsic signal imaging experiments, differences between the evoked potential characteristics of coronal and sagittal slices imply that the relative contributions of inhibition and excitation lead to a larger discriminative capacity within the coronal plane. This means that within this plane the cortex should demonstrate an improved ability to spatially discriminate two near adjacent, simultaneously driven cortical columns.

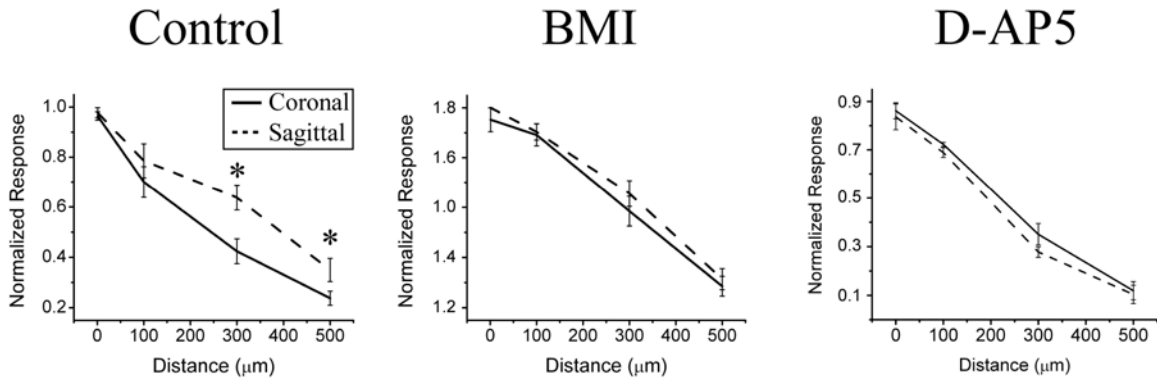


Figure 6.5. Distribution of local field potential across layer 2/3 in coronal and sagittal slices. Measurements of LFP within subjects were binned and averaged before normalizing according to peak potential in control conditions. Same bin normalized values were averaged across subjects and plotted as a function of distance from the stimulated column center (obtained from optical images). Bins were 0-100μm, 100-300μm, 300-500μm, and >500μm. * indicates locations demonstrating statistical significance between coronal and sagittal averages, $p < 0.01$.

Evoked OIS responses were imaged to multisite stimulation in order to demonstrate differences in the discriminative capacity of slices cut in each plane; that is the ability to discriminate two discrete as opposed to one contiguous pattern of activity across layer 2/3. Separations of $> 1.5\text{mm}$, $\sim 1.0\text{mm}$, and $\sim 0.5\text{mm}$ were used between the two stimulus electrodes. These distances were chosen based on results of the response distribution to single site stimulation; for example we predicted that significant differences in the response distribution at distances of $\sim 0.5\text{mm}$ (from Figures 6-3 - 6-5) would lead to differences in the discriminative capacity of slices stimulated at distances $\sim 1.0\text{mm}$ apart but not $> 1.5\text{mm}$. Figure 6.6 shows responses evoked by multisite stimulation in exemplary slices cut in each plane perfused with normal ACSF (Control) and after application of $2\mu\text{mol}$ BMI (multisite stimulation trials were not conducted under conditions of NMDA block due to lack of effect on OIS spatial characteristics).

The transmittance distribution measured across all of layer 2/3 is shown beneath each image. When the distance between the stimulus electrodes was $> 1.5\text{mm}$ two distinct patterns of columnar activation are apparent in slices cut in both planes under both conditions, two columns were also clearly discernable by the identification of independent FWHM. When the stimulus electrodes were located $\sim 1.0\text{mm}$ apart, under control conditions, the coronal slice displays a pattern of activity which permits the identification of two discrete columnar patterns of activation in layer 2/3, however, the same conditions in the sagittal slice do not. Following treatment with BMI two independent columns of activation are no longer distinguishable in either type of slice at this separation. Although there are observable differences in the transmittance distributions displayed under the images, when the stimulus electrodes were separated by $\sim 0.5\text{mm}$, two discrete patterns of activation were not observed in either slice or under either condition.

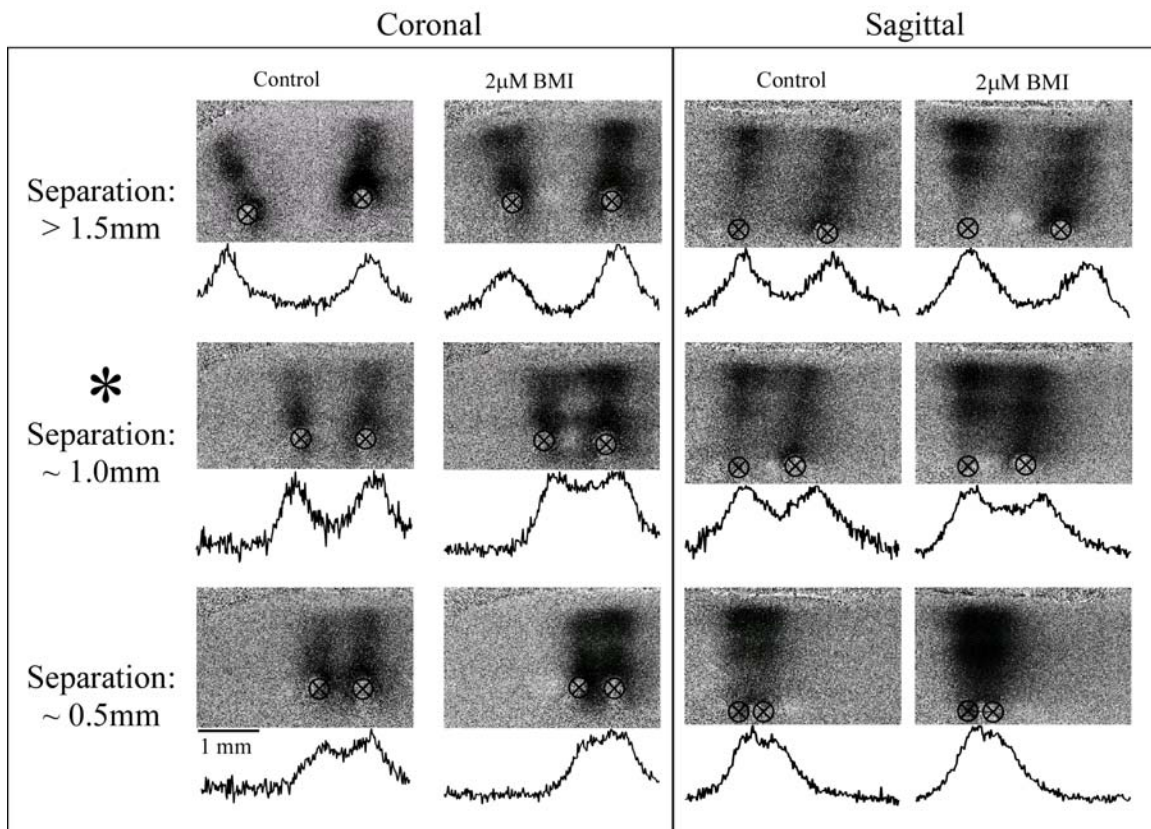


Figure 6.6. OIS responses evoked by multisite stimulation. Electrodes were separated by three distances (>1.5, ~1.0, and ~0.5mm) and the response evoked by simultaneous dual site stimulation of layer V/VI was measured in normal ACSF (control) and after pharmacological block with BMI. Location of stimulus electrodes is indicated by circled x. Traces under each image display the transmittance distribution measured across layer 2/3. * indicates significant differences were observed at the 1.0mm electrode separation between coronal and sagittal slices according to visual inspection of OIS images as well as using FWHM criterion.

Discussion

In this report we have described differences between the stimulus evoked activity in layer 2/3 of rat sensorimotor cortical slices sectioned in the coronal and sagittal planes. The results of this study demonstrate that the tangential span of cortical activity in layer 2/3 in the coronal slice (evoked by stimulation of layer 5/6) is more strongly attenuated

when compared with similarly evoked activity in the sagittal slice. Application of BMI eliminated these differences indicating an important role of GABA_A in the sculpting of this intrinsic activity. NMDA block by D-AP5 produced a robust decrease in intrinsic signal strength within the stimulated column but very little difference in the response of layer 2/3 neurons outside of the stimulated column suggesting that at the level of block achieved with this concentration, the NMDA system had a smaller impact on the spatial attributes of the acquired signal. Measurements of evoked potential strongly supported the conclusions of the intrinsic imaging experiments indicating that neuroelectrical activity was impacted in a consistent fashion.

Many in vitro studies of cortical function have used the coronal slice preparation, and its importance as a model for the investigation of intrinsic mechanisms of cortical information processing has been invaluable (Lee et al. 1992; Staiger et al. 1999; Kohn et al. 2000; Wirth and Luscher 2004; Ajima and Tanaka 2006). However our results suggest that caution should be exercised when interpreting the results of these studies and extrapolating them to local mechanisms of cortical processing in general. To our knowledge this is the first study to examine the differences in the functional properties of rat sensory cortex using the sagittal cortical slice. As with the coronal slice preparation there is always a potential that the functional connectivity has been disturbed by the sectioning process (this may be especially true in the case of long range horizontal connections); however the strong columnar responses observed during our intrinsic imaging studies as well as the robust impact of BMI on these responses suggests that at least within the region studied these vertical and shorter range horizontal connections were functional.

The anisotropic spread of activity in the rat barrel cortex, which extends further along a barrel row than across them, is well documented in vivo (Derdikman et al. 2003; Petersen et al. 2003). Even more studies have reported in detail on the anatomical connections which serve as the substrate for these differences in the spread of activation (Akers and Killackey 1978; Bernardo et al. 1990; Bernardo et al. 1990; Staiger et al. 1999; Fox et al. 2003). Fewer studies have examined the electrophysiological differences responsible for the generation of these activity patterns. Ajima et al characterized the differences in excitatory and inhibitory currents in single cells along and across barrel rows in vitro and found no differences in the strength of GABA_A mediated inhibitory currents, although differences in the strength of excitatory currents were observed. The stronger impact of GABA_A observed in our experiments can thus possibly be attributed to differences in the locations of stimulus delivery (layer 2/3 in study by Ajima et al) or differential recruitment of these connections which could result from repetitive stimulation of lower cortical layers (Ajima and Tanaka 2006). To this end, stimulation of lower cortical layers in the sensorimotor cortical slice, especially layer VI/ white matter, has been shown to more closely reproduce the response to thalamocortical afferent drive and therefore may be a better model for investigation of normally activated intrinsic cortical circuitry (Kohn et al. 2000).

The role of GABAergic inhibition in the spatial sculpting and temporal tuning of intrinsic cortical activity has been characterized in great detail in the rat sensory/ barrel cortex. Salin and Prince reported that the maximum horizontal distance that an ipsc could be recorded was largest in infragranular layer 5, which could contribute to the increased role for GABA which was observed in our studies (Salin and Prince 1996).

Additionally, it was reported by Kyriazi et al. that GABAA block with BMI produced the largest proportional effect on the responses of cells which were initially smaller (Kyriazi et al. 1996). This is in direct agreement with the observations of our study which showed that the impact of BMI on both types of slices was largest in columns which were located ~500µm away from the stimulated site rather than in the maximally activated column. Thus locations which displayed the largest proportional increase in their activity in response to BMI typically demonstrated the smallest evoked response to stimulation during control conditions.

It seems clear that the activity within the rat (and potentially other animal models) sensory cortex is modulated differentially along different cortical axis although the reason for such a mechanism is still a subject of speculation. Many researchers have proposed that these differences exist to maximize the contrast which is generated during whisking behaviors, a process which occurs by the sweeping of multiple whiskers within a barrel row across a surface. If this is the case then the stronger inhibition which was observed in the coronal plane (approximately across the barrel row) in this study would seem to exist in order to limit the influence of a single barrel row on an adjacent barrel row and could be evidence for the segregation of each barrel row as an independent higher order element of sensory processing.

The results of this and other studies lead us to conclude that intercolumnar processing in the sensorimotor cortical slice is anisotropic with respect not only to a given cortical area but also within a single cortical area. Differences in the horizontal spread of activity likely are a result of differences in the balance of excitation and inhibition along each cortical axis. Here we have shown that the impact of GABAergic

inhibition is stronger along the coronal axis and thus provides a heightened capacity for spatial discrimination along this dimension. Further studies are needed to discover the exact mechanism by which this increase in GABAergic efficacy occurs as well as to elucidate its purpose.

References

- Ahmed B., Anderson J., Douglas R., Martin K., and Nelson J. (1994). "Polyneuronal innervation of spiny stellate neurons in cat visual cortex." *J Comp Neurol* 341(1): 39-49.
- Ajima A., and Tanaka S. (2006). "Spatial patterns of excitation and inhibition evoked by lateral connectivity in layer 2/3 of rat barrel cortex." *Cereb Cortex* 16(8): 1202-11.
- Akers R. M., and Killackey H. P. (1978). "Organization of corticocortical connections in the parietal cortex of the rat." *J Comp Neurol* 181(3): 513-37.
- Allison T., McCarthy G., and Wood C. (1992). "The relationship between human long-latency somatosensory evoked potentials recorded from the cortical surface and from the scalp." *Electroen Clin Neuro* Jul-Aug; 84(4): 301-314.
- Allison T., McCarthy G., Wood C., Darcey T., Spencer D., and Williamson P. (1989a). "Human cortical potentials evoked by stimulation of the median nerve. I. cytoarchitectonic areas generating short-latency activity." *J Neurophys* Sep; 62(3): 694-710.
- Allison T., McCarthy G., Wood C., Williamson P., and Spencer D. (1989b). "Human cortical potentials evoked by stimulation of the median nerve. II. cytoarchitectonic areas generating long-latency activity." *J Neurophys* Sep; 62(3): 711-722.
- Arthurs O., Williams E., Carpenter T., Pickard J., and Boniface S. (2000). "Linear coupling between functional magnetic resonance imaging and evoked potential amplitude in human somatosensory cortex." *Neurosci* 200; 101(4): 803-806.
- Ba A., Guiou M., Pouratian N., Muthialu A., Rex D., Cannestra A., Chen J., and Toga A. (2002). "Multiwavelength optical intrinsic signal imaging of cortical spreading depression." *J Neurophys* Nov; 88(5): 2726-35.
- Backes W., Mess W., van Kranen-Mastenbroek V., and Reulen J. (2000). "Somatosensory cortex responses to median nerve stimulation: fMRI effects of current amplitude and selective attention." *Clin Neurophys* Oct; 111(10): 1738-1744.
- Bensmaia S., Leung Y., Hsiao S., and Johnson K. (2005). "Vibratory adaptation of cutaneous mechanoreceptive afferents." *J Neurophys* 94(5): 3023-36.
- Bernardo K. L., McCasland J. S., and Woolsey T. A. (1990). "Local axonal trajectories in mouse barrel cortex." *Exp Brain Res* 82(2): 247-53.

- Bernardo K. L., McCasland J. S., Woolsey T. A., and Strominger R. N. (1990). "Local intra- and interlaminar connections in mouse barrel cortex." *J Comp Neurol* 291(2): 231-55.
- Brumberg J., Pinto D., and Simons D. (1996). "Spatial gradients and inhibitory summation in the rat whisker barrel system." *J Neurophys* Jul; 76(1): 130-140.
- Burton H., and Fabri M. (1995). "Ipsilateral intracortical connections of physiologically defined cutaneous representations in areas 3b and 1 of macaque monkeys: projections in the vicinity of the central sulcus." *J Comp Neurol* May; 355(4): 508-38.
- Cannestra A., Pouratian N., Shomer M., and Toga A. (1998). "Refractory periods observed by intrinsic signal and fluorescent dye imaging." *J Neurophys* 80(3): 1522-32.
- Chen L., Friedman R., Ramsden B., LaMotte R., and Roe A. (2001). "Fine-scale organization of SI (Area 3b) in the squirrel monkey revealed with intrinsic optical imaging." *J Neurophys* Dec; 86(6): 3011-3029.
- Chen L., Friedman R., and Roe A. (2003). "Optical imaging of a tactile illusion in area 3b of the primary somatosensory cortex." *Science* Oct 31; 302(5646): 881-885.
- Chung S., Li X., and Nelson A. (2002). "Short-term depression at thalamocortical synapses contributes to rapid adaptation of cortical sensory responses in vivo." *Neuron* 34(3): 331-2.
- Connor C., Hsiao S., Phillips J., and Johnson K. (1990). "Tactile roughness: neural codes that account for psychophysical magnitude estimates." *J Neurosci* Dec; 10(12): 3823-3836.
- Craig J. (1985). "Attending to two fingers: two hands are better than one." *Percept Psychophys* Dec; 38(6): 496-511.
- Derdikman D., Hildesheim R., Ahissar E., Arieli A., and Grinvald A. (2003). "Imaging spatiotemporal dynamics of surround inhibition in the barrels somatosensory cortex." *J Neurosci* Apr; 23(8): 3100-3105.
- Diamond M., Favorov O., Tommerdahl M., Kelly D., and Whitsel B. (1986). "Organization of somatic sensory cortex: the detection of discrete topographic units and evidence for their integrative function." *University of North Carolina, Chapel Hill* Dissertation.
- Douglas R., Koch C., Mahowald M., Martin K., and Suarez H. (1995). "Recurrent excitation in neocortical circuits." *Science* 269: 981-85.

- Essick G., and Whitsel B. (1988). "The capacity of human subjects to process directional information provided at two skin sites." *Som Mot Res* 6(1): 1-20.
- Ferster D. (1992). "The synaptic inputs to simple cells of the cat visual cortex." *Prog Brain Res* 90: 423-41.
- Foeller E., Celikel T., and Feldman D. (2005). "Inhibitory sharpening of receptive fields contributes to whisker map plasticity in rat somatosensory cortex." *J Neurophys* 94(6): 4387-400.
- Fox K., Wright N., Wallace H., and Glazewski S. (2003). "The origin of cortical surround receptive fields studied in the barrel cortex." *J Neurosci* 23(23): 8380-91.
- Frostig R., Lieke E., Ts'o D., and Grinvald A. (1990). "Cortical functional architecture and local coupling between neuronal activity and the microcirculation revealed by in vivo high-resolution optical imaging of intrinsic signals." *Proc Natl Acad Sci USA* Aug; 87(16): 6082-6086.
- Grinvald A. (1985). "Real-time optical mapping of neuronal activity: from single growth cones to the intact mammalian brain." *Ann Rev Neurosci* 1985(8): 263-305.
- Grinvald A., Bonhoeffer T., Malonek D., Shoham D., Bartfeld E., Arierli A., Hildesheim R., and Ratzlaff E. (1991). Optical imaging of architecture and function in the living brain. In Memory Organization and Locus of Change. L. Squire, N. Weinberger, G. Lynch and J. McGaugh. N.Y., Oxford Univ. Press: 49-85.
- Grinvald A., Frostig R., Siegel R., and Bartfeld E. (1991). "High-resolution optical imaging of functional brain architecture in the awake monkey." *Proc Natl Acad Sci USA* 88(24): 11559-63.
- Guclu B., and Bolanowski S. (2002). "Modeling population responses of rapidly-adapting mechanoreceptive fibers." *J Comp Neurosci* May-Jun; 12(3): 201-218.
- Hlushchuk Y., and Hari R. (2006). "Transient suppression of ipsilateral primary somatosensory cortex during tactile finger stimulation." *J Neurosci* 26(21): 5819-24.
- Holthoff K., and Witte O. (1996). "Intrinsic optical signals in rat neocortical slices measured with near-infrared dark-field microscopy reveal changes in extracellular space." *J Neurosci* Apr; 16(8): 2740-2749.
- Hubel D., and Wiesel T. (1962). "Receptive fields, binocular interaction, and functional architecture in the cat's visual cortex." *J Physiol* Jan; 160: 106-154.
- Iguchi Y., Hoshi Y., Tanosaki M., Taira M., and Hashimoto I. (2002). "Selective attention regulates spatial and intensity information processing in the human primary somatosensory cortex." *NeuroReport* Dec; 13(17): 2335-2339.

- Iwamura Y., Tanaka M., Iriki A., Taoka M., and Toda T. (2002). "Processing of tactile and kinesthetic signals from bilateral sides of the body in the postcentral gyrus of awake monkeys." *Behav Brain Res Sep*; 135(1-2): 185-190.
- Johnson K. (1974). "Reconstruction of population response to a vibratory stimulus in quickly adapting mechanoreceptive afferent fiber population innervating glabrous skin of the monkey." *J Neurophys* 37(1): 48-72.
- Jones E. (1986). Connectivity of the Primate Sensory-Motor Cortex. In Cerebral Cortex: Sensory-Motor Areas and Aspects of Cortical Connectivity. E. Jones and A. Peters. New York, Plenum Press. 5.
- Jones E., and Porter R. (1980). "What is area 3a?" *Brain Res May*; 203(1): 1-43.
- Juliano S., Hand P., and Whitsel B. (1981). "Patterns of increased metabolic activity in the somatosensory cortex of monkeys subjected to controlled cutaneous stimulation: A 2-deoxyglucose study." *J Neurophys Dec*; 46(6): 1260-1284.
- Juliano S., Hand P., and Whitsel B. (1983). "Patterns of metabolic activity in cytoarchitectural area SII and surrounding cortical fields of the monkey." *J Neurophys Oct*; 50(4): 961-980.
- Juliano S., and Whitsel B. (1987). "A combined 2-deoxyglucose and neurophysiological study of primate somatosensory cortex." *J Comp Neurol Sep*; 263(4): 4514-4525.
- Kleinfeld D., and Delaney K. (1996). "Distributed representation of vibrissa movement in the upper layers of somatosensory cortex revealed with voltage-sensitive dyes." *J Comp Neurol* 375(1): 89-108.
- Kohn A., Metz C., Quibrera M., Tommerdahl M., and Whitsel B. (2000). "Functional neocortical microcircuitry demonstrated with intrinsic signal optical imaging in vitro." *Neurosci* 95(1): 51-62.
- Korvenoja A., Wikstrom H., Huttunen J., Virtanen J., Laine P., Aronen H., Seppalainen A., and Ilmoniemi R. (1995). "Activation of ipsilateral primary sensorimotor cortex by median nerve stimulation." *Neuroreport Dec*; 6(18): 2589-2593.
- Kyriazi H., Carvell G., Brumberg J. C., and Simons D. J. (1998). "Laminar differences in bicuculline methiodide's effects on cortical neurons in the rat whisker/barrel system." *Som Mot Res* 15(2): 146-56.
- Kyriazi H. T., Carvell G. E., Brumberg J. C., and Simons D. J. (1996). "Quantitative effects of GABA and bicuculline methiodide on receptive field properties of neurons in real and simulated whisker barrels." *J Neurophys* 75(2): 547-60.

- Lee C., and Whitsel B. (1992). "Mechanisms underlying somatosensory cortical dynamics: I. In vivo studies." *Cereb Cortex* Mar-Apr; 2(2): 81-106.
- Lee C., Whitsel B., and Tommerdahl M. (1992). "Mechanisms underlying somatosensory cortical dynamics II. In vitro studies." *Cereb Cortex* 2: 107-33.
- Lee J., Tommerdahl M., Favorov O., and Whitsel B. (2005). "Optically recorded response of the superficial dorsal horn: dissociation from neuronal activity, sensitivity to formalin-evoked skin nociceptor activation." *J Neurophys* June; 94(1): 852-64.
- Leung Y. (1995). Adaptation of mechanoreceptive afferents to continuous sinusoidal vibration. Baltimore, Johns Hopkins University Dissertation.
- Ling D., and Benardo L. (1995). "Recruitment of GABAA inhibition in rat neocortex is limited and not NMDA dependent." *J Neurophys* 74(6): 2329-2335.
- Lipton M. L., Fu K. M., Branch C. A., and Schroeder C. E. (2006). "Ipsilateral hand input to area 3b revealed by converging hemodynamic and electrophysiological analyses in macaque monkeys." *J Neurosci* 26(1): 180-5.
- MacVicar B., and Hochman D. (1991). "Imaging of synaptically evoked intrinsic optical signals in hippocampal slices." *J Neurosci* May; 11(5): 1458-1469.
- McKenna T., Whitsel B., and Dreyer D. (1982). "Anterior parietal cortical topographic organization in macaque monkey: a reevaluation." *J Neurophys* Aug; 48(2): 289-317.
- Moore C., Nelson S., and Sur M. (1999). "Dynamics of neuronal processing in rat somatosensory cortex." *Trends Neurosci* 22(513-520).
- Mountcastle V., Poggio G., and Werner G. (1963). "The relation of thalamic cell response to peripheral stimuli varied over an intensive continuum." *J Neurophys* Sep; 26: 807-834.
- Nelson A., Staines W., Graham S., and McIlroy W. (2004). "Activation in SI and SII; the influence of vibrotactile amplitude during passive and task-relevant stimulation." *Cog Brain Res*(19): 174-184.
- Nihashi T., Naganawa S., Sato C., Kawai H., Nakamura T., Fukatsu H., Ishigaki T., and Aoki I. (2005). "Contralateral and ipsilateral responses in primary somatosensory cortex following electrical median nerve stimulation - an fMRI study." *J Neurophys* Apr; 116(4): 842-8.
- OMara S., Rowe M., and Tarvin R. (1988). "Neural mechanisms in vibrotactile adaptation." *J Neurophys* Feb; 59(2): 607-622.

- Petersen C. C., Grinvald A., and Sakmann B. (2003). "Spatiotemporal dynamics of sensory responses in layer 2/3 of rat barrel cortex measured in vivo by voltage-sensitive dye imaging combined with whole-cell voltage recordings and neuron reconstructions." *J Neurosci* 23(4): 1298-309.
- Powell T., and Mountcastle V. (1959a). "The cytoarchitecture of the postcentral gyrus of the monkey macaca mulatta." *Bulletin of the Johns Hopkins Hospital* Sep; 105: 108-131.
- Salin P. A., and Prince D. A. (1996). "Electrophysiological mapping of GABAA receptor-mediated inhibition in adult rat somatosensory cortex." *J Neurophys* 75(4): 1589-600.
- Shoham D., and Grinvald A. (2001). "The cortical representation of the hand in macaque and human area s-i: high resolution optical imaging." *J Neurosci* Sep 1; 21(17): 6820-6825.
- Simons D. (1978). "Response properties of vibrissa units in rat SI somatosensory neocortex." *J Neurophys* May; 41(3): 798-820.
- Simons S., Tannan V., Chiu J., Favorov O., Whitsel B., and Tommerdahl M. (2005). "Amplitude-dependency of response of SI cortex to vibrotactile stimulation." *BMC Neurosci* 6(1): 43.
- Simons S. B., Chiu J., Favorov O. V., Whitsel B. L., and Tommerdahl M. (2007). "Duration-dependent response of si to vibrotactile stimulation in squirrel monkey." *J Neurophys* 97(3): 2121-9.
- Somers D., Nelson A., and Sur M. (1995). "An emergent model of orientation selectivity in cat visual cortical simple cells." *J Neurosci* 15(8): 5448-65.
- Staiger J. F., Kotter R., Zilles K., and Luhmann H. J. (1999). "Connectivity in the somatosensory cortex of the adolescent rat: an in vitro biocytin study." *Anat Embryol (Berl)* 199(4): 357-65.
- Sur M., Nelson R., and Kaas J. (1982). "Representations of the body surface in cortical areas 3b and 1 of squirrel monkeys: comparisons with other primates." *J Comp Neurol* Oct; 211(2): 177-192.
- Tan H., Wuhle A., and Braun C. (2004). "Unilaterally applied stimuli in a frequency discrimination task are represented bilaterally in primary somatosensory cortex." *Neurol Clin Neurophys* \Nov; 2004: 83.
- Tannan V., Dennis R., and Tommerdahl M. (2005b). "Stimulus-dependent changes in spatial acuity." *Behavioral and Brain Functions* Oct; 1(18).

- Tannan V., and Tommerdahl M. (2006). "Vibrotactile adaptation enhances spatial localization." *Brain Res* Submitted for Review.
- Tommerdahl M. (1989). "Stimulus evoked activity patterns in somatosensory cortex: evidence for an opponent mechanism." The University of North Carolina at Chapel Hill Dissertation.
- Tommerdahl M., Delemos K., Whitsel B., Favorov O., and Metz C. (1999a). "Response of anterior parietal cortex to cutaneous flutter and vibration." *J Neurophys* Jul; 82(1): 16-33.
- Tommerdahl M., Favorov O., and Whitsel B. (2002). "Optical imaging of intrinsic signals in somatosensory cortex." *Behav Brain Res* Sep; 135(1 - 2): 83-91.
- Tommerdahl M., Simons S., Chiu J., Favorov O., and Whitsel B. (2005d). "Response of SI cortex to ipsilateral, contralateral and bilateral flutter stimulation in the cat." *BMC Neurosci* Apr; 6(1): 29.
- Tommerdahl M., Simons S., Chiu J., Tannan V., Favorov O., and Whitsel B. (2005b). "Response of SII cortex to ipsilateral, contralateral and bilateral flutter stimulation in the cat." *BMC Neurosci* 6(11).
- Tommerdahl M., and Whitsel B. (1996a). Optical imaging of intrinsic signals in somatosensory cortex. In Somesthesia and the Neurobiology of Somatosensory Cortex. O. Franzen, R. Johansson and L. Terenius. Basel, Birkhauser Verlag AB: 369-384.
- Torquati K., Pizzella V., Penna S., Franciotti R., Babiloni C., Rossini P., and Romani G. (2002). "Comparison between SI and SII responses as a function of stimulus intensity." *NeuroReport*(13): 813-819.
- Vierck Jr. C., Favorov O., and Whitsel B. (1988). "Neural mechanisms of absolute tactile localization in monkeys." *Som Mot Res* 6(1): 41-61.
- Werner G., and Mountcastle V. (1965). "Neural activity in mechanoreceptive cutaneous afferents: stimulus-response relations, weber functions, and information transmission." *J Neurophys* Mar(28): 359-397.
- Whitsel B. (1987). "A combined 2-deoxyglucose and neurophysiological study of primate somatosensory cortex." *J Comp Neurol* 263(4): 514-25.
- Whitsel B., Favorov O., Tommerdahl M., Diamond M., Juliano S., and Kelly D. (1989). Dynamic processes govern the somatosensory cortical response to natural stimulation. In Sensory Processing in the Mammalian Brain. J. S. Lund. New York, Oxford Univ. Press: 79-107.

- Whitsel B., and Franzen O. (1989). Dynamics of Information Processing in the Somatosensory Cortex. In Brain and Reading. C. Euler, I. Lundberg and G. Lennerstrand. London, Macmillan Press: 129-137.
- Whitsel B., and Juliano S. (1984). Imaging the responding neuronal population with ¹⁴C2DG: the somatosensory cerebral cortical signature of a tactile stimulus. In Somatosensory Mechanisms. C. von Euler, O. Franzen, U. Lindblom and D. Ottoson. London, Macmillan: 61-80.
- Whitsel B., and Kelly D. (1988). Knowledge acquisition ("learning") by the somatosensory cortex. In AAAS Selected Symposium. J. L. Davis, R. W. Newburgh and E. Wegman. Boulder, Westview Press. In Brain Structure, Learning and Memory: 93-131.
- Whitsel B., Kelly E., Delemos K., Xu M., and Quibrera P. (2000). "Stability of rapidly adapting afferent entrainment vs responsivity." *Som Mot Res* 17(1): 13-31.
- Whitsel B., Kelly E., Quibrera M., Tommerdahl M., Li Y., Favorov O., Xu M., and Metz C. (2003). "Time-dependence of SI RA neuron response to cutaneous flutter stimulation." *Som Mot Res* 20(1): 45-69.
- Whitsel B., Kelly E., Xu M., Tommerdahl M., and Quibrera M. (2001). "Frequency-dependent response of SI RA-class neurons to vibrotactile stimulation of the receptive field." *Som Mot Res* 18(4): 263-285.
- Wirth C., and Luscher H. (2004). "Spatiotemporal evolution of excitation and inhibition in the rat barrel cortex investigated with multielectrode arrays." *J Neurophys* 91(4): 1635-47.